N71-33611

NASA TECHNICAL TRANSLATION

NASA TT F-13,798

# ANALYSIS OF THE RELATIONS BETWEEN ACOUSTIC AND AERODYNAMIC PARAMETERS FOR A SERIES OF DIMENSIONALLY SIMILAR CENTRIFUGAL FAN ROTORS

J. Weidemann

Translation of: "Beitrag zur Analyse der Beziehungen zwischen den akustischen und strömungstechnischen Parametern am Beispiel geometrisch ähnlicher Radialventilator-Laufräder", Deutsche Luft-und Raumfahrt, DLR-FB-71-12, 1971, 95 pages.

CASE FILE COPY

NATIONAL AERONAUTICS AND SPACE ADMINISTRATION
WASHINGTON, D. C. 20546 AUGUST 1971

TABLE OF CONTENTS


| | | Page |
|---|---|---|
| SYMBOL LIST | | iii |
| 1. | INTRODUCTION | 1 |
| 2. | SUMMARY OF FLOW-ACOUSTIC PROBLEMS OF VENTILATORS | 3 |
| 2.1. | Analysis of the Flow-Acoustic Problems | 3 |
| 2.2. | Overview of Results in the Literature | 5 |
| 2.2.1. | Summary of the Results of Flow-acoustic Theories | 5 |
| 2.2.2. | Empirically Determined Laws for the Description of Ventilator Noise | 6 |
| 2.2.3. | Investigations of Mechanisms of Aerodynamic Sound Production | 9 |
| 3. | GOAL OF THE INVESTIGATIONS | 12 |
| 4. | ESTABLISHMENT OF THE MODEL LAWS FOR THE PROBLEM | 14 |
| 4.1 | Conditions | 14 |
| 4.2. | System of Equations for the Problem | 15 |
| 4.3. | Boundary Conditions | 16 |
| 4.4. | Parameters of the Problem | 17 |
| 4.5. | Special Cases | 19 |
| 4.5.1. | Spectral Analysis | 20 |
| 4.5.2. | Constant Parameters | 21 |
| 5. | INTRODUCTION OF THE SYSTEM FREQUENCY CHARACTERISTICS | 22 |
| 6. | PRODUCT TRIAL SOLUTION FOR THE DESCRIPTION OF THE VENTILATION NOISE | 25 |
| 7. | EXPERIMENTAL INSTALLATION | 26 |
| 7.1. | Simplifications | 26 |
| 7.2. | Perturbing Bodies for the Simulation of the Blade | 27 |
| 7.3. | Description of the Rotor | 27 |
| 7.4. | Experimental Conditions | 31 |
| 8. | FUNDAMENTAL PROPERTIES OF THE NOISE SPECTRUM | 33 |
| 9. | INVESTIGATION OF THE ROTATIONAL SOUND | 35 |

Page

9.1. Measurement Method and Measurement Program ..... 35
9.2. Determination of the Exponents for the Reynolds Number and Mach Number ..... 38
9.3. Determination of the System Frequency Characteristics .. 42
9.4. Determination of the Excitation Spectrum ..... 43
9.5. Verification of the Product Trial Solution ..... 45
9.6. Rapid Measurements for the Direct Determination of the Excitation Spectrum ..... 48
9.7. Similarity of the Excitation Spectra and System Frequency Characteristics ..... 52

10. INVESTIGATION OF THE FLOW NOISE ..... 55

10.1. Measurement Program ..... 55
10.2. Determination of the Exponents for the Reynolds Number and Mach Number ..... 56
10.3. Determination of the System Characteristics ..... 61
10.4. Determination of the Power Spectral Function ..... 64
10.5. Verification of the Product Trial Solution ..... 70
10.6. Similarity of the Power Spectrum Functions and System Frequency Characteristics ..... 71

11. COMPARISON OF THE NOISE COMPONENTS ..... 72

11.1. Total Sound Level of the Rotational Sound ..... 73
11.2. Total Sound Level of the Flow Noise ..... 74
11.3. Noise Synthesis ..... 75

12. ADDITIONAL MEASUREMENTS ..... 76

12.1. Influence of the Perturbing Body ..... 76
12.2. Influence of the Edge Distance ..... 78
12.3. Directional Effect of the Sound Radiation ..... 80
12.4. Reproducibility ..... 84

13. DISCUSSION OF THE RESULTS ..... 87

14. MEASUREMENT INSTALLATIONS ..... 92

14.1. Measurement Apparatus and Control Apparatus Used ..... 92
14.2. Follower Control Device for the Measurement of the Rotational Sound ..... 93

15. SUMMARY ..... 95

APPENDIX ..... 99

REFERENCES ..... 100

## SYMBOL LIST

| | | |
|---|---|---|
| $c$ | [m/s] | speed of sound |
| $c_p$, $c_v$ | [cal/g °C] | heat capacity |
| $D$ | [m] | rotor diameter |
| $f$ | [Hz] | frequency, bandwidth |
| $F$ | - | non-specified function |
| $g$ | [$m/s^2$] | gravitational force |
| $G$ | - | system frequency process |
| He | - | Helmholtz number, see text |
| $i$ | - | ordinal number of sound elements |
| $k$ | - | constant |
| $K$ | - | sound pressure coefficient |
| Ma | - | Mach number, derived from angular velocity |
| $n$ | [Hz] | rotation frequency, rotation coefficient |
| $p$ | [bar] | pressure |
| $p_0$ | [bar] | relative sound pressure, $2 \cdot 10^{-4}$ µbar |
| $P_0$ | [bar] | ambient air pressure |
| $r$ | [m] | radius of the polar coordinates |
| Re | - | Reynolds number |
| $s$ | [mm] | edge distance |
| $s$ | [W/Hz] | power spectral density |
| $s_0$ | [W/Hz] | relative power effect density formed with $\tilde{p}_0^2$ |
| $S$ | [$m^2$] | surface |
| St | - | Strouhal number |
| $T$ | [m] | division of rotor |
| $T$ | [K] | absolute temperature |
| $U$ | [m/s] | angular velocity of rotor |
| $v$ | [m/s] | absolute flow speed |
| $\dot{V}$ | [$m^3/s$] | volume flux |
| $w$ | [m/s] | relative flow speed |
| $W$ | [W] | sound power |

| | | |
|---|---|---|
| $x$ | - | exponent |
| $X_i$ | [m] | general point coordinates |
| $z$ | - | blade number |
| $\beta$ | [°] | blade angle |
| $\delta$ | [mm] | boundary layer thickness |
| $\vartheta$ | [°] | angle of the polar coordinates |
| $\kappa$ | - | isentropic exponent |
| $\lambda$ | [m] | sound wave length |
| $\nu$ | [$m^2/s$] | kinematic viscosity |
| $\rho$ | [$kg/m^3$] | air density |
| $\phi$ | - | efficiency factor |
| $\psi$ | - | pressure factor |

| | |
|---|---|
| $\bar{}$ | denotes mean value over time |
| $\sim$ | denotes effective value |
| $\cdot$ | denotes alternating variables |

# ANALYSIS OF THE RELATIONS BETWEEN ACOUSTIC AND AERODYNAMIC PARAMETERS FOR A SERIES OF DIMENSIONALLY SIMILAR CENTRIFUGAL FAN ROTORS

J. Weidemann

ABSTRACT. Through the example of free-running centrifugal rotors blowing against a sharp edge, the author shows that the fan laws of blade-passage and broad-band noise can be described by product notations. In particular, it is shown that the frequency dependence of the sound pressure established in the free field is essentially determined by velocity fluctuations on the edge and, independently thereof, by the dimension to the wavelength ratio. Finally, the measurements provide information on the accuracy with which the noise can be calculated for homologous fan series up to a size ratio of 1:10.

## 1. INTRODUCTION

/9

One important goal of mechanical engineering in the area of machine construction is the increase of the power per unit weight of force conversion machines and working machines. In the case of flow machines, this leads to ever increasing rates of revolution and circumferential velocities, which can exceed the speed of sound in special cases. The amount of noise produced by these machines is closely connected with this development, because an increase in the converted mechanical energy also brings about an increase in the produced acoustic power. In addition, as the revolution rate is increased, the noise spectrum is displaced towards the higher frequencies. In the most disadvantageous case, the maximum of the spectrum can be located in the frequency region corresponding to the maximum sensitivity of the ear, so that

---

*Numbers in the margin indicate pagination in the original foreign text.

the annoyance factor of the noise becomes considerable.

The increasing importance of the noise problem can easily be traced using the example of development of aircraft engines. The piston engine used for propeller drive was displaced by the gas turbine, and the propeller itself was replaced by the jet engine and turbo jet engine in most cases. The jet engine leads to a strong annoyance not only because of the large spectral power density of the wide-band jet noise, but also because the so-called rotational pitch of the jet is superimposed. The latter is almost completely produced in the axial compressor. The frequencies of the tones which make up the rotational sound are many octaves higher than in the case of the propeller, and lie above the midpoint of the audible frequency range. Since the rotational sound is more strongly attenuated in the case of sound propagation than the low-frequency jet noise, it can only be heard in the vicinity of the jet engine. It is especially annoying in the interior of the aircraft.

The noise production also increases with the progress in the development and application of air conditioning and cold climate control units. This means that the importance of flow-acoustics processes increases. Today there is a tendency to decrease the channel cross sections in order to increase the flow velocities for reasons of economy. In addition, the climate control of closed skyscrapers requires even more powerful ventilation installations. In so-called high velocity installations, the flow velocities can be three to four times higher than in conventional units.

The aerodynamic noise, which threatens to reduce the comfort of the installations, also consists of a noise component and a sound component. The noise component is produced in the ventilator, in the channel system and at the grids of the air exhaust. The rotational sound is only produced in the ventilator. Since the ventilator noise in general contributes to the total sound production, it becomes necessary to separate the ventilator from the channel system with sound depressors. In order to design these in an

/10

optimum way, that is, in order to obtain sufficient sound suppression for the least flow resistance, it is necessary to know the source and field parameters of the ventilator.

The acoustic power produced in ventilation installations is several orders of magnitude smaller than in the case of aircraft engines. However, the permissible acoustic levels at the outlets of these installations are considerably smaller in the case of ventilation installations. On the other hand, there are many ways in which the sound production of ventilation installations can be reduced. In particular, suitable ventilators can be chosen. This explains why just in recent years numerous theoretical and experimental investigations have been carried out in this area of flow acoustics. The present paper is an attempt to obtain better insights into the structure of the noise of radio ventilators.

## 2. SUMMARY OF FLOW-ACOUSTIC PROBLEMS OF VENTILATORS

### 2.1. Analysis of the Flow-Acoustic Problems

The purpose of flow-acoustic investigations of ventilators is to give an explanation for the sound production mechanisms in order to be able to suppress them. This is not immediately possible, because the power production of existing flow machines is maintained due to the nonsteady component of the flow, which of necessity is converted to part of the sound. Therefore, it is necessary to obtain the minimum ratio between the sound production and the power of the flow by suitable design and operational conditions for the ventilators. In the following we will present the various paths leading to the solution of this problem. These will be discussed in the later chapters.

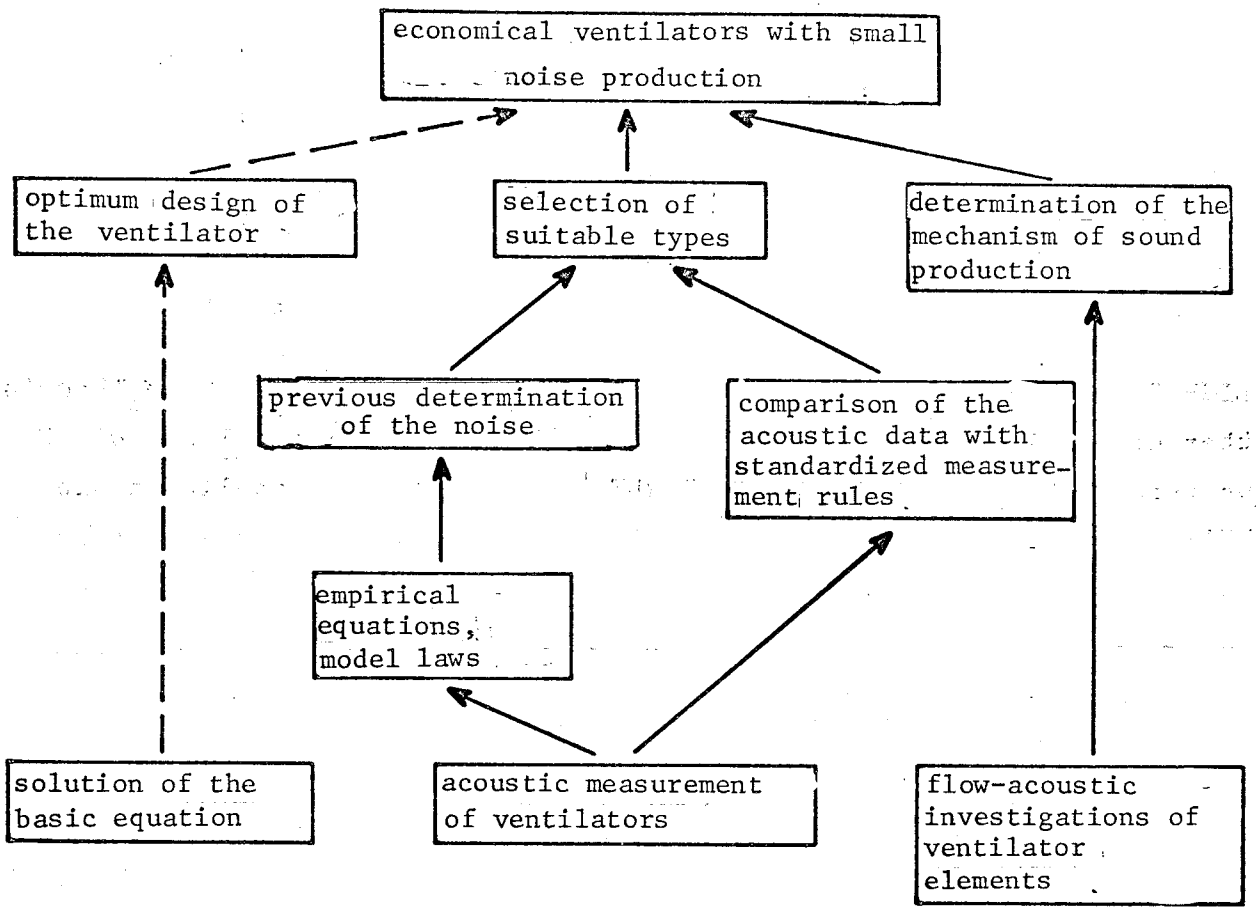
economical ventilators with small noise production
optimum design of the ventilator
selection of suitable types
determination of the mechanism of sound production
previous determination of the noise
comparison of the acoustic data with standardized measurement rules
empirical equations, model laws
solution of the basic equation
acoustic measurement of ventilators
flow-acoustic investigations of ventilator elements

## 2.2. Overview of Results in the Literature /11

### 2.2.1. Summary of the Results of Flow-acoustic Theories

If the noise from the ventilator could be exactly calculated, then it would be possible to immediately find an optimum design of the machine by taking into account the flow, technical and acoustic requirements. However, it is not possible to carry out such a calculation in advance, because the flow field cannot be calculated exactly and therefore the boundary conditions for the rotor, which acts as an acoustic source, cannot be given in closed form.

In the case of a propeller, it was possible for ERNSTHAUSEN [1] to calculate the nonsteady component of the aerodynamic forces acting on the profile. This was done using suitable trial solutions, for a radial velocity distribution and by ignoring compressibility. From this he derived the radiated acoustic power, its spectral distribution and the directional characteristics. ERNSTHAUSEN only considered the rotational sound and showed in particular that the power of the individual harmonics depends on the $7.5^{th}$ to $14^{th}$ power of the circumferential velocity. The corresponding directional /12 characteristics depend on the ratio of the diameter of the radiating complex divided by the acoustic wavelength.

On the other hand, there is no corresponding theory for the radial ventilator up to the present. This is because the flow field in the rotor is extremely complex due to secondary flows and strong turbulence.

In his work, LIGHTHILL [2] furnished the basis for the theory of aerodynamic sound production due to free turbulence. The expansions of this theory due to CURLE [3] and DOAK [4] include cases in which the turbulent source region has a boundary with rigid walls and the case where it contains rigid bodies. Since then, investigations have been carried out on the turbulence noise of closed systems in order to bring the experimental

observations into agreement with the theoretical results. The dimensionless notation of the equations makes a comparison of the terms easier. In this way, one obtains model laws for geometrically similar configurations. The results of the theories state that sound production can be traced to the following three flow phenomena: temporal fluctuations of the mass flow; fluctuations of the force field at body surfaces and oscillating shear forces in the flowing medium.

The noise due to compression effects and boundary layers, for example in the case of sirens, zero incidence profiles or diffusers, can be traced to variations of the mass flow. These acoustic sources have the effect of a flow monopole, the sound production of which consists of a power term per unit surface, an area term and a Mach number term:

$$W_m \sim \frac{\rho \cdot v^3}{2} \cdot S \cdot \frac{v}{c} \quad . \tag{1}$$

Variations in the thrust, caused by vortex shedding at a profile, result in a flow dipole. The acoustic power, compared with that of a monopole, differs only by the Mach number term:

$$W_d \sim \frac{\rho \cdot v^3}{2} \cdot S \cdot \left(\frac{v}{c}\right)^3 . \tag{2}$$

In the case of very fast jets of aircraft and rocket engines, the flow- /13
quadrupole component dominates. These are produced in the turbulent mixing zone during transition of the jet into the ambient air. In this case, the following is obtained for the sound production:

$$W_q \sim \frac{\rho \cdot v^3}{2} \cdot S \cdot \left(\frac{v}{c}\right)^5 . \tag{3}$$

2.2.2. Empirically Determined Laws for the Description of Ventilator Noise

Since it is not possible to calculate the acoustic properties of radial ventilators beforehand, one is forced to measure the sound power, the spectral distribution of the sound energy, the acoustic impedance, the

directional characteristics, etc. Another goal of this paper will be to experimentally verify the general validity of equations found for geometrically similar ventilators. This would mean an important step in the direction of calculating the ventilator noise beforehand using the model laws found. When general laws are determined, one must consider the varied installation possibilities of ventilators, which determine the produced noise to a considerable extent. Therefore, it is only possible to make a comparison when acoustic measurements are carried out under standardized conditions. We cannot describe the numerous problems here which can result. The references WIKSTROM [5] and YEOW [6] give good summaries of the problems.

The first empirically derived equations for the estimation of radial ventilator noise can be found in the work of BERANEK, REYNOLDS and WILSON [7] as well as PIESTRUP and WESLER [8]. The equations for the sound power only contain the mechanical input power given on the ventilator housing plate as well as the number of blades. The deviations of the calculated values from the measured values amount to $\pm$ 4 dB. Improved formulas due to ALLEN [9] and MADISON and GRAHAM [10] consider the delivery pressure, the rotation rate as well as the size of the ventilator. WIKSTROM [5] discussed these laws and showed that they can all be cast in the unified form

$$W \sim u^5 \cdot D^2 \qquad (4)$$

His own measurements on radial ventilators confirm this law. GOLDMAN /14
and MALING [11] investigated ventilators with almost identical dimensions but having different characteristic curves. Using an empirical equation, which contains a shape parameter for the rotor, the static pressure difference and the volume flow, it becomes possible to calculate the sound power within a bandwidth of 75 - 10 kHz with uncertainty from $\pm$ 2 dB to - 3 dB.

However, formulas such as those given above are unsatisfactory, because it is not possible to precalculate the noise from various sized ventilators or to obtain insight into the structure of the noise. The first attempts

to establish model laws for ventilator noise were made by MADISON [12]. However, he did not require strict similarity of the ventilators, but instead only included the rotor diameter in the calculation formulas. This meant that the ventilators considered had different characteristic curves $\psi = F(\phi)$ in general. MADISON obtained the following equation for the sound power:

$$W = \frac{h(\varphi)}{\rho \cdot c^2} \cdot \dot{V} \cdot (\Delta p)^2 . \tag{5}$$

If the volume flow $\dot{V}$ and the static pressure difference $\Delta p$ are expressed by the flow coefficient $\phi$ or the pressure number $\psi$, then Equation (8) can be transformed into Equation (4) in the case of geometrically similar ventilators which operate at the same characteristic curve point.

MALING [13], on the other hand, required strict geometric similarity of the ventilators. For this assumption, the ventilators have the same characteristic curve, if we first ignore the influence of viscosity. This means that the operating point is uniquely determined by specifying the flow coefficient. In addition, MALING considered the normalized power spectral density "$E/\rho c^2 D^3$" in his similarity analysis, which in particular depends on the normalized frequency St. He found the following description of the problem using dimensional analysis:

$$E/\rho c^2 D^3 = F(Ma, \varphi, St) . \tag{6}$$

The evaluation of the measurements of three radial ventilators having 28 blades inclined in the forward direction showed that a Mach number term could be split off in Equation (6):

$$E/\rho c^2 D^3 = Ma^3 \cdot g(St, \varphi). \tag{7}$$ /15

$g(St, \phi)$ is the dimensionless power spectral function which as assumed does not depend on the Reynolds number because the diameter was only varied in the ratio 1:1.4. The deviations of the power density from the averaged function

Equation (7) amount to $\pm$ 3 dB for various frequencies and flow coefficients. In order to obtain the sound power, Equation (7) must be integrated over all dimensionless frequencies from St = a to St = $\infty$. MALING obtained the following for $\phi$ = const

$$W_{a-\infty} = \rho c^3/\pi \cdot Ma^4 \cdot D^2 \int_a^\infty g(St)\, d(St) . \qquad (8)$$

MALING explained the difference of his law from the $u^5D^2$ law by the fact that the lower limiting frequency of the measuring instruments is usually held constant. For a continuously decreasing power spectral function, which MALING approximated by the function $g \sim St^{-2.67}$, the following was obtained for the integral of Equation (8)

$$\int_a^\infty (St)^{-2,67}\, d(St) \sim (St)^{-1,67} = \left(\frac{u}{f \cdot D}\right)^{1,67}.$$

For a constant lower limiting frequency $f = f_a$, that is, for non-similar bandwidth of the spectra under consideration, the following is obtained for the sound power:

$$W_{a-\infty} \sim u^4 D^2 \cdot \left(\frac{u}{D}\right)^{1,67} = u^{5,67} \cdot D^{0,33} . \qquad (9)$$

From this it follows that in a precalculation of the ventilator noise, which contains primarily a continuous spectrum, using similarity laws, it is necessary to have similarity between the widths of the frequency spectra under consideration.

2.2.3. Investigations of Mechanisms of Aerodynamic Sound Production /16

In addition to a detailed description of ventilator noise, it is also important to analyze the mechanisms which bring about the ventilator noise. Only knowledge of these mechanisms will make it possible to carry out a systematic noise suppression at the point of origination. By this we mean

flow-acoustic mechanisms, in contrast to those in which the imbalance of rotating parts leads to oscillations of machine components and therefore to sound production.

Since the establishment of power laws for the sound production of monopole, dipole and quadrupole sources, attempts have been made to reduce the sound due to turbulences in the flow machines to the sources mentioned above. The exponent of the characteristic velocity, which depends on the measured acoustic power, is determined and it is compared with the power laws (1), (2) and (3). If the radiation type is known, then it is possible to draw conclusions regarding the sound production mechanism. In order to separate the noise components from the rotational sound, it is not positioned to dissect the spectrum into tertiary bands. Instead it is necessary to carry out a narrow band analysis. The bandwidths can only amount to a few percent of the central frequency or only a few Hertz.

According to YEOW [6], ALLEN [9] is the first who pointed to the difference between the production of the sound component and the noise component. The rotational sound (rotational component) is produced by impulses at a fixed point of the housing by the air after passing around the blade. On the other hand, the noise component, also often called vortex noise (vortex component), is produced by vortex separation at the trailing edge of the blade. Here we should mention that the term "vortex noise" is not precise for the noise component. Then vortex shedding can also be periodic, just as in the case of the Karman vortex pattern, so that lines will dominate in the frequency spectrum, just as in the case of a strongly developed rotational sound.

Several experimental and theoretical papers have investigated the sound production of individual components of the ventilator.

SHARLAND [14] showed that three mechanisms bring about fluctuations of the lift in the case of turbulent flow around a flat plate. Therefore they have the effect of dipole sources:

1. vortex shedding at the profile trailing edge /17

2. fluctuations of the angle of attack, caused by turbulent fluctuations of the flow

3. fluctuations of the plate boundary layer.

SHARLAND was able to estimate that the boundary layer noise can be ignored in comparison with the other components. Measurements of the directional characteristic of the sound radiation confirm the dipole properties of the sound source.

The aerodynamic sound production of an installation consisting of two cylinders clamped between two rotating disks was investigated in detail by STUBER [15]. He found that the vortex shedding occurred at the cylinders at a preferred frequency, the Aeolian tone. The two disks represent a cavity resonator, the eigenresonances of which modify the spectrum further. In addition, the measurement results showed that the cavity resonance causes a distinct directional characteristic of the radiating body. This explains why the sound intensity determined at a fixed point of measurement can clearly deviate from the $u^6$ dipole law.

In investigations of the noise production in radial ventilators, the aerodynamic interactions between the rotor and the switchblade are of primary importance, because they determine the production and properties of the rotational sound, as was already mentioned above. Here the question arises of which radiation type is dominant, whether it is the dipole which is produced due to the interaction forces applied to the switchblade and the blade, or whether it is the monopole, which is produced by the pulsating mass flow produced at the switchblade.

CHANAUD [16] discussed the discrepancy which exists between the $u^4$ law of the monopole, the $u^6$ law of the dipole, and the $u^5$ law of

radial ventilators. His measurements of geometrically similar ventilators without housings confirmed the $u^5$ law only in terms of the dependence of the sound power and the power density at low frequencies. On the other hand, at higher frequencies this dependence agrees with the $u^6$ law of the dipole. CHANAUD explained the deviations in terms of the near field influences. Using the example of sound production at a knife edge, used to simulate the switchblade of the ventilator, CHANAUD pointed out that the knife edge acts as a dipole radiator using the power law and sound pressure distribution /18
he determined in the chamber, which is relatively free of reflections. The direction of maximum sound radiation is perpendicular to the knife edge surface. This is the same result as the one SHARLAND obtained.

The further investigations of EMBLETON [17], LYONS and PLATTER [18] and LEIDEL [19] attempted to suppress the rotational sound as much as possible by shaping the switchblade in an appropriate way, for example by rounding it off, inclining it with respect to the blade, dividing it into two switchblades displaced by one half the division or by suitably adjusting the switchblade distance. Without going into the details further, it should be noted that it is possible to reduce the sound level by more than 12 dB with such measures.

## 3. GOAL OF THE INVESTIGATIONS

In most investigations, especially in the Anglo-Saxon investigations of radial ventilator noise, rotors having short blades and curved in the forward direction, so-called drum rotors, are considered. In contrast to this, in this paper we carried out acoustic measurements of a type of ventilator having long blades curved in the aft direction. The purpose of this investigation was to find experimental verification of model laws and to determine laws governing the noise structure. The works of MALING [13] and CHANAUD [16] have been extended in the following ways:

1. In order to determine the influence of the Reynolds number on the produced sound in a more accurate way, it is not sufficient to vary the rotor diameter only in the ratio range 1:1.4 or 1:2, as was done in the case of MALING or CHANAUD. Therefore, five rotors with a diameter of 1:10 were investigated.

2. The rotational sound is especially important in this paper, because it was especially well developed compared with the flow noise. This was done with appropriate measures. The sound component and the noise components of the ventilator noise are treated separately.

3. The literature on aerodynamic sound production [1, 5, 14, 15, 16, 19, 20, 21] shows that the radiation properties of the systems considered are characterized by directional characteristics and resonance effects. Since both only depend on the ratio of the dimensions to the acoustic wavelength, this frequency dependence has the effect of a frequency characteristic on the sound intensity measured at a fixed point. It will be shown that /19
this "system frequency characteristic" can be separated from the laws of aerodynamic sound production and can be introduced into the model laws. Measurements of the magnitude of sound velocity at the slit between the rotor and the switchblade were used to verify the validity of the theory.

4. In order to satisfy the requirements for geometric similarity of the ventilators as much as possible, we used specially produced rotors with very close production tolerances.

It is sufficient for an analysis of the structure of ventilator noise to establish relationships between the acoustic and flow parameters for one characteristic curve point alone. Since it is also necessary to restrict the number of measurement points, there was no variation of the working point.

## 4. ESTABLISHMENT OF THE MODEL LAWS FOR THE PROBLEM

If the field quantities are first normalized by the characteristic quantities of the problem, for example if the acoustic pressure is referred to the ambient pressure of the experimental medium, then they can be represented as a function of the independent variables which are normalized in the same way. The relationships represented in this dimensionless form represent universal laws for the problem, which in general depend on several normalized parameters. In the case of geometrically similar experimental installations, the parameters specify how the experimental conditions must be adjusted in order to obtain similar processes or, stated in another way, so that the normalized field quantities will be equal. If the parameters are held constant, then the model dimensions can be immediately given. For example, if the size of the experimental arrangement is changed, as is done in model experiments, then it follows that the other adjustable quantities must be varied according to some specified ratio with respect to each other. The considered physical processes are then similar. The establishment of model laws is therefore equivalent to finding all the essential parameters on which the problem depends. If we start with the fundamental equations and boundary conditions for the problem, then we will also specify the range of validity of the developments and possibly also the effects which have been ignored. The adjustable quantities result naturally and with them the dimensionless parameters. Experiments must then be used to test whether the laws are universally valid. If this is the case within the framework of the measurement accuracy, then all essential parameters have been considered. /20

### 4.1. Conditions

Before the system of equations is established, we must specify the conditions for which the following development applies.

1. The medium which is moved by the working machine to be investigated consists of a frictionless and ideal gas. The working machine is assumed to

be an "ideal machine" and has no losses. The heat conductivity of the medium is assumed negligible.

2. Changes of the position energy are now taken into account. Heat source densities are ignored.

3. The specific heats of the thermal equation of state $p = \rho(c_p - c_v)\,T$ and the caloric equation of state are constants.

4. The flow is steady on the average. We only consider the effective values of the fluctuating pressure components as the only dependent quantities. These radiate the sound. The amplitudes are small with respect to the steady average value.

5. The acoustic measurements are carried out in the free field which is simulated by a chamber with low reflection. The incident flow effects on the microphone are negligible.

6. The working machines under consideration are geometrically similar.

## 4.2. System of Equations for the Problem

The complete set of equations for the thermodynamic description of the flow-acoustic phenomena is a consequence of the conservation laws for momentum, mass and energy as well as the thermal equation of state. The corresponding equations are given as follows considering the conditions stated above:

Euler equations of motion:

$$\rho \frac{Dv_i}{Dt} = -\frac{\partial p}{\partial x_i}\,, \tag{10}$$

Continuity equation:

$$\frac{D\rho}{Dt} + \rho \frac{\partial v_i}{\partial X_i} = 0 , \tag{11}$$

Energy equation for the open system:

$$\rho c_p \frac{DT}{Dt} = \frac{Dp}{Dt} , \tag{12}$$

Thermal equation of state

$$p = \rho(c_p - c_v) T , \tag{13}$$

4.3. Boundary Conditions

The boundary conditions for the flow field inside the blade channels state that the normal components of the vector of relative velocity vanish on the blade. Assuming that only a series of geometrically similar ventilators are being considered, the coordinates of the rotors can be specified by a characteristic dimension, for example, the wheel diameter D. If the circumferential velocity U at the exhaust of the rotor is specified for a certain shape, then the motion of the blade channel edges is completely specified.

The velocity field also depends on the degree of throttling of the ventilator, in addition to the shape and motion of the rotor. For example, it is characterized by the volume flux

$$\dot{V} = \int_{\text{inlet}} v_1 \cdot dS$$

with the inlet velocity $v_1$.

The thermodynamic state of the working medium is specified by the pressure $P_0$ and temperature $T_0$ at a point, for example, at the inlet cross

sections.

## 4.4. Parameters of the Problem

/22

By means of a dimensional analysis [22], the normalized parameters can be derived on which the problem depends. They are also called characteristic numbers or characteristics values. They consist of the independent variables, the dependent variables and the adjustment quantities of the system of equations and the boundary conditions. The normalized parameters form a complete set which is characterized by the fact that no parameter can be obtained by combination of other parameters from the set. A check of the system of equations and the boundary conditions will show that no quantities which are important in the problem have been missed and that the set of parameters is not over specified.

In addition to the dependent variables, the field quantities

$$p,\ v_i,\ \rho,\ T$$

and the independent variables

$$X_i,\ t$$

the boundary conditions and the system of equations contain seven adjustment quantities:

$$D,\ U,\ \dot{V},\ P_o,\ T_o \quad \text{or} \quad c_p,\ c_v\ .$$

If friction were taken into consideration, then the kinematic viscosity $\nu$ would have to be included in the list of adjustment quantities.

The following dimension matrix corresponds to the adjustment quantities

| | $c_p$ | $c_v$ | $\dot{V}$ | D | U | $P_o$ | $T_o$ |
|---|---|---|---|---|---|---|---|
| dimension | 2 | 2 | 3 | 1 | 1 | -1 | 0 |
| time | -2 | -2 | -1 | 0 | -1 | -2 | 0 |
| mass | 0 | 0 | 0 | 0 | 0 | 1 | 0 |
| temperature | -1 | -1 | 0 | 0 | 0 | 0 | 1 |

The last four quantities are dimensionally independent and can therefore be selected as the fundamental parameters of the problem. The following complete set of characteristic numbers results from the variables and the other adjustment quantities and consists of the following normalized field quantities:

$$\frac{p}{P_o}\ ,\quad \frac{v_i}{U}\ ,\quad \frac{\rho}{P_o/U^2}\ ,\quad \frac{T}{T_o}\ , \qquad /23$$

The normalized coordinates of position in time

$$\frac{X_i}{D}\ ,\ \frac{t}{D/U}$$

and the normalized parameters $\Pi_\nu$ of the adjustment quantities

$$\Pi_1 = c_p T_o/U^2$$
$$\Pi_2 = c_v T_o/U^2$$
$$\Pi_3 = \dot{V}/D^2 U \quad .$$

If the following combinations are formed with the parameters $\Pi_\nu$

$$\Pi_1/\Pi_2,\ \sqrt{\Pi_2}/\Pi_1(\Pi_1-\Pi_2),\ \frac{4}{\pi}\Pi_3,$$

then the following parameters which are usually used are obtained which are equivalent to the $\Pi_\nu$ :

the isentropic exponent

$$\varkappa = c_p/c_v\ , \qquad (14)$$

the ("circumferential") Mach number

$$Ma = U/c \tag{15}$$

with the sound velocity

$$c = \sqrt{(c_p - c_v)\, T_o} \tag{16}$$

and the flow coefficient

$$\varphi = 4\dot{V}/\pi\, D^2 U \ . \tag{17}$$

If friction is taken into account, then the Reynolds number must be added to the $\Pi_v$

$$Re = UD/\nu \ . \tag{18}$$

4.5. Special Cases /24

The pressure in the flow field consists of a constant component, the average pressure $\bar{p}$ and a fluctuating component p'. The pressure ratio $\psi$ is formed from them, and is the normalized fluctuating pressure $p'/P_0$, which is recorded outside of the flow field in the form of acoustic pressure. This is the most important acoustic field quantity in noise investigations, so that it is sufficient to investigate the following relationship

$$p'/P_o = F\ (X_i/D,\ tU/D,\ Ma,\ \varphi\ ,\ \varkappa).$$

Since the functional dependence on the isentropic exponent it is not of interest here, then it would be possible to also relate the acoustic pressure to the compression modulus $K = \kappa \cdot P_0$ and thus obtain a characteristic acoustic parameter.

4.5.1 Spectral analysis

In order to obtain reproducible results in the analysis of noise, the complex temporal course of the acoustic pressure is transformed into a frequency spectrum by means of a Fourier transformation. In this transformation, the mean square values of the spectrum amplitudes are formed, so that the normalized field quantity to be investigated is given by :

$$K = \tilde{p}/P_o \quad . \tag{19}$$

The temporal dependence of the normalized acoustic pressure, which is characterized by the independent variable tU/D, is therefore transformed into a dependence on frequency. The "Strouhal number" St $\sim$ fD/U is obtained as the reciprocal of the normalized time, which is usually used. For convenience in the case of the present problem, the Strouhal number is multiplied by the factor $\pi/z$:

$$St = \frac{\pi D}{z} \cdot \frac{f}{U} \quad . \tag{20}$$

This means that the characteristic length of the Strouhal number is the division T of the rotor which is obtained by dividing the circumference by the number of blades:

$$T = \pi D/z \, . \tag{21}$$

/25

In the case of symmetric flow through the rotor, the flow field observed from a fixed point is repeated in a periodic way, every time the rotor has moved by one division. The problem then takes on the form

$$K = F\,(X_i/D,\ St,\ Ma,\ \varphi\ ,\ \varkappa\ ).$$

Since in general noise contains non-periodic pressure fluctuations in addition to periodic ones, a continuous spectrum is superimposed on the discrete

line spectrum, which is a so-called power spectrum, the characteristic of which is the power spectrum density s. It specifies the magnitude of the mean square value $p^2$ if the spectrum were to be analyzed at a bandwidth which goes to zero. The power density is obtained by dividing the measured mean square value by the bandwidth $\Delta f$ of the analyzer. This quotient then no longer depends on the bandwidth of the filter used. The defining equation of the power spectrum density then becomes:

$$s = \overline{p^2} / \Delta f = \tilde{p}^2 / \Delta f \ . \tag{22}$$

The following is then obtained for the power spectrum density normalized together with the fundamental parameter:

$$s^* = \frac{(\tilde{p}/p_o)^2}{\Delta f \ D/U} \ . \tag{23}$$

The mean square value of the acoustic pressure for a small frequency band is obtained from the power density as follows:

$$K^2 \sim s^* \ \Delta(St) \ .$$

4.5.2. Constant Parameters

In order to verify the similarity of the ventilator noise it is sufficient, as pointed out in Section 3, to operate the ventilators at a constant working point. In addition, this measure is necessary in order to reduce the number of data points to a reasonable value. This restriction is defensible, because knowledge of the variation of ventilation noise as a function of the working point gives no further information on the fundamental structure of the noise. The measurements of MALING [13] show that the acoustic power level increases only by 2 dB when the flow coefficient is doubled. This means that the parameters $\phi$ and $\kappa$ remain constant, because all the measurements are carried out in air. /26

Since the decrease of the acoustic pressure with increasing distance is known, as long as base points in the far field of the acoustic source are considered and also the sound propagation takes place under free field conditions as is the case here, it is not necesaary to vary the distance r between the microphone and the ventilator. This means that the ratio r/D can be held constant in all measurements. In order to experimentally verify the similarity of the ventilation noise, it is sufficient to carry out measurements at only individual and geometrically similar microphone positions. If r and $\vartheta$ are the polar coordinates of the microphone for measurement planes having similar positions, then the following total number of parameters can be held constant.

$$r/D, \ \vartheta, \ \varphi, \ \varkappa = \text{const} .$$

## 5. INTRODUCTION OF THE SYSTEM FREQUENCY CHARACTERISTICS

In his paper "Radiation Groups with a Rotation Phase", ERNSTHAUSEN [1] showed that the directional factor and the radiation resistance of the acoustic source under consideration depend on the parameter $\pi D/\lambda$, which gives the ratio of the radiator dimensions to the acoustic wavelength. But the directional characteristics of the sound radiation have been considered not only in the case of the propeller, but also in the case of acoustic measurements of ventilators. BERANEK, REYNOLDS and WILSON [7]investigated their frequency dependence. They carried out acoustic measurements in front of the inlet nozzle, and in plotting their measurement data they selected the ratio of the nozzle circumference to the acoustic wavelength as the parameter.

On the other hand, if resonance phenomena in ventilators are investigated, then one finds that it is best to represent the frequency dependence by means of the ratio of the characteristic length to the acoustic wavelength. STUBER [15] was able to show that a rotor consisting of two parallel and closed circular disks has cavity resonances which can be traced to standing waves between the disks and also to cylindrical waves. The eigenfrequencies can /27

be estimated by means of an analogy to the organ pipe open at one end. The ratio of the cavity dimensions to the acoustic wavelength is a whole number.

Closed systems have a similar frequency dependence, for example, in the case of a spiral housing of a radial ventilator. It includes a relatively large air volume at a small inlet cross section. The Helmholtz resonator is related to this shape, the resonant frequency of which satisfies the following relationship:

$$f = \frac{c}{2\pi} \sqrt{S/l \cdot V} = \frac{c}{2\pi} \cdot 1/D,$$

where V is the included volume, S the inlet surface and l is the length of the throat. The square root expression corresponds to the reciprocal of a characteristic dimension D if geometrically similar resonators are considered. This means that for a given shape the expression

$$\frac{f \cdot D}{c} = D/\lambda \qquad (24)$$

represents a universal parameter for the resonance frequencies. This means that the parameter $D/\lambda$ is an important quantity for the description of the radiation and resonance properties of a system if the wavelength of the generated noise spectrum is of a similar order of magnitude as the system dimensions. According to a suggestion by CREMER, the quantity $D/\lambda$ is called the "Helmholtz number" as a consequence of the other parameter notations

$$He = D/\lambda = f \cdot D/c \qquad (25)$$

It represents a normalized frequency similar to the Strouhal number, but in which the motion of the system is not taken into account. If we consider only one example of geometrically similar systems, then the ratio D/c is a constant. The Helmholtz number then only depends on the frequency. Because of the similarity with the quadrupole theory of communication theory, the dependence of any field quantity on the Helmholtz number is called the "system frequency

characteristic" G (He). In the case of an acoustically complicated system such as the radial ventilator, the system frequency characteristic does not specify whether the frequency dependence of the acoustic pressure is due to the directional characteristic, the near field interferences or resonances. Both effects superimpose and a separation can only be done by carrying out appropriate experiments. /28

The system frequency characteristic can be considered as a partial solution of the system of equations and it must be possible to make up the Helmholtz number from a combination of characteristic numbers from the complete set. If it is multiplied by the constant $\pi/z$ and if the product is multiplied by the circumferential velocity so that

$$\frac{\pi}{z} He = \frac{U}{c} \cdot \frac{\pi}{z} \frac{f \cdot D}{U} , \tag{26}$$

then we obtain

$$He = \frac{z}{\pi} Ma \cdot St . \tag{27}$$

As far as dimensional analysis is concerned, the Helmholtz number thus only represents an abbreviation for a product of two characteristic numbers. However, as we will show, it is the suitable independent variable of the spectrum to be used in the determination of the system frequency characteristic. This means that in a Fourier transformation, the Strouhal number must be multiplied by the Mach number. Since both quantities are related to each other according to Equation (27), it is only possible to select one of the two parameters independently. The following two equivalent formulations of the problem results:

$$K = F(He); \quad St = \text{Parameter}; \quad r/D, \varphi, \varkappa = \text{const} \tag{28}$$

or

$$K = F(He); \quad Ma = \text{Parameter}, \quad r/D, \quad \varphi, \quad \varkappa = \text{const.} \qquad (29)$$

We will show later which of the two parameters should be used for convenience.

## 6. PRODUCT TRIAL SOLUTION FOR THE DESCRIPTION OF THE VENTILATION NOISE

The inclusion of the system frequency characteristic in the development means that the normalized acoustic pressure depends on three quantities which are no longer linearly independent, but are characteristic parameters for various physical processes: /29

1. The Strouhal number characterizes the frequencies caused by the motion of the rotor. The nonsteady component of the flow depends in general on periodic and non-periodic fluctuations.

2. the Helmholtz number specifies, in the form of a system frequency characteristic, at which frequencies the sound radiation is preferred in certain determined directions and at which frequencies the amplitude of the acoustic pressure is influenced by resonance effects.

3. The circumferential Mach number can be looked upon as a measure for the magnitude of sound production. This is independent of what the dimensions of the rotor are with respect to the wavelengths of the produced spectrum. Following the results of flow acoustic theory, which was outlined in Equation (1) - (3), it will be assumed that the acoustic pressure produced by a ventilator depends on the circumferential velocity of the rotor in the form of a power law.

4. In case the normalized acoustic pressures depend on the size of the ventilators, it will be assumed that this influence can be reduced to the

influence of air viscosity in the first approximation. The characteristic parameter is the Reynolds number. Just as in the case of the Mach number, the normalized acoustic pressure can depend on the Reynolds number according to another power of law.

We will now assume that the four laws are independent in the first approximation and that they can be linearly superimposed on a logarithmic scale. A corresponding equation results in the following product trial solution

$$K = k \cdot Ma^{x_1} Re^{x_2} F(St) \cdot G(He). \tag{30}$$

It will be the goal of the measurements to verify this product trial solution, to separate the laws from each other and to make quantitative statements. We must determine whether the functions are generally valid for a series of geometrically similar ventilators, provided the measurements have been carried out under similar experimental conditions, so that r/D, $\vartheta$, $\phi$, $\kappa$ = const.

## 7. EXPERIMENTAL INSTALLATION

/30

### 7.1. Simplifications

In order to verify the product trial solution and the similarity laws, we will exclude all effects which do not have a primary effect on sound production. Therefore, the components of the test band must be made as stiff as possible, so that when excited by body noise and air noise it will only oscillate slightly and will not lead to any noticeable amount of sound radiation. In addition, cavities, which include air volumes capable of carrying out oscillations and therefore capable of resonance, should be avoided. Since we do not intend to vary the flow coefficients, the measurements are carried out without housings and without connected piping.

## 7.2. Perturbing Bodies for the Simulation of the Blade

Since the radial ventilator noise depends on the blade of the housing in a decisive way, it is replaced by a suitable perturbation body in order to take into account the part of the housing important for the acoustics. The distance of the blade to the rotor determines how much the rotational sound differs from the flow noise. The perturbing body consists of a rigid wood wedge, the exterior surfaces of which are perpendicular to each other and make a sharp edge. The edges of the square surfaces are $\sqrt{2}$ times the rotor diameter. Therefore the dimensions are not an integral ratio in order to avoid possible interferences. Figure 1 shows the experimental installation. The measurement plane of the microphone passes through the axis of the rotor and the edge of the perturbing body. The polar coordinates of the microphone position are shown in Figure 2. Figures 3 shows the dimensions of the perturbing body and the details of the slit between the edge and the rotor. In contrast to the experimental installation of CHANAUD [16], who selected a flat, radial and sharpened knife edge, we have added a tangential surface close to the rotor. This makes it possible to simulate the "braking" of the flow in the blade channels when these are momentarily pointed at the surface.

## 7.3. Description of the Rotor

/31

The flow characteristics of the rotors used were investigated at the Hermann-Fottinger-Institut to a considerable degree. The delivery properties are characterized by the ventilator characteristic. It specifies how large the normalized total pressure difference, the pressure ratio $\psi$ and the normalized volume flux and the flow coefficient are for given degrees of throttling. The report by GIESE [25] gives a description and photographs of the test stand. It is possible to vary the degree of throttling and to determine the characteristic. Since the ring diffuser rotating with the unit and used by GIESE was left off, the pressure ratio is decreased. Figure 4 shows the recalculated characteristic. Figure 5 shows the details of the rotor. Six blades with a strong curvature in the backwards direction were

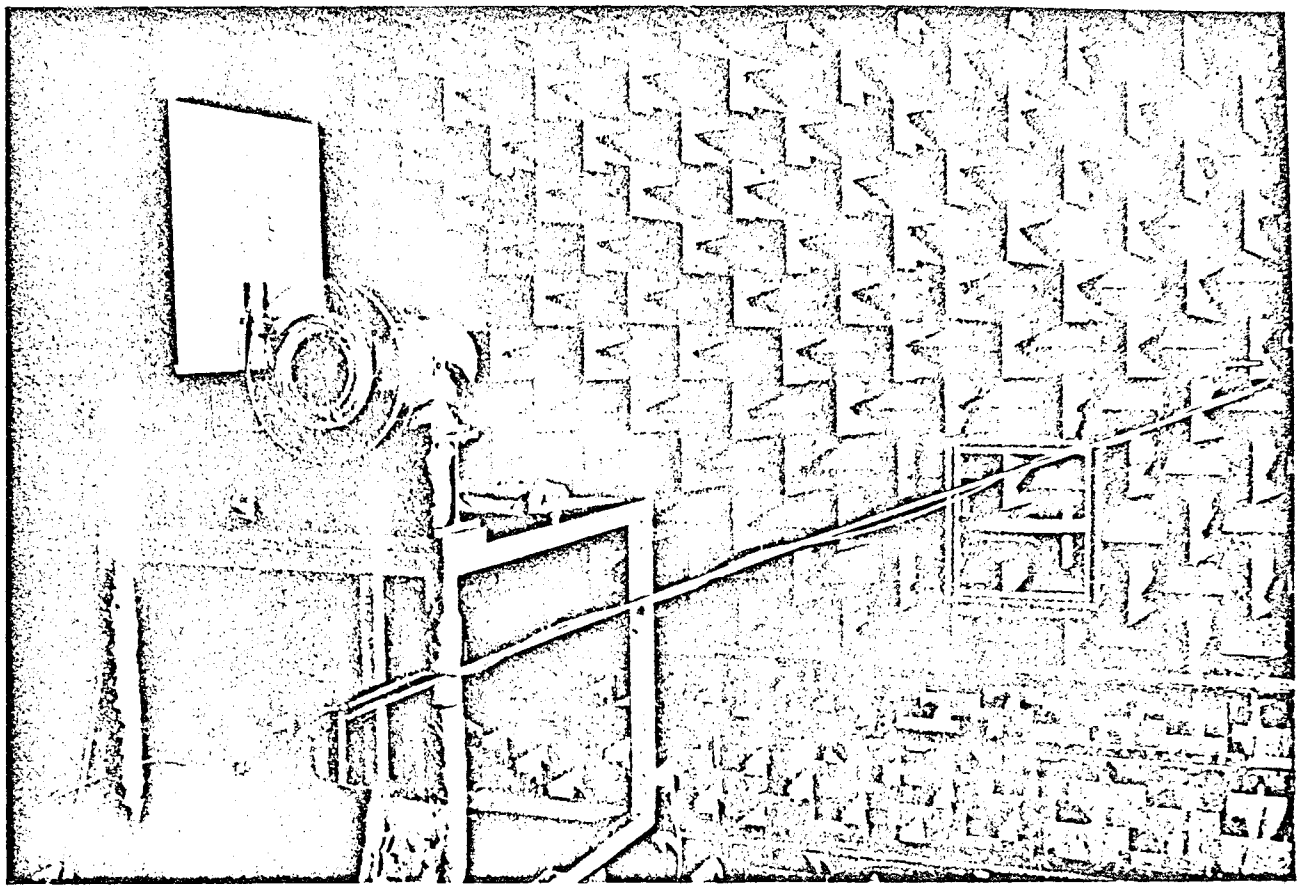

Figure 1. View of the experimental installation

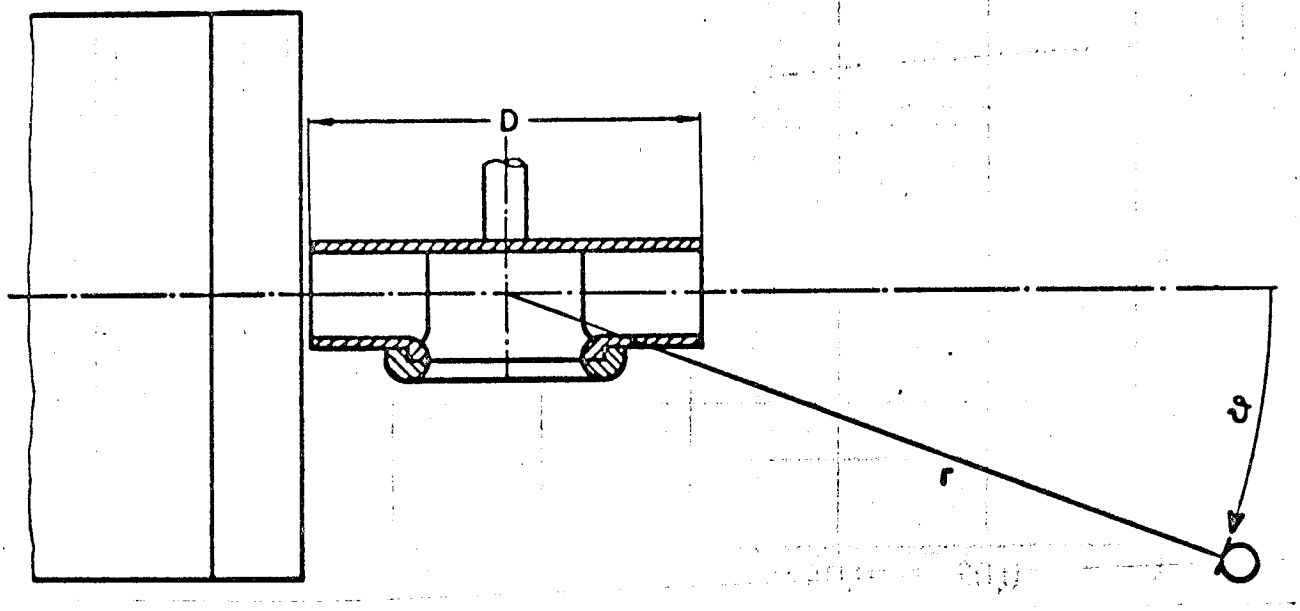


Figure 2. Coordinates of the microphone position.

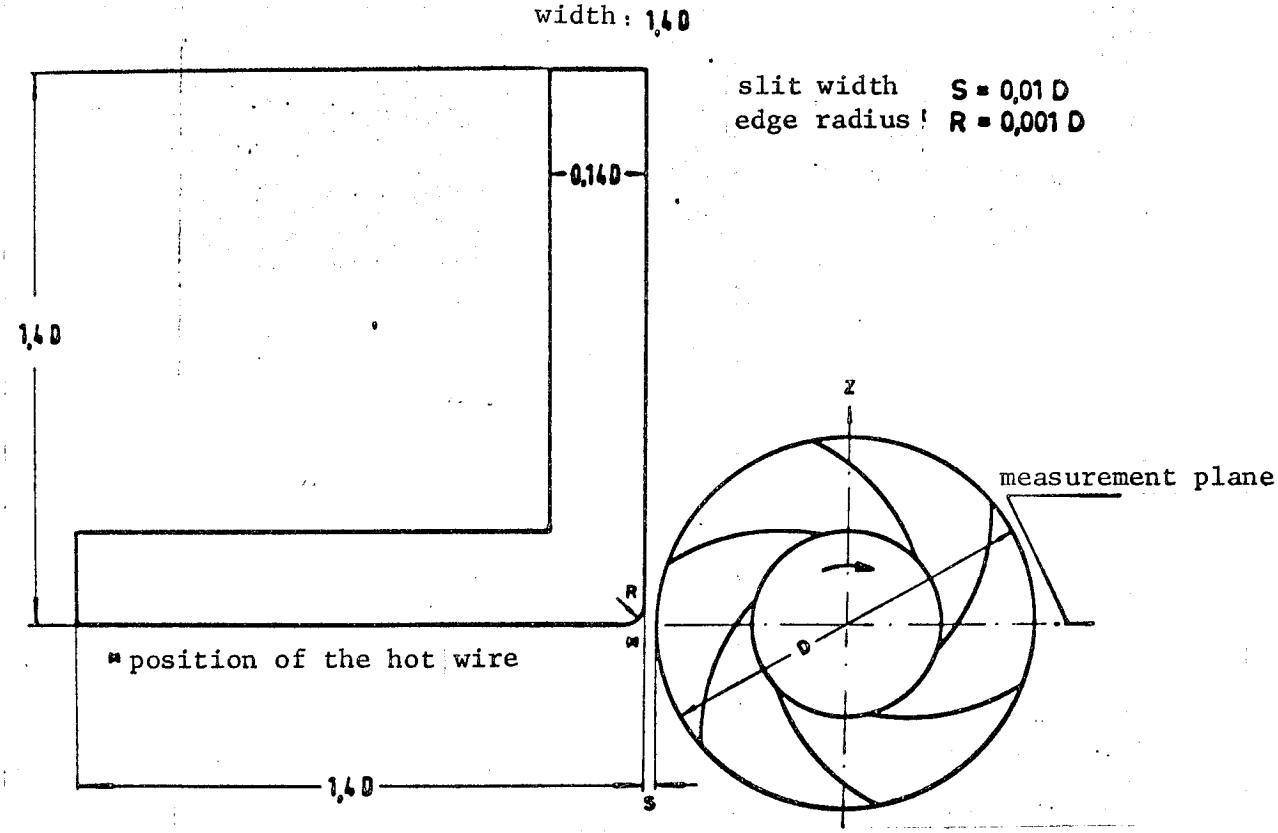


Figure 3. Dimensions of the experimental installation.

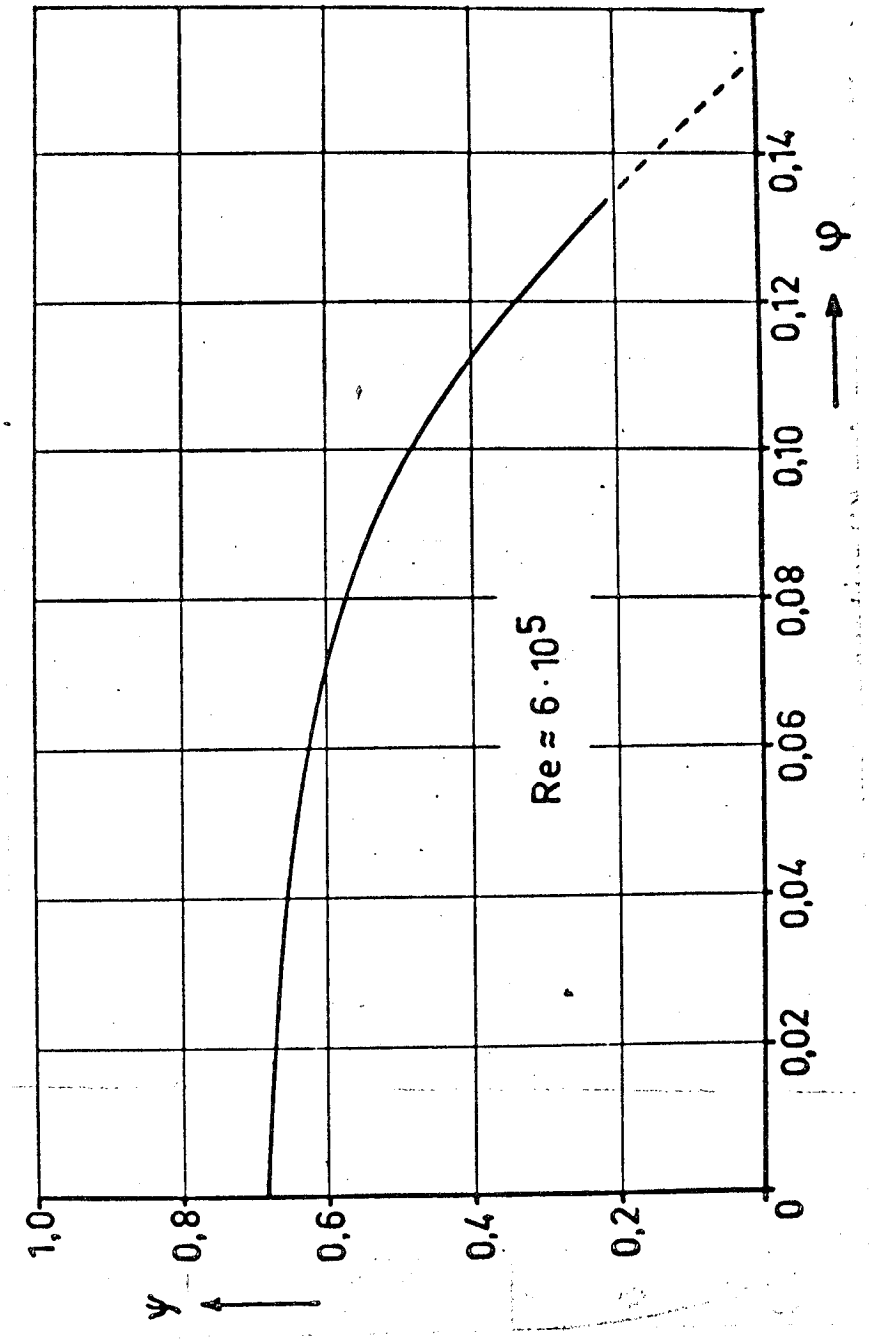


Figure 4. Characteristic of the ventilator.

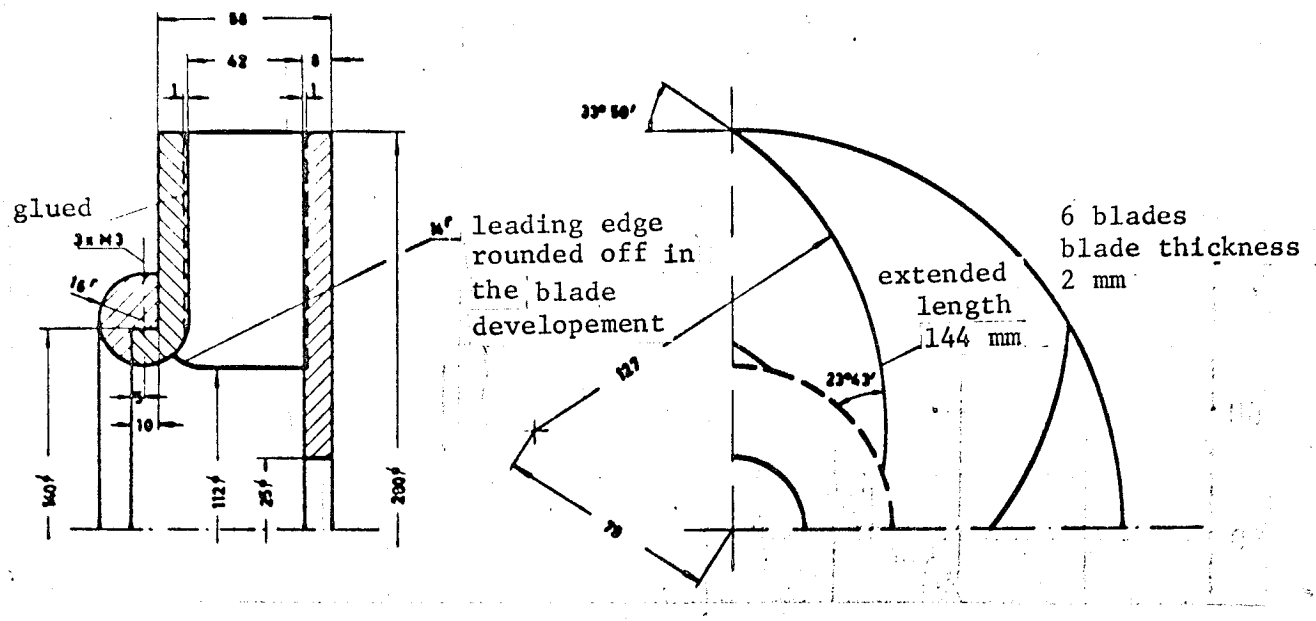


Figure 5. Dimensions of a rotor.

used in order to reduce the tendency to separation. In order to maintain geometric similarity of the five rotors as much as possible, they are provided with circular arch dummy blades. The diameter ratio and width ratio are 0.4 and 0.15, respectively. The details of the blades are shown in Figure 6. The inclination of the blade trailing edge results by rotating the rotors to a prescribed degree. In the manufacture of the rotors, we were especially careful to assure proper balancing. The required weights for dynamic mass balance were determined from oscillation measurements using a digital computer. Balancing was carried out in conjunction with the drive motor.

## 7.4. Experimental Conditions

The simplifications described, which essentially consist of the fact that the rotor is operated in a free function mode and a free exhaust mode, mean that the working point on the characteristic of Figure 4 lies extremely far into the overload region. This means that the flow input is not free of impulses. The throttling is only due to the drag coefficient of the rotor.

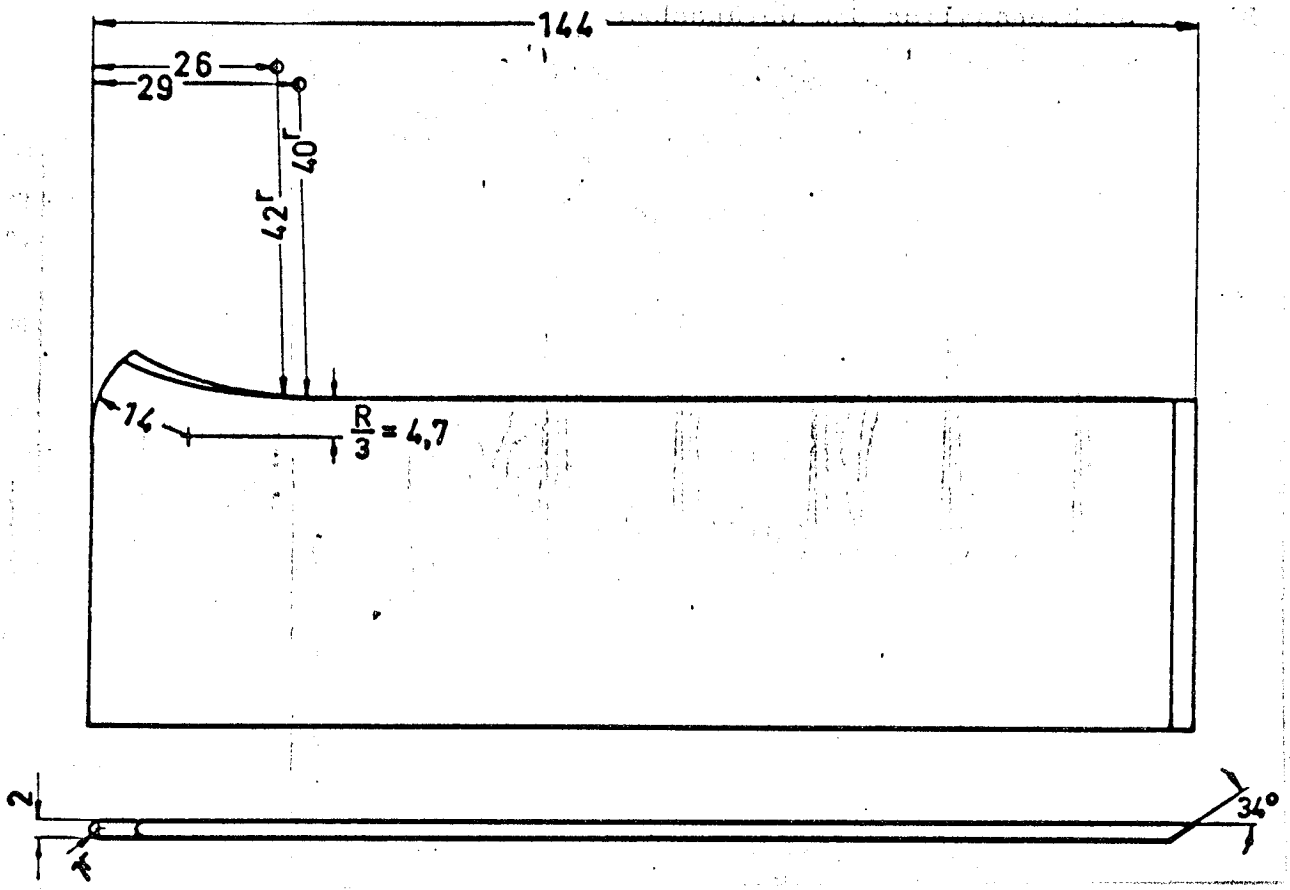


Figure 6. Details of the blade.

Since it is equipped with a co-rotating nozzle, as Figure 5 shows, the flow coefficient should be about

$$\varphi_{max} \approx 0,14$$

Direct current shunt-wound electric motors are used to drive the ventilators. /32
The motor axials carry the corresponding rotor. They are supplied by a Leonardo generator, the direct current of which has a negligible wave component. The generator is excited by means of a direct current-power amplifier. It is designed in such a way that, depending on the amplitude of the control

direct current, which can be ten V, the rotation rate of the rotors can be adjusted almost proportional to an electrical control parameter. The latter can either be given manually or by means of an electronic control unit. The motors are designed in such a way that the five rotors used can be operated up to the same maximum circumferential velocity of $U_{max} = 60$ m/s.

The acoustic measurements are carried out in a chamber with low reflectivity. The lower limiting frequency is about 120 Hz. The maximum distance r between the microphone and the rotor is given by the chamber dimensions and the largest rotor diameter, which is D = 560 mm. We selected r = 7D. The microphone position can be rotated around an axis which passes through the center of the rotor and lies in a plane given by the rotor axis and the edge of the perturbing body. All acoustic measurements were analyzed with a constant filter bandwidth of $\Delta f = 7.1$ Hz. The following gives the experimental conditions in tabular form:

$$\begin{aligned} r/D &= 7 \\ c &= 345 \text{ m/s} \\ P_o &= 1 \text{ bar} \\ \varkappa &= 1{,}4 \\ \varphi &\approx 0{,}14 \\ U_{max} &= 60 \text{ m/s} \\ D &= 56,\ 100,\ 140,\ 280,\ 560 \text{ mm} \end{aligned} \tag{31}$$

## 8. FUNDAMENTAL PROPERTIES OF THE NOISE SPECTRUM

The typical dependence of the acoustic pressure level on frequency is shown in Figure 7. For narrow bandwidth filtering of the noise, the line spectrum of the rotational sound emerges distinctly from the continuous spectrum of the flow noise. The level differences between the spectral conponents depend on the filter bandwidth. They increase with increasing bandwidth. At $\Delta f = 7.1$ Hz there is a good separation of the noise components. /33
On the other hand, the level differences lie within the dynamic range of the

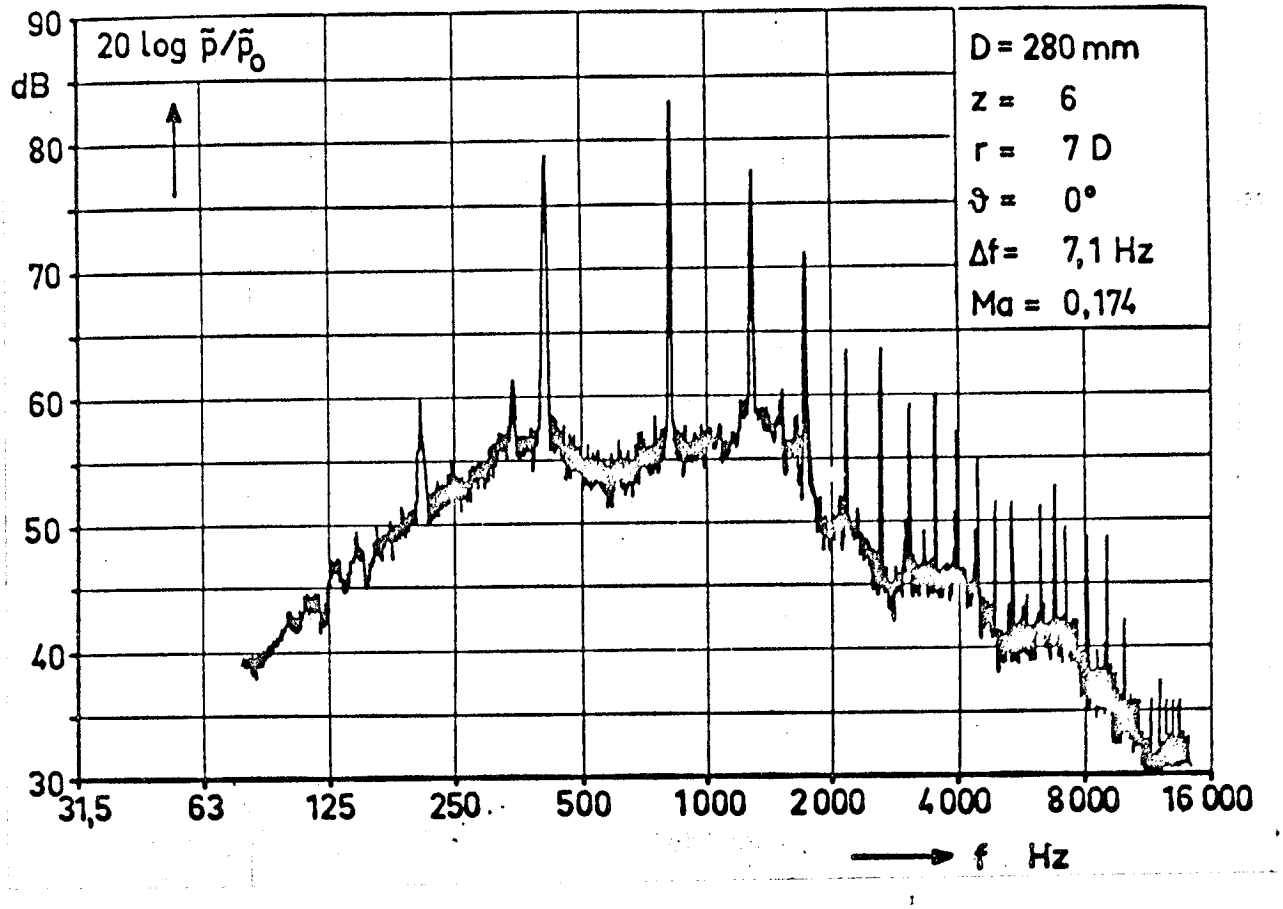


Figure 7. Heterodyne analysis of noise

measurement instruments, which is about 60 dB.

The tones of about 200 and 350 Hz, which lie below the first harmonic of the rotational sound of 410 Hz, can be traced to the oscillation excitations due to the third or fifth harmonic of the rotational frequency. This is because the imbalance of the rotor cannot be completely excluded. In the following considerations, this "rotational frequency spectrum" is not considered.

The continuous spectrum of the flow noise has two maxima and decreases in a continuous way to both sides. In a later section we will give a comparison of the two components of the spectrum and we will show that for a selected

slit width of 1% of the rotor diameter, the power of the noise component can be ignored with respect to the sound component. Measurements of the total level, averaged over all frequencies between 20 Hz to 20 kHz, show that the deviations from the power corresponding to the summation of the first seven harmonics of the rotational sound are on the order of the measurement accuracy. Since the flow noise can dominate in other cases, and therefore is of importance, it will be investigated afterwards with the same methods used for the rotational sound.

## 9. INVESTIGATION OF THE ROTATIONAL SOUND

### 9.1. Measurement Method and Measurement Program

Investigation of the rotational sound is done to give an experimental verification of the product trial solution and to determine the structure of the line spectrum. An attempt is made to isolate the properties of the sound production mechanisms which are then no longer "falsified" by the system frequency characteristic, i.e., which would be additionally colored as far as the spectrum is concerned. In addition, the first seven harmonics must be tested to determine whether the generalized laws found are generally valid for the series of geometrically similar experimental installations.

Figure 8 shows recordings from a heterodyne analysis which was carried out at an average circumferential velocity. It can be seen that the rotational sound is formed in the form of an equidistant line spectrum for a linear frequency scale. The frequencies of the harmonics obey the law: /34

$$f_i = i \cdot z \cdot n \,, \qquad i = 1,2,3,\ldots \tag{32}$$

Here i is the order of the harmonic, z the blade number and n the rotational rate, which means the rotational frequency of the driving shaft. If the circumferential velocity is replaced in Equation (20) using the relationship

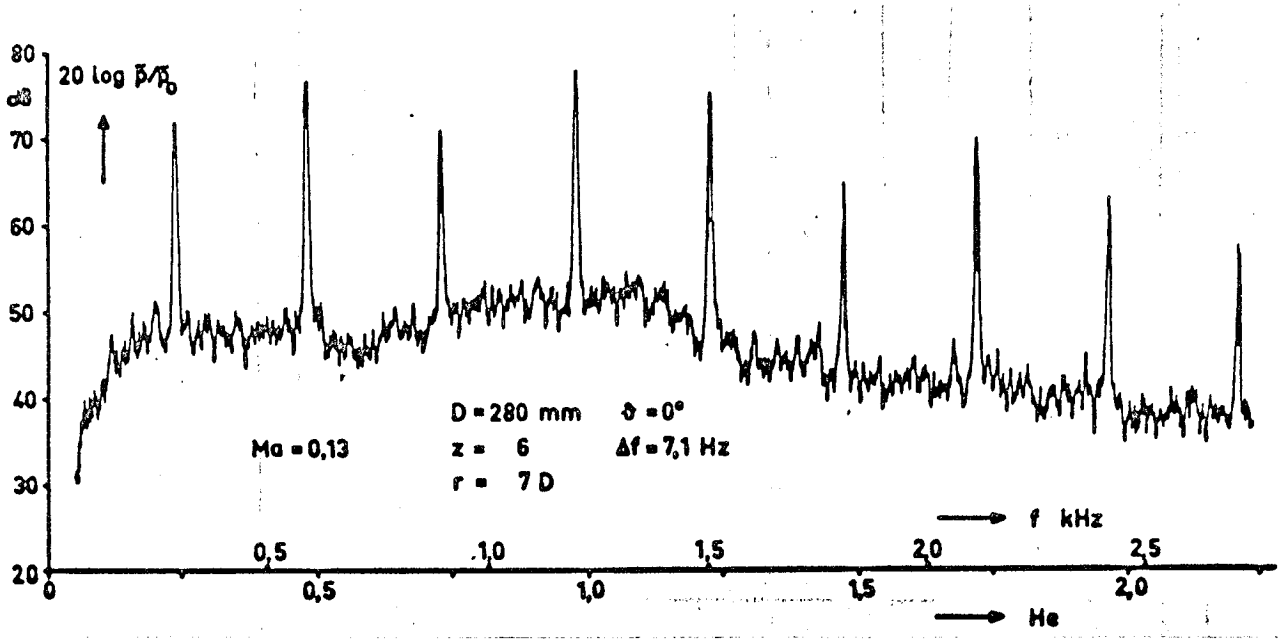


Figure 8. Representation of the rotational sound.

$$U = \pi D \cdot n \tag{33}$$

by the rotational rate, then we obtain

$$St = \frac{1}{z} \cdot \frac{f}{n} \, . \tag{34}$$

If we consider the formation law for the rotational sound frequencies, Equation (32), it follows that the Strouhal number coincides with the order number for $f = f_i$ and decreases only for the discrete values

$$St = 1,2,3, \ldots \quad ; \quad f = f_i \tag{35}$$

Therefore, it is possible to represent the rotational sound using the family of curves defined by Equation (28) up to, for example, the seventh harmonic. This can be done without a gap and in a continuous fashion for all frequencies and rotational rates.

Therefore, the following relationship must be measured in the investigation of the rotational sound:

$$K_d = F(He);\ St = 1,2,3, \ldots 7;\ Re = \text{Parameter};\ r/D,\ \vartheta,\ \varphi,\ \varkappa = \text{const} \tag{28}$$

or, in a detailed description

$$K_d = F\left(\frac{D}{c} \cdot f\right);\ \frac{1}{z} \cdot \frac{f}{n} = 1,2,3, \ldots 7;\ \frac{U}{V} D = \text{Parameter};\ r/D,\ \vartheta,\ \varphi,\ \varkappa = \text{const}. \tag{36}$$

In order to provide for accuracy and completeness of the measurement data, an attempt is made to record the relationship given by Equation (36) directly by the measurement instrument, so that it is not necessary to reprocess the data afterwards. In order to do this a special follower control device is used. If there is a variation of the frequency f at the heterodyne analyzer, it makes the rotational rate n of the wheel follow the frequency in a proportional way, so that the ratio f/n remains constant. If this ratio is selected as follows, taking into account the fact that the blade number is z = 6

$$f/n = 6,\ 12,\ 18,\ \ldots,$$

then the amplitude course of the individual harmonics is recorded immediately as a function of the frequency when the circumferential velocity is varied. The variation is carried out in such a way that the highest frequencies which are reached by the individual harmonics correspond to the maximum circumferential velocity of U = 60 m/s. In this way, in measurements of the rotational sound, the Mach number range up to

/35

$$Ma_{max} = 0,174$$

is traversed in a continuous fashion.

There is a fixed relationship between the normalized reference acoustic pressure $\tilde{p}_0$ and the ambient pressure $P_0$ which is just at the reference point.

In order to obtain the normalized acoustic pressure of the rotational sound

$$K_d = \tilde{p}/P_o$$

from the acoustic pressure recorded on a logarithmic scale, a constant value must be added to the measured levels, which results from the ratio $\tilde{p}_0/P_0$.

In addition, the scale of the frequency axis in recording of the rotational sound is given by the factor D/c, see Equation (36). In this way the rotational sound of the rotors under consideration is plotted as a function of the Helmholtz number so that similarity of the spectra can be immediately evaluated. If this similarity is satisfied, then the family of curves must be similar except for measurement errors.

Figure 9 shows measurements of the rotational sound carried out according to the principle described for a rotor with D = 280 mm. In order to make the comparison with the usual plotting methods in which the rotational number is held constant as in Figure 8, both representations were given in Figure 10. It can be seen that the "continuous" recording contains an arbitrary number of narrow band analysis in the usual representation. By presenting the data in this way, the flow noise is separated at the same time. /36

## 9.2. Determination of the Exponents for the Reynolds Number and Mach Number

Since the Reynolds number and the Mach number are formed with the circumferential velocity, the measurements must be carried out in such a way that for a variation of the diameter, the same regions of the circumferential velocity are considered. The rotational rate ranges must therefore be adjusted corresponding to the five rotor diameters. In order to determine the exponent of the Reynolds number, the total acoustic pressure levels are measured. It is important to be sure thet important parts of the spectra do not exceed the limiting frequencies of the measurement apparatus either at low frequencies, in the case of the largest rotor at low rotational rates,

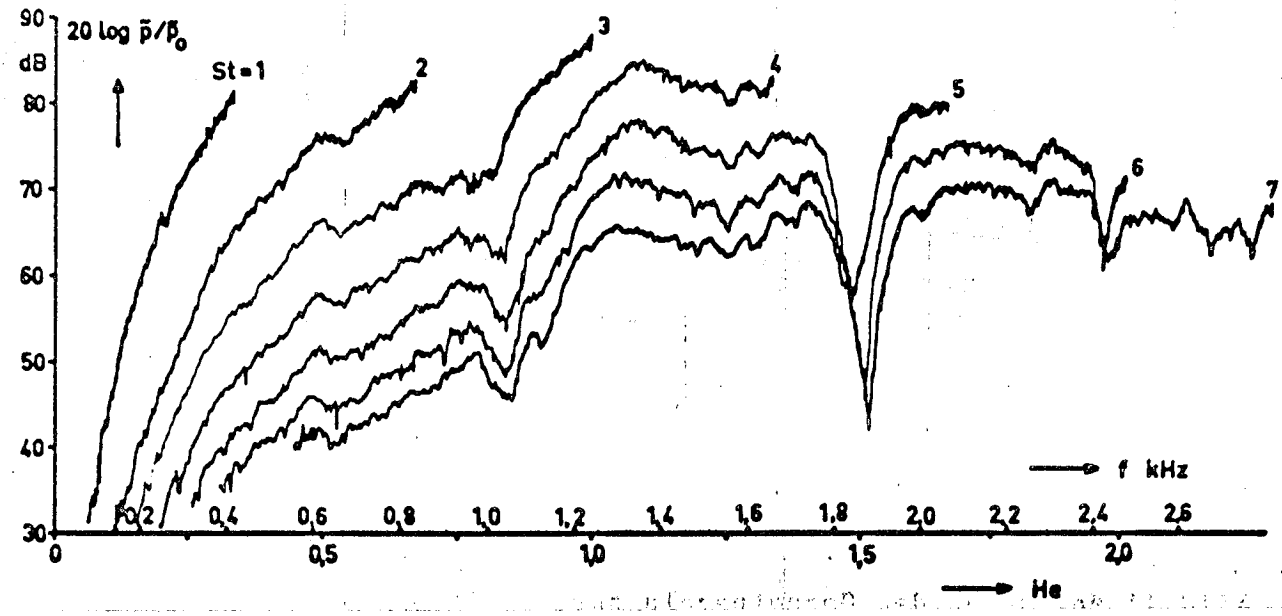


Figure 9. Measurement of the rotational sound.

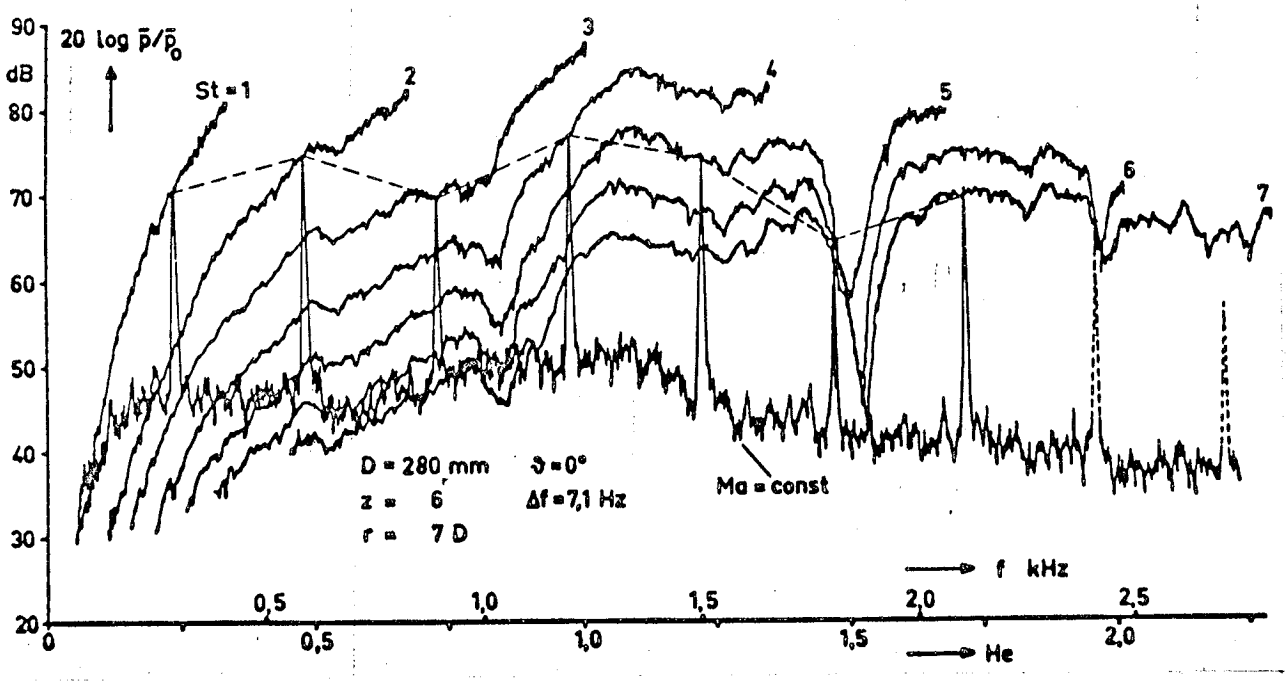


Figure 10. Comparison of various representations of the rotational sound.

or at high frequencies, in the case of the smallest rotor at the maximum rotational rate. Since the ratio of the smallest to the larges rotor is 1:10, the circumferential velocity can only be varied in the range 1:2. Thus, the following is obtained for the product trial solution Equation (30):

$$K_d \sim \left(\frac{U}{c}\right)^{x_1} \cdot \left(\frac{U \cdot D}{\nu}\right)^{x_2} \tag{37}$$

or

$$\tilde{p} \sim U^{x_1 + x_2} \cdot D^{x_2} . \tag{38}$$

The total measured acoustic pressure levels are shown in Figure 11 as a function of D on a double logarithmic scale. It is seen that the measurement points deviate only slightly from the parallel lines U = const shown in the figure. The value $x_2 = 0.2$ can be derived from the slope of the lines. Therefore, we have

$$\tilde{p} \sim D^{0,2} . \tag{39}$$

The level differences between the lines are shown in Figure 12 as a function of the circumferential velocity. From the slope of the lines drawn through the points it follows that /37

$$\tilde{p} \sim U^{2,8} , \tag{40}$$

so that a comparison with Equation (38) results in :

$$x_1 + x_2 = 2,8 . \tag{41}$$

For $x_2 = 0.2$ it follows that $x_1 = 2.6$. Equation (37) and the above values result in the following for the rotational sound, because its total level determines the total noise in a decisive way:

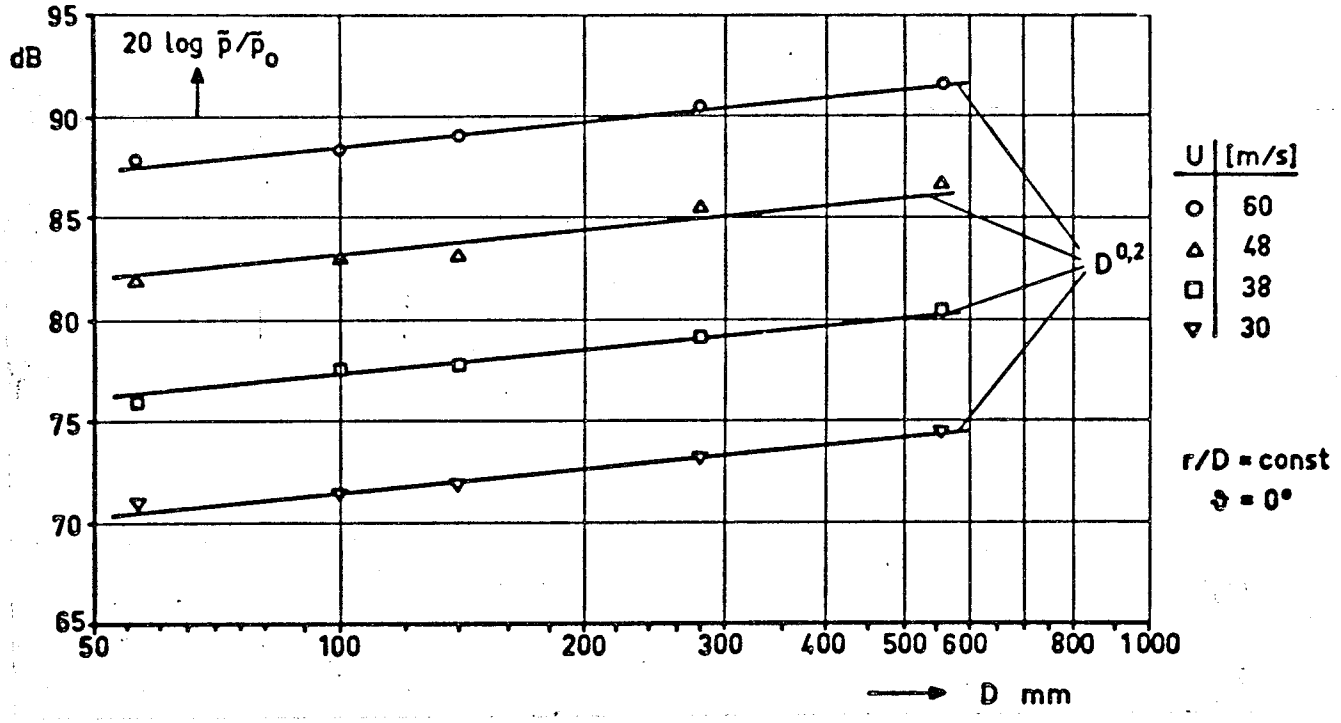


Figure 11. Measurements of the total level for the determination of one exponent of the Reynolds number.

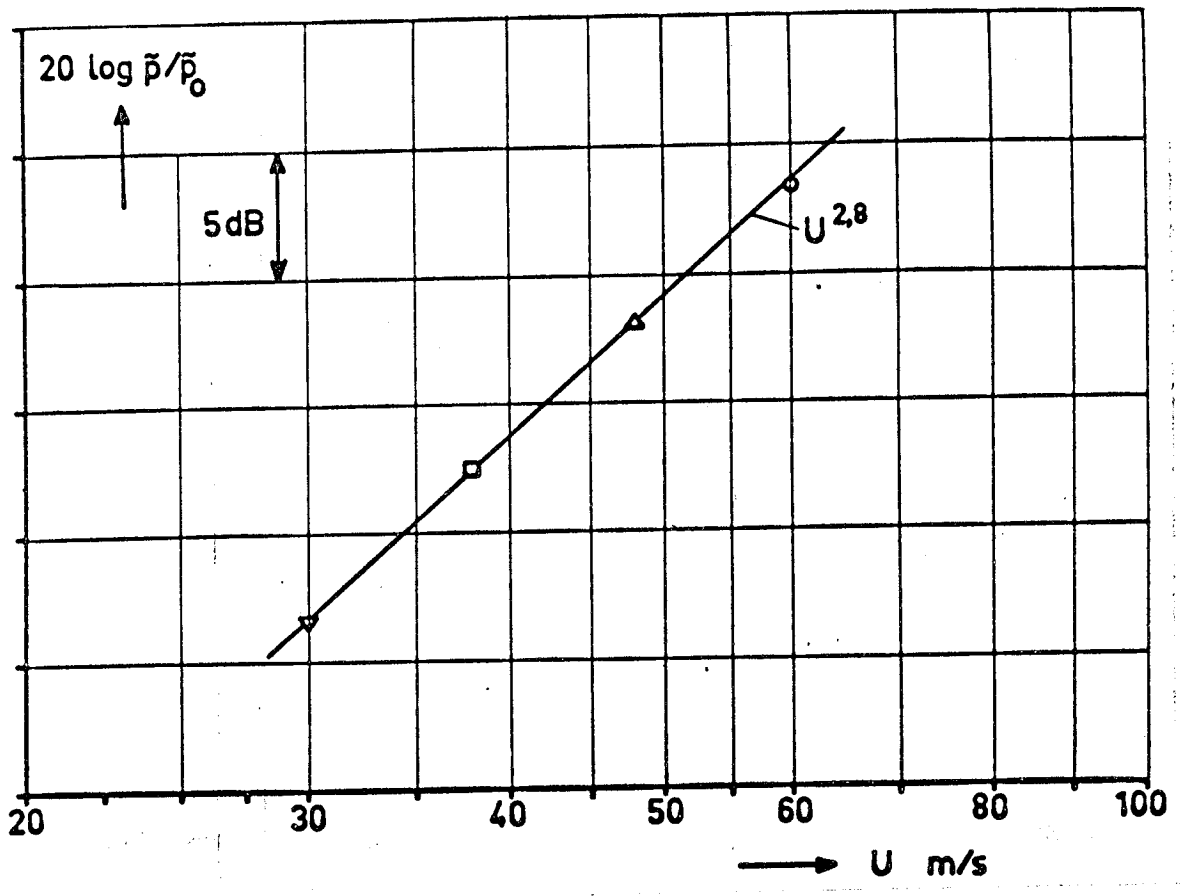


Figure 12. Determination of the exponent of Mach number from Figure 11.

$$K_d \sim Ma^{2,6} \cdot Re^{0,2} \cdot \tag{42}$$

From the fact that the measurement values in Figure 11 and 12 have only small deviations from the power laws, it follows that the system frequency characteristics will hardly influence the total level when integration of the entire spectrum is carried out.

## 9.3. Determination of the System Frequency Characteristics

As Figure 9 shows, the curves ST = const have the same qualitative course plotted as a function of the Helmholtz number. They only differ by

level differences which are almost constant. After subtracting these level differences, these curves deviate by not more than $\pm$ 3 dB from an imaginary average curve $F_2$ (He), as is shown in Figure 13. If the level differences are plotted versus the Strouhal number according to another function $F_1$(St), then this function specifies the factor by which $F_2$(He) must be multiplied in order to obtain the quantitative course of the harmonic of the rotational sound under consideration. This means that the acoustic pressure depends on the product of two functions:

$$K_d \sim F_1(St) \cdot F_2(He) \quad . \tag{43}$$

The function $F_2$(He) is approximated by the power function

$$He^{2,6} \sim Ma^{2,6} \cdot St^{2,6} \tag{44}$$

drawn on the curve. In order to take into account the $Ma^{2.6}$ law of the product trial solution given by Equation (42), we use the system characteristic to define the course of the deviations which occur between the functions $F_2$(He) and $He^{2.6}$: /38

$$G_d(He) = \frac{F_2(He)}{Ma^{2,6} \cdot St^{2,6}} \quad . \tag{45}$$

The subscript "d" refers to applicability to the rotational sound for which the system frequency characteristic was determined. The average deviations between the measured curve and the power function were determined from Figure 13 and were plotted versus the Helmholtz number. The system frequency characteristic obtained in this way is shown in Figure 14.

## 9.4. Determination of the Excitation Spectrum

The level differences at He = const, which exist between the curves St = const in Figure 9 and their functional dependence on the Helmholtz number, which was ignored, can be represented by the function

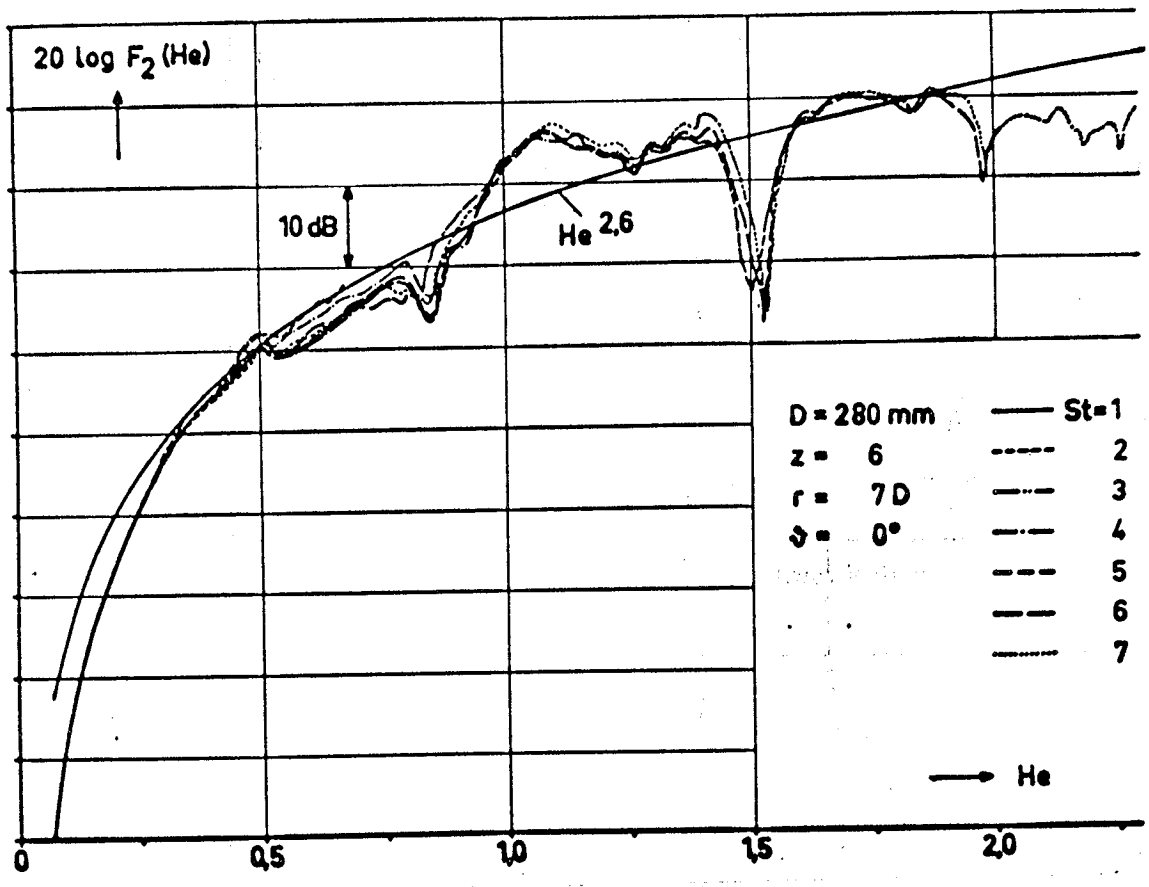


Figure 13. Comparison of curves St = const from Figure 9.

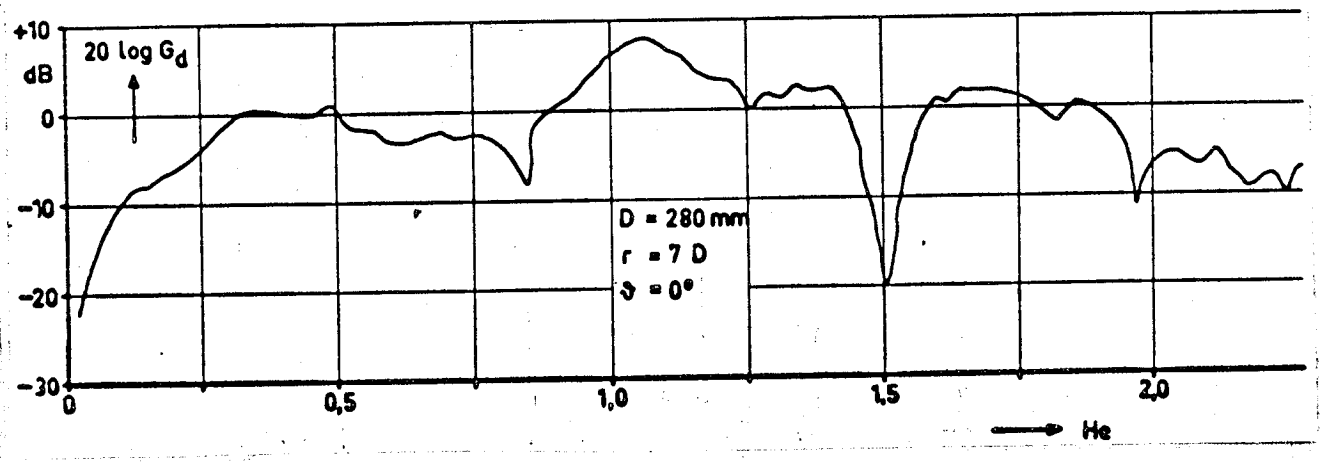


Figure 14. System frequency characteristics.

$$K_d \sim F_1(St = 1,2,3, \ldots)$$

Figure 15 shows the average values of the level differences plotted as a function of the Strouhal number. The amplitude of the first harmonic is used as the reference level. For a clearer representation, the discrete function values were connected by lines. This function is again put into a power function and a so-called "excitation spectrum" $F_d(St)$ which represents the deviations from the power function. A good approximation results when the power function is formed with the negative Mach number exponents. The excitation spectrum is defined in the following way, in analogy to the definition of a system frequency characteristic:

$$F_d(St) = \frac{F_1(St)}{St^{-2,6}} \; . \tag{46}$$

The discrete values of this function are shown in Figure 16. The normalization was carried out in such a way that

$$F_d(St = 1) = 1$$

9.5. Verification of the Product Trial Solution /39

The evaluation of the rotational sound which leads to Equation (43) shows that the acoustic pressure depends on the product of the two independent functions $F_1(St)$ and $F_2(He)$. If Equations (45) and (46) are substituted in (43), then we obtain

$$K_d \sim St^{-2,6} \cdot F_d(St) \cdot Ma^{2,6}\, St^{2,6} \cdot G_d(He) \; .$$

Since the power functions of the Strouhal number can be cancelled, we obtain the following results considering the relationship [Equation (42)] already found:

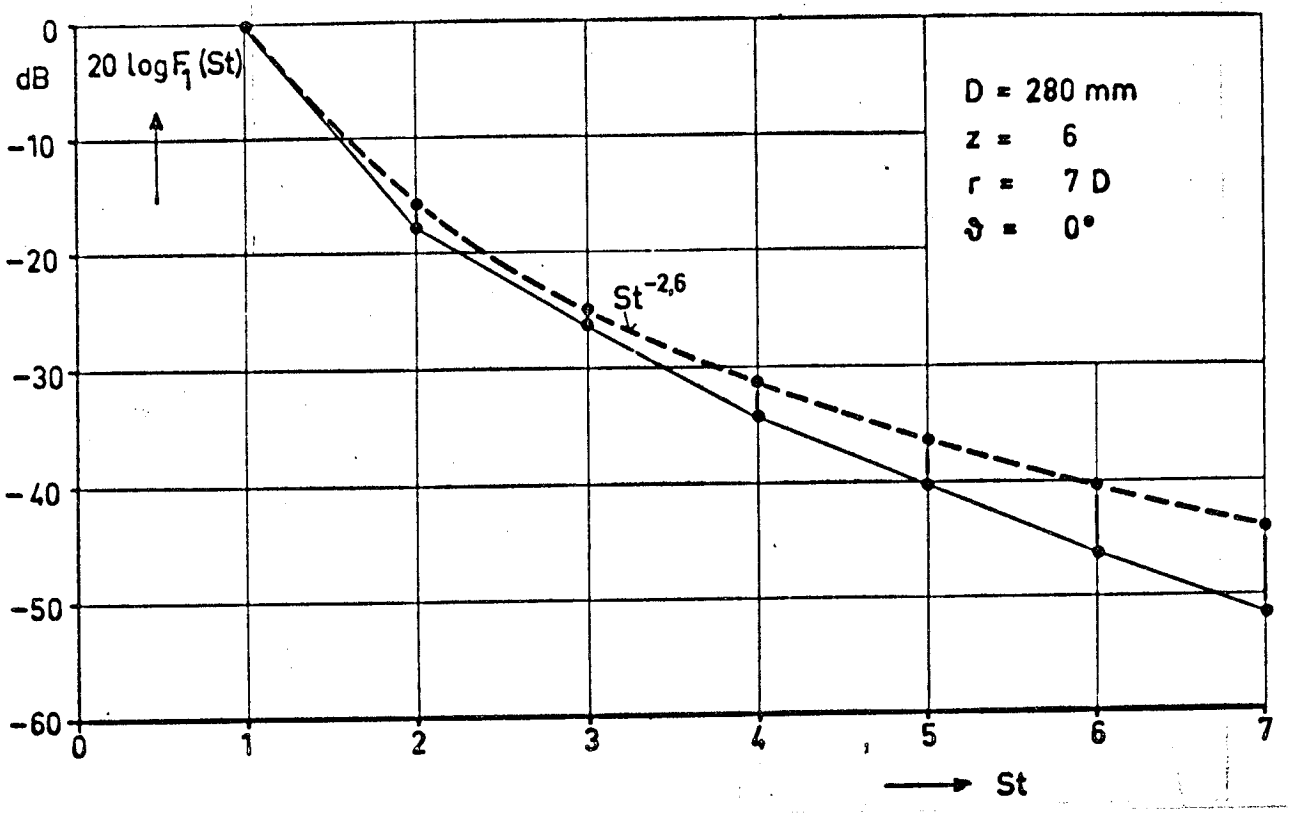


Figure 15. Average level differences between the curves St = const from Figure 9.

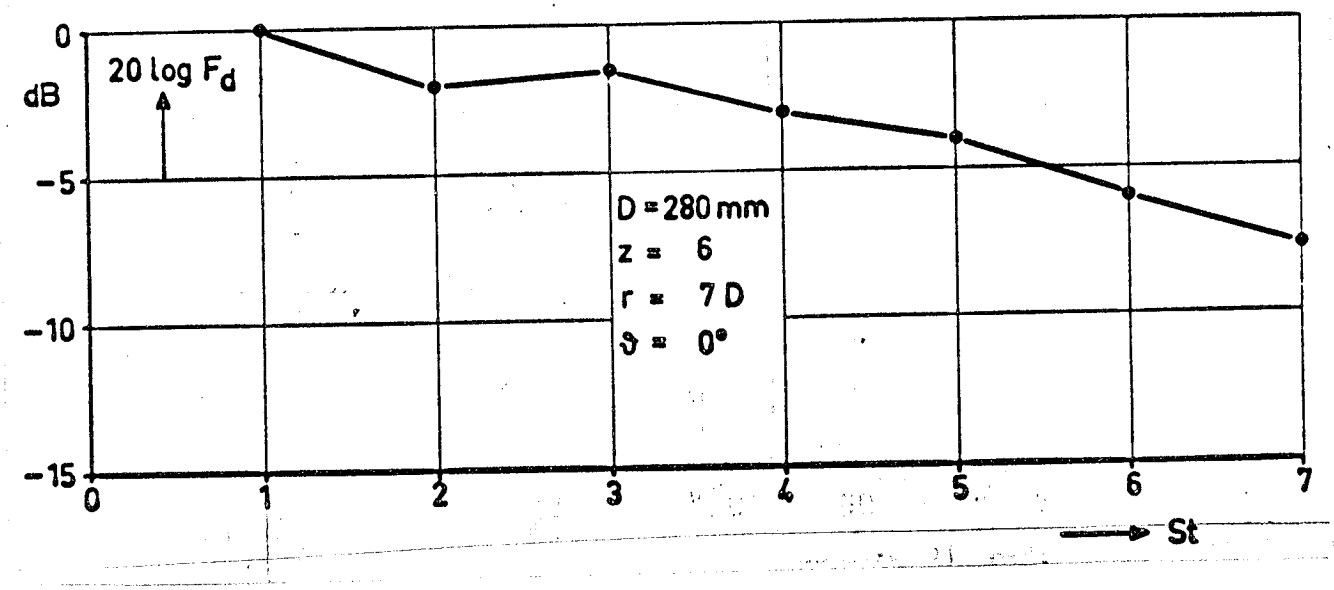


Figure 16. Excitation spectrum

$$K_d = k_d \cdot Ma^{2,6} Re^{0,2} \cdot F_d(St) \cdot G_d(He) \; . \qquad (47)$$

This means that the product trial solution has been experimentally verified by evaluation of rotational sound measurements. The range of applicability is given by Equation (31).

In order to give the numerical value of the acoustic pressure, it is necessary to determine the constant $k_d$:

$$k_d = \frac{\tilde{p}}{P_o} \cdot Ma^{-2,6} \; Re^{-0,2} \cdot F_d^{-1}(St) \cdot G_d^{-1}(He) \; . \qquad (48)$$

A pair of values $\tilde{p}_k/\tilde{p}_0 = F(He_k)$ is taken from Figure 9, which shows the measurement data of the rotational sound. This is substituted into Equation (48). In order to obtain a good average value when the constants are determined, the acoustic pressure $\tilde{p}_k$ is taken at a Helmholtz number at which the curves in Figure 13 have as little scatter as possible, for example at He = 1. The following values were taken from Figure 9:

$$20 \log(\tilde{p}_k/\tilde{p}_0) = 86 \text{ dB corresponding to } \tilde{p}_k = 4 \text{ µbar}$$

at He = 1 and St = 3;

Equations (31) and D = 280 mm lead to the following for the Mach number and Reynolds number:

$$Ma = \frac{\pi}{z} \cdot \frac{He}{St} = 0,174$$

$$\text{or } Re = \frac{c \cdot D}{\nu} Ma = 1,12 \cdot 10^6 .$$

From the excitation spectrum, Figure 16, and the system characteristic, Figure 14, the following values can be derived:

$$F_d(St = 3) = 0,84$$

$$\text{or } G_d(He = 1) = 2$$

After substituting these characteristic numbers in Equation (48) we obtain

$$k_d = 0,14 \cdot 10^{-4}. \qquad (49)$$

In order to calculate the acoustic pressure with these constants, Equation (47) is transformed as follows:

$$\tilde{p} = 0,14 \cdot 10^{-4} \cdot P_o \cdot Ma^{2,6} Re^{0,2} \cdot F_d(St) \cdot G_d(He). \qquad (50)$$

For

$$k_d \cdot \frac{P_o}{\tilde{p}_o} = 7 \cdot 10^4$$

and Equation (31), the following is obtained for the acoustic pressure level:

$$20 \log(\tilde{p}/\tilde{p}_o) = 20 \log(Ma^{2,6} Re^{0,2}) + 20 \log F_d(St) + 20 \log G_d(He) + 97 \text{ dB}. \qquad (51)$$

The errors, which can be expected in the calculation of the acoustic pressure level from Equation (51), correspond to the scatter of the curves in Figure 13. Thus, for example, at a frequency of 400 Hz the following acoustic pressure level is obtained for the first harmonic which is equal to

$$20 \log (\tilde{p}/\tilde{p}_o) = 81 \text{ dB}.$$

The calculated value is only too large by 1 dB as compared with the measured level taken from Figure 9.

## 9.6. Rapid measurements for the Direct Determination of the Excitation Spectrum

It is possible to measure the magnitude of the flow velocity and the temporal course of the velocity fluctuations using hot wire measurement

methods [23]. This method is primarily used in turbulence investigations. It is natural to investigate the flow between the rotor and the perturbing edge using a hot wire anemometer. It is especially important to carry out /41
a heterodyne analysis of the velocity fluctuations within the framework of this paper. The same measurement apparatus can be used as for recording the spectra of the acoustic pressure. At this point it should be mentioned that, because of the characteristics of the hot wire measurement technique, measurements of the speed of sound are only possible when the hot wire is in a uniform additional field, so that the "rectification" effect is avoided by formation of the absolute magnitude in the hot wire probe. This condition is satisfied for the selected position of the hot wire shown in Figure 3. The hot wire, whose length and diameter was about 2 mm and 5 μm, respectively, was situated in the immediate vicinity of the perturbing edge. A DVL hot wire anemometer was used a a measuring instrument. Essentially it contains a control loop for maintaining the hot wire temperature constant as well as a linearization stage. The latter establishes proportionality between the voltage indicated by the control loop and the incidence flow velocity. Since the transmission function of the linearization stage is approximated by a polygon, it is possible for additional lines to appear in the spectrum in the frequency analysis of periodic processes which do not correspond to the flow processes. Therefore a separate linearization stage was used which, among other things, contains two constant squaring stages and can be programmed for the King Formula (28) which describes the heat transfer through the hot wire. In the present case the linearization deviations obtained were about $\pm$ 0.3 dB of the final value.

Figure 17 shows a recording of the level frequency spectrum of the velocity at the perturbing edge taken for an average circumferential velocity. It can be seen that the amplitudes of the line spectra and the power spectrum of the noise component decrease monotonically as the frequency increases. This of course is typical for flow processes and is distinctly different from the spectrum corresponding to the far field of the acoustic pressure.

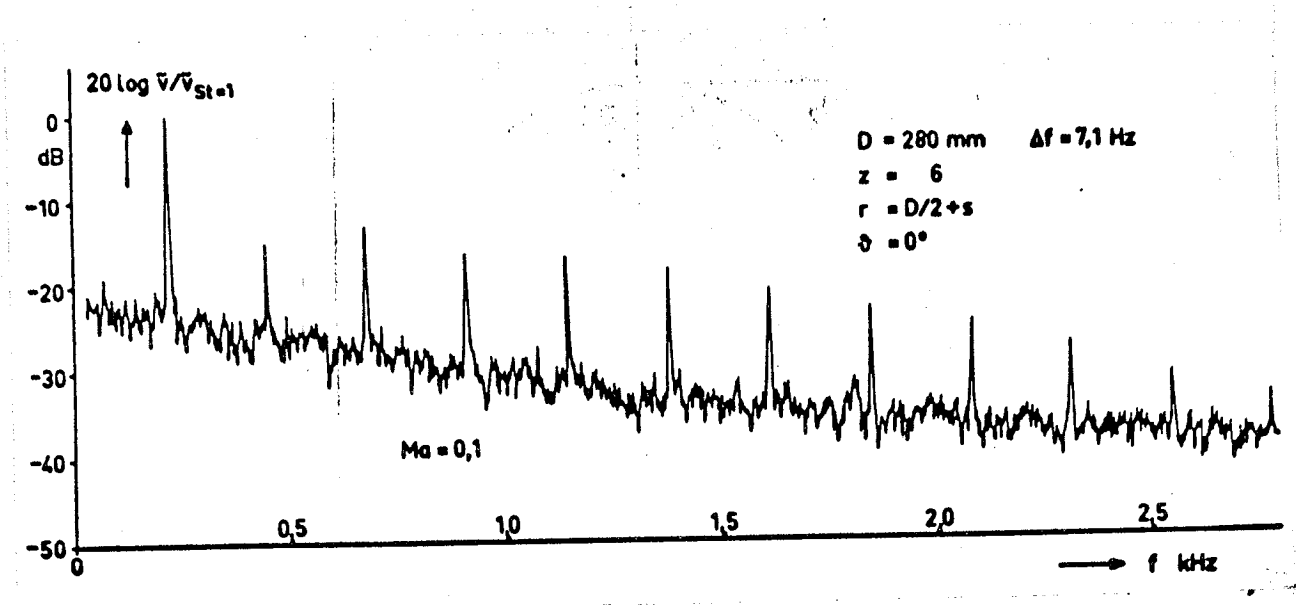


Figure 17. Heterodyne analysis of the velocity fluctuations at the slit.

On the other hand, if the harmonics of the excitation spectrum and the spectrum of the velocity fluctuations are compared, then there is good agreement of the spectra except for the first harmonic, as Figure 18 shows. The reference velocity selected was the amplitude of the first harmonic. Since we only wish to show agreement between the drop in the spectra, the constant level difference between them can be ignored. We would especially like to note that the $U^{2.8}$ law found in Equation (40) leads to the exponential functions $He^{2.6}$ and $St^{-2.6}$ only after splitting it into a Mach number term and a Reynolds number term according to Equation (42). This was used to determine the course of the excitation spectrum. Thus, agreement of the decrease in the spectra shown in Figure 18 can be interpreted as a confirmation of the validity of the product trial solution. /42

The temporal course corresponding to the excitation spectrum was investigated for the same rotor by GIESE [24], but at the design point $\phi = \phi_{opt}$. The change of the velocity triangle at a fixed point of the outlet is shown in Figure 19. A measurement instrument will record a steep increase in the velocity at this point if a blade moves by at this point. It is connected with a corresponding change in direction of the incident flow. Since the

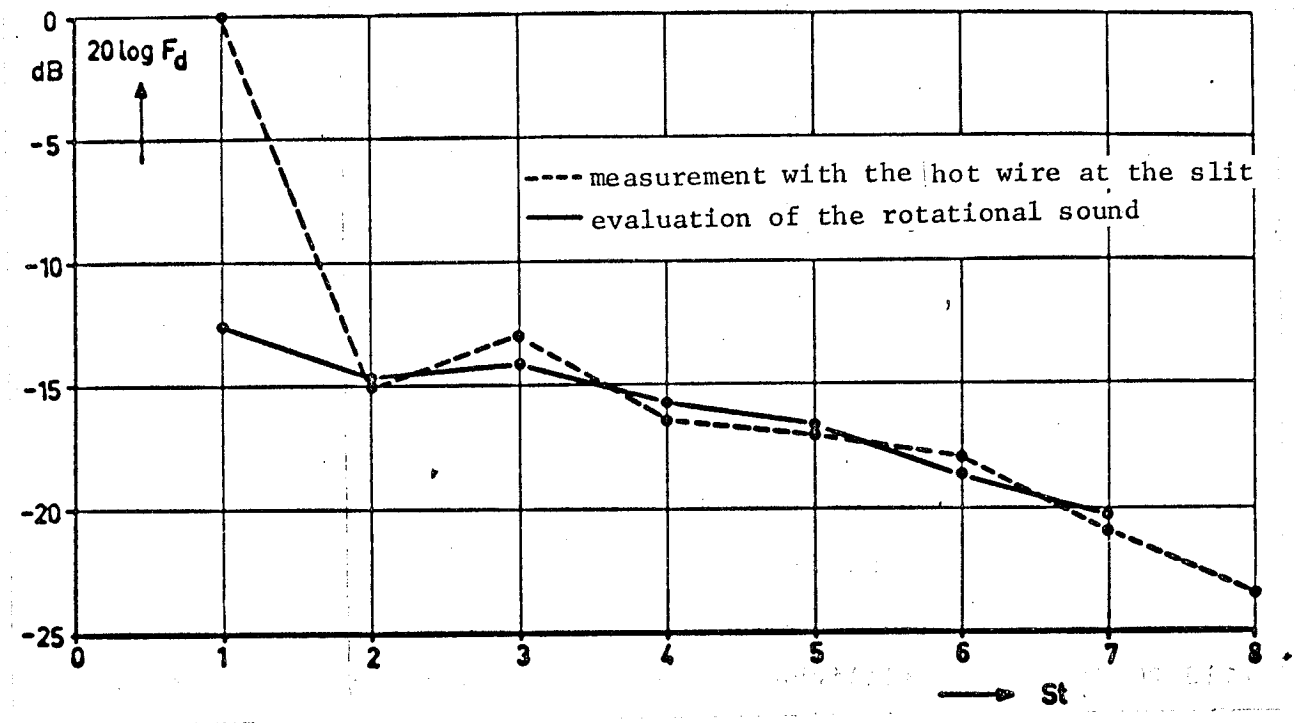


Figure 18. Comparison of the excitation spectra.

relative velocity $w_2$ behind the blade vanishes, the absolute velocity $v_2$ takes on its maximum value, which is about equal to the circumferential velocity. Figure 20 shows the average course of the absolute velocity $v_2$ averaged over several rotations. It was measured for a comparable probe distance. The curve is similar to an impulse sequence with period T, which can be roughly approximated by e functions having the time constant $\tau$. The corresponding amplitude spectrum has the same levels up to the harmonics

$$i \leq \frac{1}{2\pi} \cdot \frac{T}{\tau}$$

as can easily be shown. It decreases only above this value. The ratio for similarity of the flow process is $T/\tau$ = const.

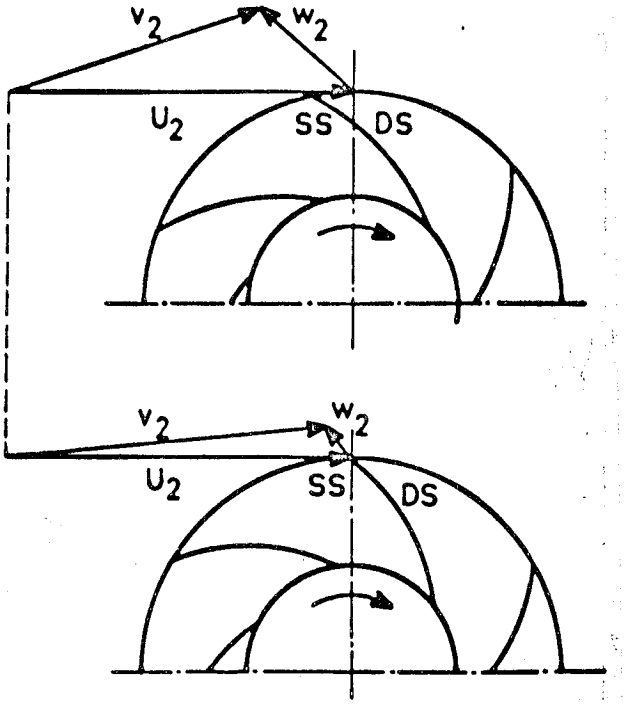


Figure 19. Velocity triangles at the exhaust.

top: next to the blades
bottom: behind the blade

## 9.7 Similarity of the Excitation Spectra and System Frequency Characteristics

It was shown that the total noise and therefore the rotational sound of the model design 1 can be recalculated for the full scale design 2 using the relationship

$$\tilde{p}/P_o = Ma^{2,6} \cdot Re^{0,2}$$

if the following regions are maintained:

$$0,5 \leq Ma_1/Ma_2 \leq 2,$$

$$0,1 \leq Re_1/Re_2 \leq 10.$$

In order to verify spectral similarity /43
of the noise, the system frequency characteristics and excitation spectra

DS: pressure side
SS: substance side
T: division

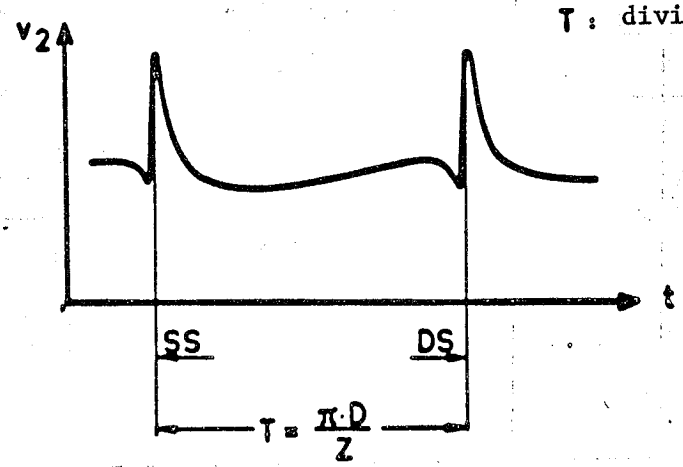


Figure 20. Average temporal course of the absolute velocity (according to GIESE [24]).

of the considered rotors must be determined and compared.

Since the drive of the smallest rotor did not make it possible to operate it over extended periods at the required rotation rate of 20,000 rpm because the accuracy of the follower control device was not sufficient to hold the harmonic frequencies within the pass span of the heterodyne analyzer, it was not possible to verify similarity of the excitation spectra and system frequency characteristics for the rotor with D = 56 mm. The frequencies of the harmonics are about up to three orders of magnitude above the filter bandwidth. However, these functions are compared in Figures 21 and 22, respectively, for the four larger rotors.

It was found that the agreement of the excitation spectra is considerably better than in the case of the system frequency characteristic, which shows large deviations at He $\approx$ 0.75. It follows from this that the periodic mechanism of sound production, which is evident in the excitation spectrum, must be traced to geometrically similar flow processes. The deviations of the system frequency characteristic, which are especially large in the shaded region, can therefore only be traced to a dissimilar sound radiation. Due to the small manufacturing tolerances for the wheels of less than 1%, it is improbable that dissimilar resonance effects cause these deviations. The explanation must therefore be found in differences in the directional characteristic.

As further measurements show, the latter is so complicated that it is hardly possible to derive laws from it. Therefore, it is possible that the acoustic field can be considerably disturbed by deviations, which might first appear insignificant, if all other details of the test stands (for example, floor stands, motor housings, frame construction) are geometrically similar. This is due to the fact that the surfaces reflect in a dissimilar way.

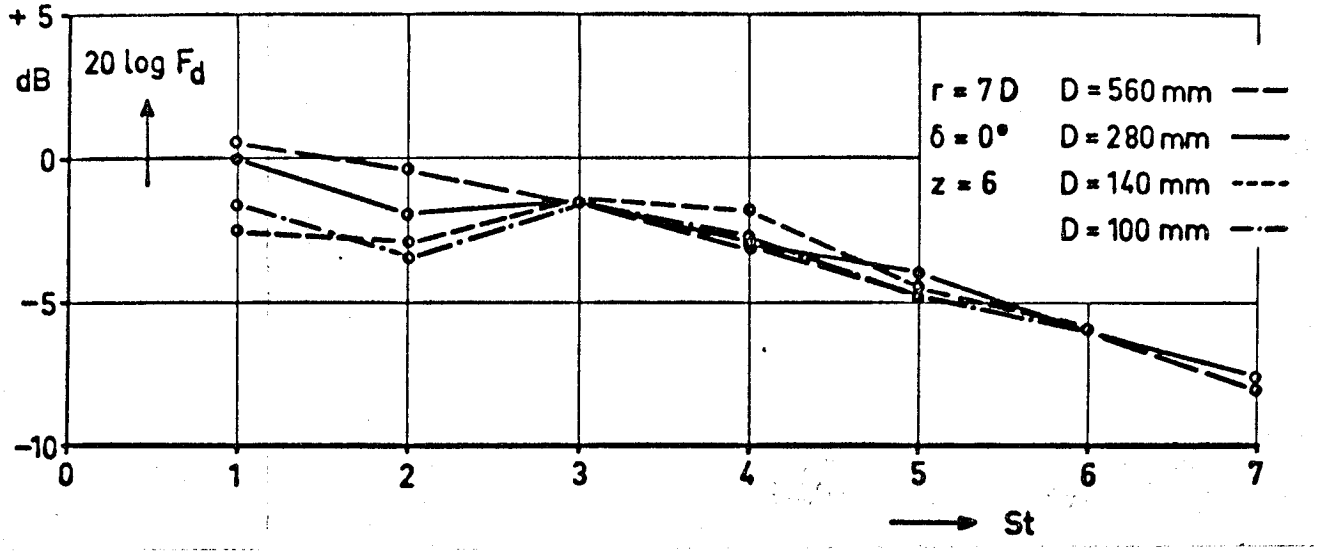


Figure 21. Similarity of the excitation spectra.

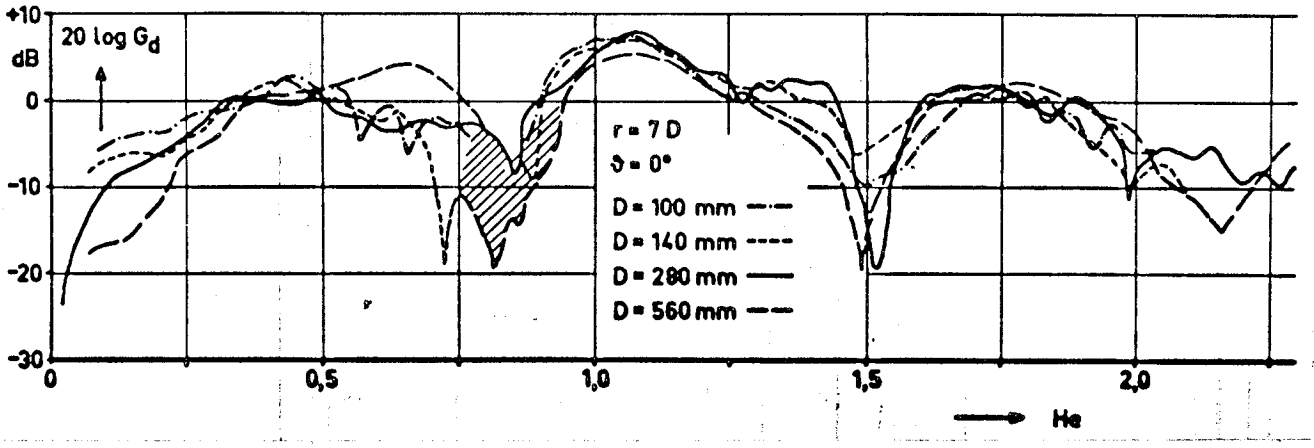


Figure 22. Similarity of the system frequency characteristics

# 10. INVESTIGATION OF THE FLOW NOISE

## 10.1. Measurement Program

The flow noise can only be incompletely analyzed, as compared with the rotational sound. This is because it is only possible to select a restricted number of Strouhal numbers from a large variety of values. Therefore, the /44
question arises as to which of the two parameters, the Mach number or the Strouhal number, must be specified. In order to obtain as complete measurement data as possible, the parameter that will be restricted is the one which will describe the smallest interval within its possible range. As was already mentioned, since the Mach number region is greatly restricted because of measurement accuracy, it is appropriate to specify discrete values for the Mach number. This results in the formulation of the measurement program from Equation (29). The Helmholtz number is varied in a continuous way at constant Mach numbers, and the Strouhal number is varied proportionally, because both parameters are coupled because of Equation (27). This representation of the flow noise also corresponds to the usual plots as shown in Figure 7. Since the range of the Helmholtz number extends over several octaves, it is preferable to use a logarithmic division of the frequency axis. In order to facilitate the later evaluation, the Mach number is also plotted logarithmically. The region from 2:1 is divided linearly three times on the logarithmic scale.

As Section 4.5.1 showed, the normalized power density $s^*$ is the appropriate characteristic number for describing the flow noise of geometrically similar ventilators. In Equation (23), $s^*$ is referred to the variable circumferential velocity. In order to establish a fixed relationship between the indicated level and the normalized power density during the course of measurements, Equation (23) is divided by the Mach number. The normalized power density then becomes

$$K_r^2 = s^*/Ma = \frac{(\tilde{p}/P_o)^2}{\Delta f \cdot D/c} = \frac{s/P_o^2}{D/c} . \qquad (52)$$

According to Equation (24) we can also write

$$K_r^2 = \frac{(\tilde{p}/P_o)^2}{\Delta(He)} \cdot \tag{53}$$

Considering the selected steps of Mach number, the following formulation of the measurement program results:

$$K_r^2 = F(He) \; ; \; Ma = 0{,}087 \; ; \; 0{,}11 \; ; \; 0{,}14 \; ; \; 0{,}174 \; ; \quad Re = Parameter \; ; \; r/D, \vartheta, \varphi, \varkappa = const. \tag{54}$$

The measurement data obtained according to this prescription are shown in Figure 23 for the rotor D = 280 mm. The curves show the average course of the spectral function, which still has considerable temporal variations, as shown in Figure 7, for example. By averaging, these are integrated graphically and at the same time the spectral components of the rotational sound are discarded. In addition, a value of 8.5 dB = 10 log 7.1 dB is subtracted from the measured levels. This corresponds to a division by the bandwidth of 7.1 Hz of the heterodyne analyzer. As Equation (53) shows, in the case of similarity of the power spectra, $K_r^2$ only then takes on the same values when the normalized bandwidth $\Delta(He)$ is held constant. This means that $\Delta f$ must be varied in such a way that the product $\Delta f \cdot D$ in Equation (52) remains constant. However, since the bandwidth of the heterodyne analyzer cannot be switched in the desired way, the analyses must be carried out for dissimilar bandwidths. In a comparison of the power spectra, we must take the fact into account that in the case of similarity, they obey the laws

/45

$$K_{r_1}^2 / K_{r_2}^2 = D_2/D_1 \tag{55}$$

10.2. Determination of the Exponents for the Reynolds number and Mach number

In order to determine the influence of the Reynolds number, an attempt is made to have the curves for the same Mach number and corresponding to D = 100, 140, 280, 560 mm lie on top of each other. These curves can be taken from the corresponding graphs, as Figure 23 shows for the rotor D = 280, for example.

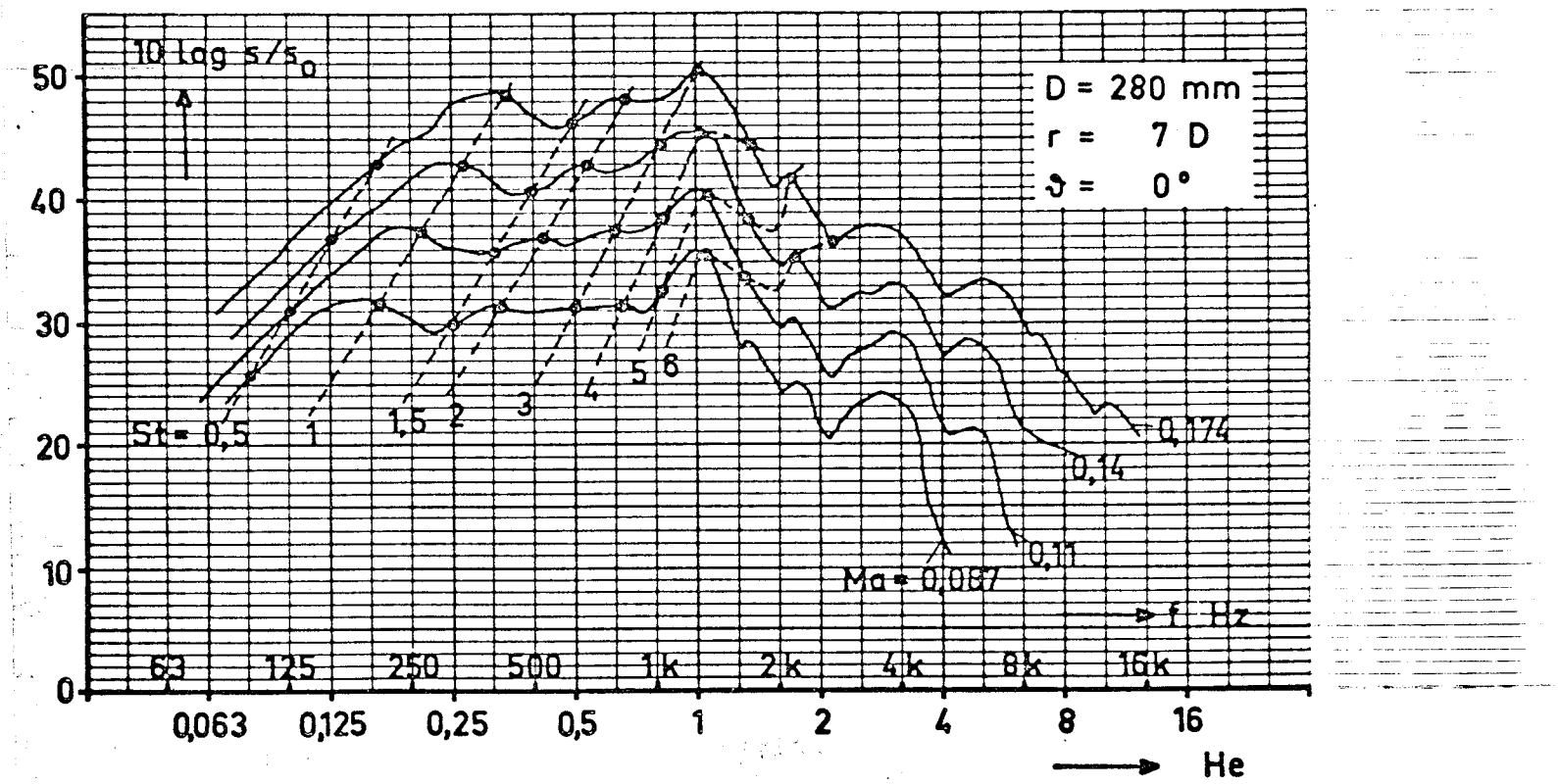


Figure 23. Measurement of the flow noise .

The level differences, by which the curves must be displaced so that there is the best agreement as is shown in Figure 24 for Ma = 0.174, are shown in Figure 25 as a function of the rotor diameter. The deviations which result at low Mach numbers are the same order of magnitude as at Ma = 0.174.

In a logarithmic representation, the level differences can be approximated by parallel lines with good accuracy as Figure 25 shows. The slopes of these lines establish the following law:

$$s \sim D \quad \text{or} \quad s/D = \text{const.} \tag{56}$$

If this law is substituted into Equation (52), then we obtain

$$K_r^2 = \text{const.} \tag{57}$$

We have thus shown that the normalized power density is independent of the size of the rotors for the same circumferential velocities. This means /46 that the flow noise does not depend on the Reynolds number. This means that the deviations in Figure 24 are measured for the similarity of the flow noise.

The Mach number exponent results from the level differences, which can be taken from Figure 25 for D = const. Figure 26 shows them plotted as a function of the logarithm of the circumferential velocity. The points lie along a straight line, which obeys the following law:

$$s \sim u^{5,2} . \tag{58}$$

The following is obtained for the power density, considering Equation (56) and (58)

$$s \sim u^{5,2} \cdot D . \tag{59}$$

The following is obtained for the normalized power density:

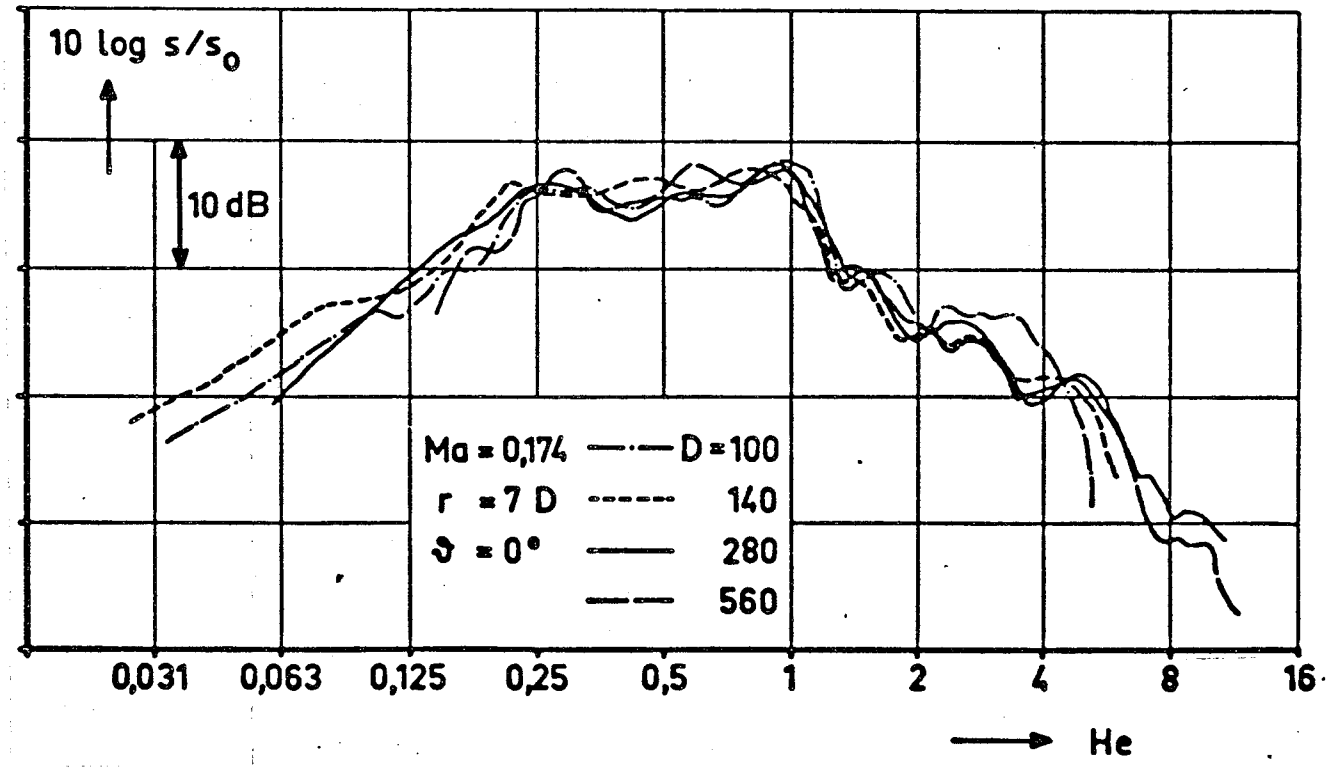


Figure 24. Achievable correspondence of the course of the power spectra density after displacement of the curve by suitable levels.

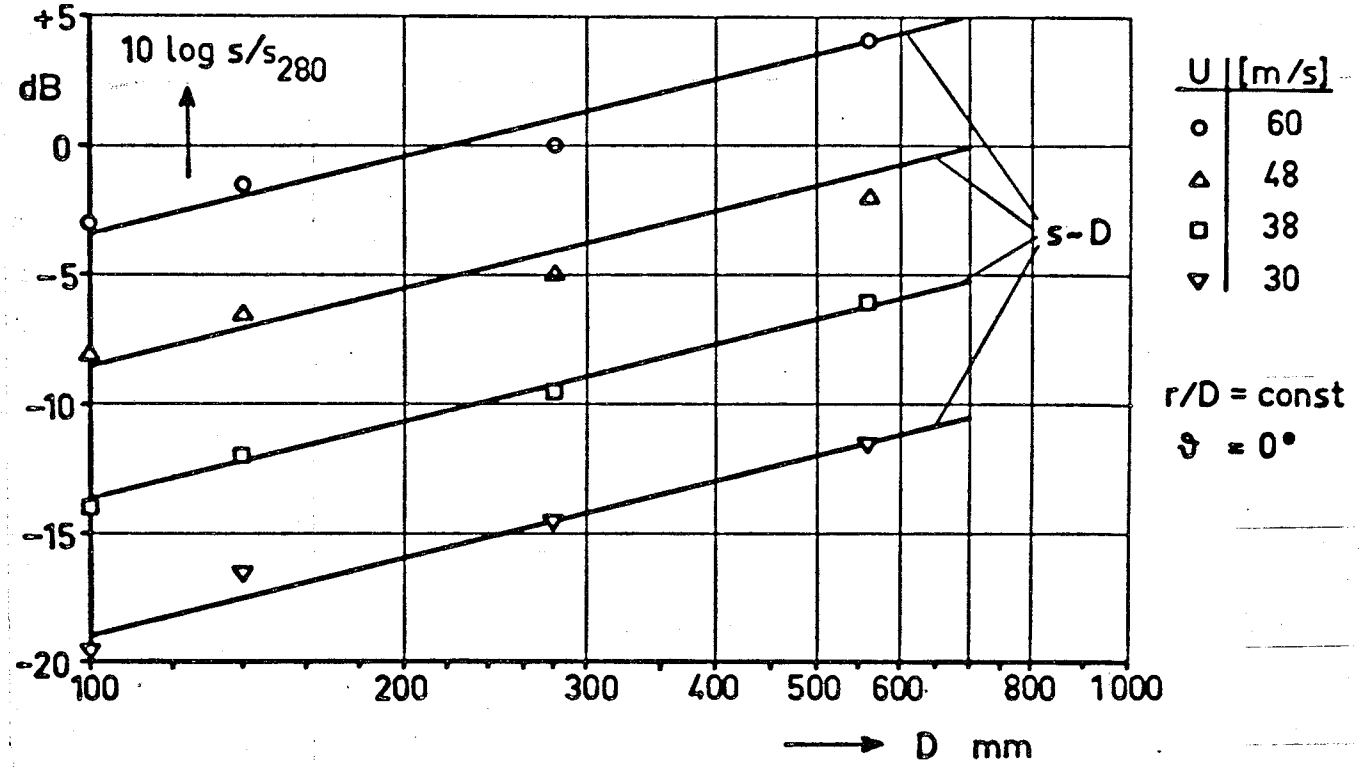


Figure 25. Dependence of the function $s/s_0 = F(He)$ on the rotor dimensions and the circumferential velocity.

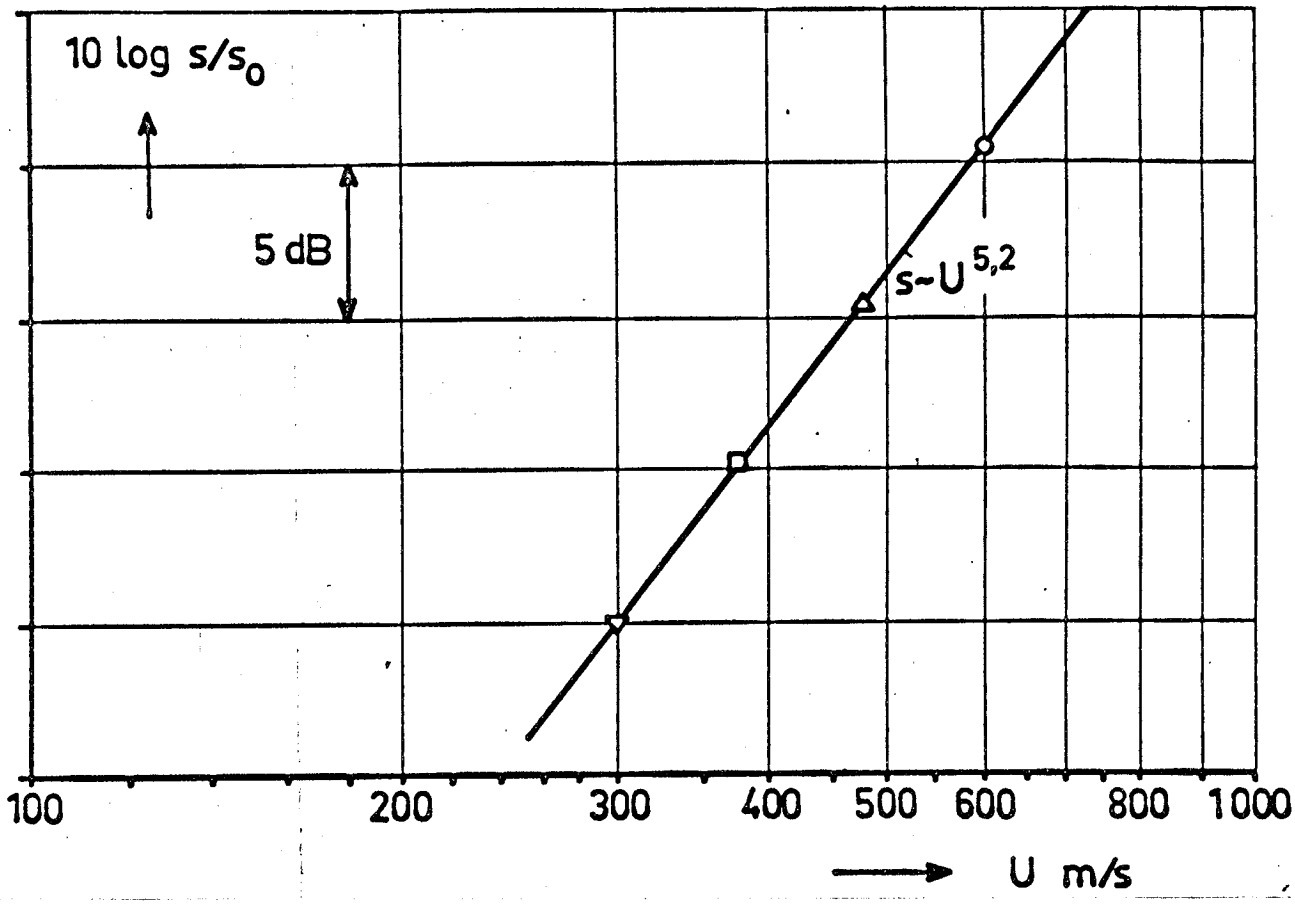


Figure 26. Determination of the Mach number exponent from Figure 25.

$$K_r^2 \sim Ma^{5,2} \cdot Re^0 \,. \tag{60}$$

10.3. Determination of the System Characteristics

In order to determine the system characteristic $G_r(He)$ from the measurements of the flow noise, the curve family Ma = const is redrawn for St as a parameter. As Figure 23 shows, this is made easier due to the fact that the Mach number steps corresponds to the 1/3 division of the frequency scale. Points with the same Strouhal number corresponding to two adjacent Ma = const curves are therefore displaced by one third. The lines connecting points

having the same Strouhal number are shown in Figure 23 as dashed lines. If we imagine that the curve Ma = const is displaced along the curves St = const, then the measurements show that in the low frequency part of the spectrum the course of the power density depends essentially only on the Strouhal number except for constant level differences. On the other hand, in the high frequency part above He = 0.5, apparently the system frequency characteristic dominates, because qualitatively there is a same course of the curves mentioned if they are plotted as a function of the Helmholtz number.

The curves ST = parameter in Figure 23 can be compared with Figure 9, /47
which shows the rotational sound, because in both cases the data have been plotted as a function of the same parameters. The only difference consists in the fact that in the case of flow noise, the Mach number region is severely restricted and it is necessary to have a finite number of selected values for the Strouhal number. Therefore, it is appropriate to split off the system frequency characteristic from the measurements of the flow noise in the same way as was done for the rotational sound. First the average course of the curve ST = const as a function of the Helmholtz number is determined, as was done for the rotational sound in Figure 9. An attempt is made to make the curves St = const overlap by displacing them in the direction He = const. The following qualitative course of the normalized power density is obtained from the average course of the curve piecewise extended curves, as is shown in Figure 27:

$$K_r^2 \sim F_2^2 (He) .$$

The numerical value of the power density depends on the factor which is given by the function $F_1^2(St)$, yet to be determined. Therefore, it becomes possible to split up the normalized power density into the two functions mentioned, in a way similar to that done for the rotational sound. Therefore, we can write:

$$K_r^2 \sim F_1^2(St) \cdot F_2^2(He) . \qquad (61)$$

By squaring functions $F_1$ and $F_2$, the system frequency characteristic is defined in the same way for the rotational sound and for the flow noise.

The function $F_2(He)$ is split into a power function and a system frequency characteristic, which specifies the deviations of the power density from the power function as a function of the Helmholtz number:

$$F_2^2(He) = He^x \cdot G_r^2(He) . \tag{62}$$

In order to consider the $Ma^{5.2}$ law in Equation (60) obtained above, the exponent $x = 5.2$ is used, so that the definition equation for the system frequency characteristic is stated as follows for the flow noise:

$$G_r^2 \sim \frac{F_2^2(He)}{He^{5,2}} . \tag{63}$$

By plotting the level differences /48

$$20 \log G_r(He) = 20 \log F_2(He) - 20 \log He^{2,6}$$

as a function of the Helmholtz number, the system frequency characteristic is obtained and is shown in Figure 28 as dashed lines.

The mentioned measurements and evaluations of the rotational sound and the flow noise result in frequency characteristics of the system. In order to compare these in a better way, the frequency characteristic obtained in Figure 14 for the rotational sound was predrawn by taking the logrithm along the frequency axis and is also shown in Figure 28. It can be seen that both curves essentially do not deviate from an average fictitious curve by no more than $\pm$ 2 dB over a region of three octaves. An exception to this can be found within narrow frequency bands at $He \approx 0.8$ and $He \approx 1.5$. At these frequencies it was also not possible to verify similarity for the rotational sound in a satisfactory way, as Figure 21 shows. Apparently the

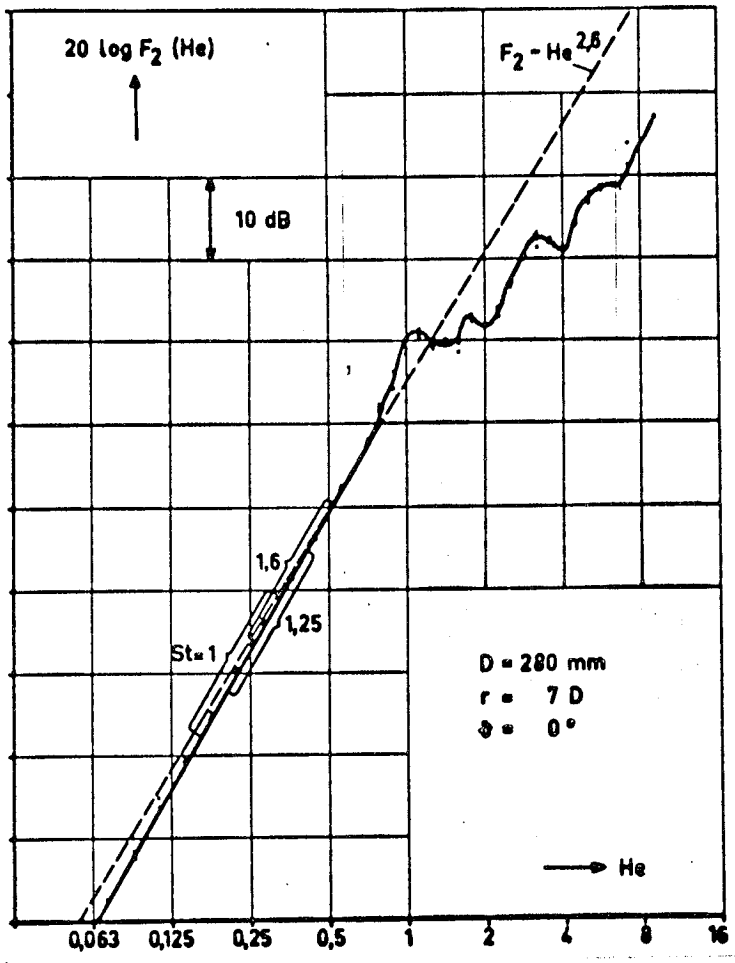


Figure 27. Course of the function $K_r^2 \approx F_2^2$ (He).

level drops, which only result due to periodic processes, can be traced to critical phase relationships in the sound radiation, which cannot be described more accurately.

Therefore, it is found that the system frequency characteristic brings about an increase or a decrease of the sound level at various frequencies, just as in the case of quadrupole theory in communications technology. Apparently it does not matter which mechanisms are responsible for the acoustic pressure at the location of sound production. The question of which characteristics of the sound radiation bring about the system frequency characteristic cannot yet be answered at this point. For this, it is necessary to carry out additional measurements in which the microphone position is varied.

## 10.4. Determination of the Power Spectral Function

The level differences by which the curves St = const in Figure 23 must be displaced in order to obtain the best agreement in Figure 27 are shown in Figure 29 as a function of Strouhal number. (The dashed curves in Figure 23 are only for clarity. Closer functions values were used in the evaluation,

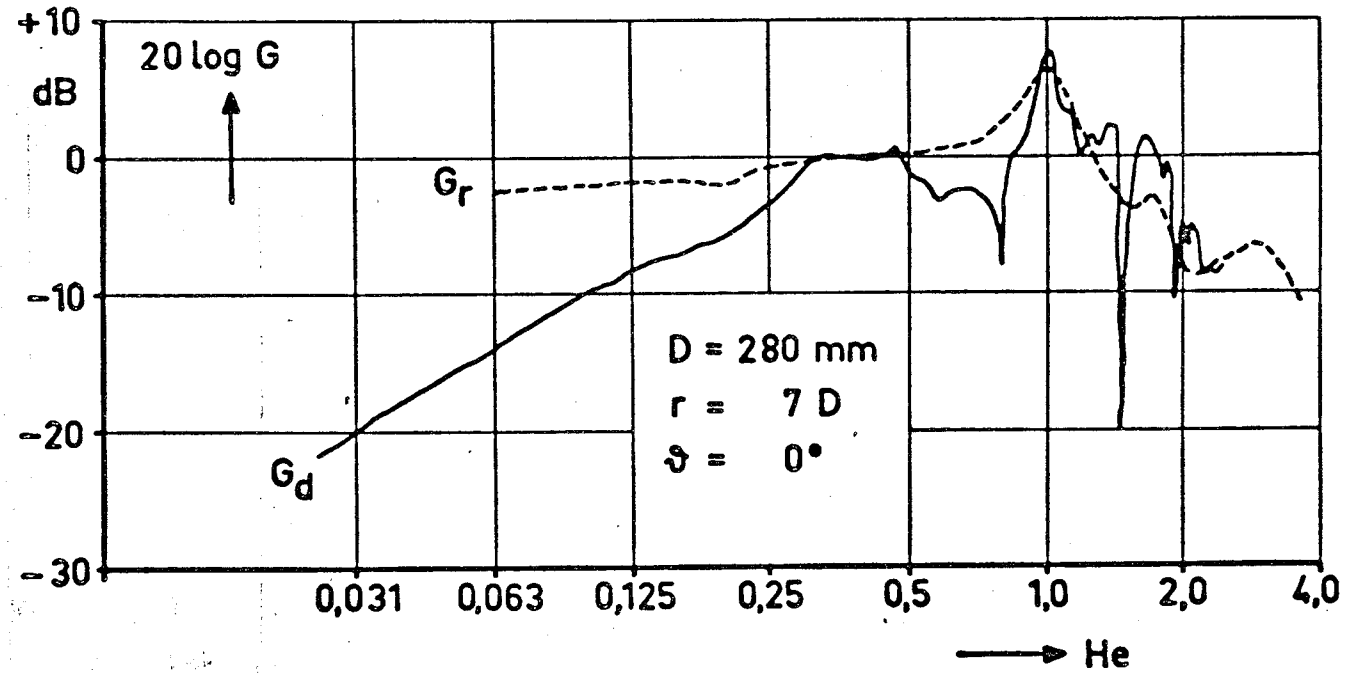


Figure 28. Comparison of the system characteristics.

and the connecting lines were left off.) The curves which connect the points establish the relationship $K_r^2 \sim F_1^2(St)$. It was also obtained as in the case of the rotational sound, see Figure 15. The function $F_1^2(St)$ is again split into a power function $St^x$ and another function $F_r^2(St)$, which gives the deviations from the power function. The same numerical value of the exponent x is selected as was used to split off the system frequency course $G_r^2(He)$, that is x = -5.2, so that



$$F_1^2(St) = St^{-5,2} \cdot F_r^2(St) \ . \tag{64}$$

It should be noted that,when the magnitude of the Mach number exponent is used, see Equation (60), the $St^{-5.2}$ law also is the best approximation for the power density.

According to the relationship

$$F_r^2(St) = \frac{F_1^2(St)}{St^{-5,2}} \tag{65}$$

the level differences

$$20 \log F_r(St) = 20 \log St^{-2,6} - 20 \log F_1(St)$$

are plotted as a function of the Strouhal number in Figure 30. The reference level defined is the value that results at St = 1. The function obtained in this way is called the "power spectral function" of the flow noise. Just as in the case of the system frequency characteristic $G_r$, which determines the basic course of the spectrum above He $\approx$ 1 in Figure 23, the power spectrum function is important for the low frequency part. The course of this function can be described as follows

$$\text{for} \quad St < 1 \quad F_r^2 \sim St^2, \tag{66}$$

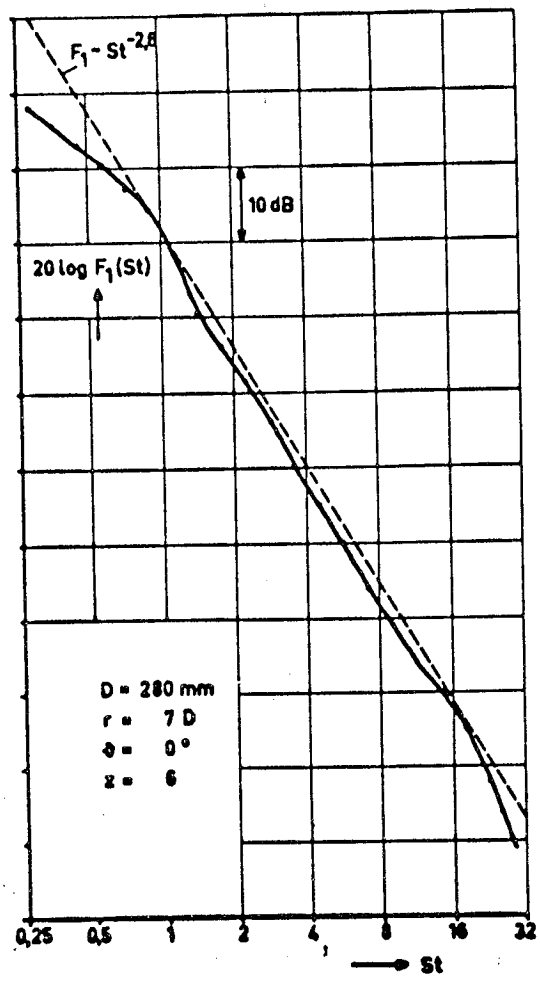


Figure 29. Course of the function $K_r^2 \approx F_1^2(St)$

for $St > 20$ $\quad F_r^2 \sim St^{-4,5}$,

for $1 > St < 20$ $\quad F_r^2 \approx$ const. (67)

The power spectral function plays the same role for the flow noise as the excitation spectrum for the rotational sound. It can also be used to draw conclusions on the sound production mechanisms. It is clearly seen that pressure fluctuations are present in the noise components. The frequencies of these agree primarily with the blade frequency

/50

$f_s = n \cdot z$ corresponding to $St = 1$

Since the Strouhal number is formed with the rotor division, see Equation (20) and (21), so that

$$St = 1 = \frac{T}{U} \cdot f, \qquad (68)$$

then the frequency of the first maximum can be written as

$$f_s = U/T \ .$$

It can be assumed that the reason for this maximum is the fact that the temporal fluctuations which are superimposed on the velocity profile at the exit of the blade channels have periodicities after each division, for example when the degree of turbulence in the individual blade channels is different.

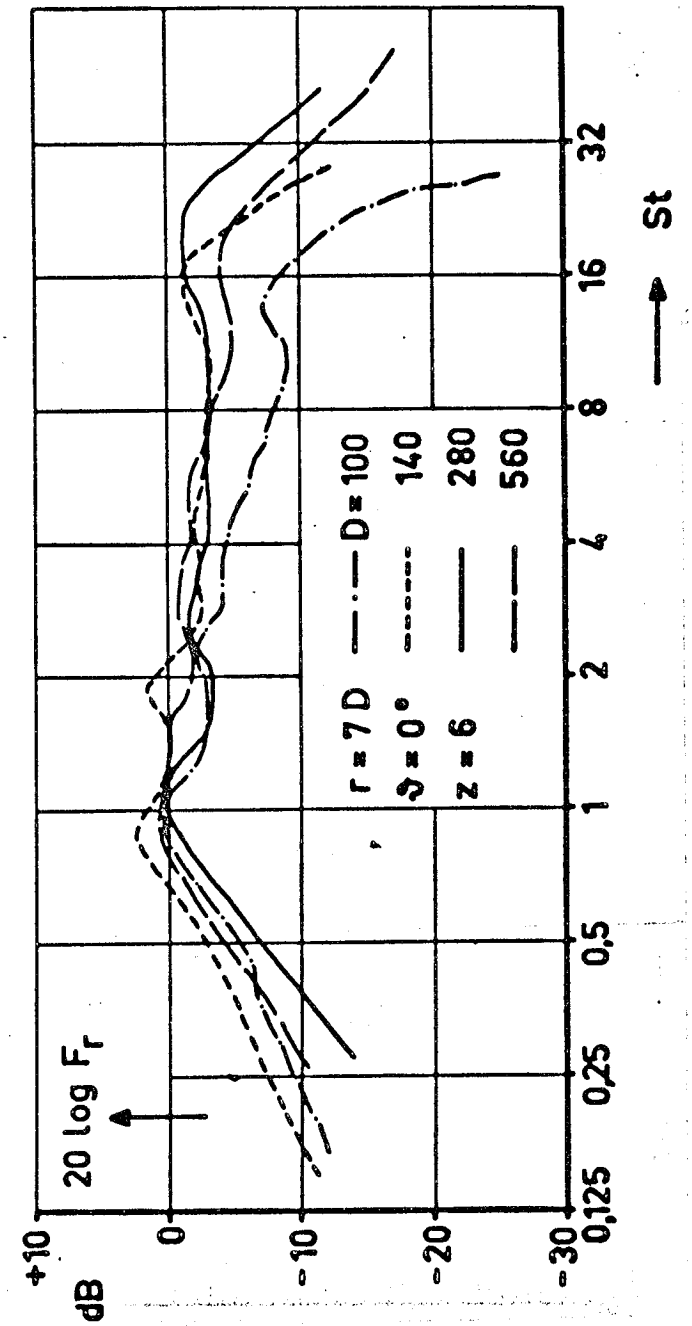


Figure 30. Similarity of the power spectral functions.

A second maximum is found at St $\approx$ 18. In the following estimation we will see whether this maximum can be traced to a natural frequency of vortex shedding. In order to test this, we determine the characteristic length which will be of importance here. ROSHKO [26] states that for Strouhal number

$$St^* = \frac{d' \cdot f}{U_s} \tag{69}$$

vortex shedding occurs if the Strouhal number takes on the value

$$St^* = 0,2 \tag{70}$$

Here f is a natural frequency of vortex separation $U_s$, the velocity at which the vortices are shed. They are produced at the free shearing layers behind a bluff body, where the distance of the shear layers d' is the characteristic length mentioned. By combining Equations (68), (69) and (70) we obtain for St = 18

$$\frac{1}{18}\frac{T}{U} \cdot f = \frac{1}{0,2}\frac{d'}{U_s} \cdot f \,. \qquad \text{/51}$$

The relative velocity at the exit of the rotor in the vicinity of the blades must be taken as the vortex velocity. Since the relative velocity $w_2$ and therefore $U_s$ are smaller than the rotational velocity U, as can be seen from the velocity triangles in Figure 19, it follows that

$$d' \leq \frac{0,2}{18}\frac{\pi}{z} \cdot D \,.$$

For D = 280 mm and z = 6 we obtain

$$d' \leq 1,6 \text{ mm} \,.$$

The distance of the corresponding shear layers therefore has the same order of magnitude as the blade thickness, which is the smallest essential dimension

of the experimental installation. By slanting the blade trailing edge, shown in Figure 6, the wake will certainly be smaller than the blade thickness. Therefore we have shown that the second maximum at St = 18 must be attributed to vortex separations at the blade trailing edge.

## 10.5. Verification of the Product Trial Solution

As shown in Equation (61), the measurement evaluation can be split into the following terms:

$$K_r^2 \sim F_1^2(St) \cdot F_2^2(He) . \tag{61}$$

If Equations (64) or (62) are substituted in Equation (61) then, considering Equations (60 and (27) we obtain

$$K_r^2 \sim St^{-5,2} \cdot F_r^2(St) \cdot Ma^{5,2} St^{5,2} \cdot G_r^2(He) \cdot Re^0$$

$$K_r^2 = k_r^2 \cdot Ma^{5,2} \cdot F_r^2(St) \cdot G_r^2(He) \tag{71}$$

Therefore, the product trial solution for the description of the flow noise has been experimentally verified by measurement evaluations. It is shown that friction does not have an influence in the case of flow noise in contrast to rotational sound within the range in which the variation was carried out: /52

$$D_{min} : D_{max} = 1 : 5,6 .$$

In order to determine the constant $k_r^2$, Equation (71) is transformed. Using Equation (52), we obtain

$$k_r^2 = \frac{s/P_o^2}{D/c} \cdot Ma^{-5,2} \cdot F_r^{-2}(St) \cdot G^{-2}_r(He) . \tag{72}$$

From Figure 23, a power level of 10 log $s/s_0$ = 48.5 dB is derived from measurements at Ma = 0.174 and St = 1. The Helmholtz number is He = 0.33.

After substituting these values in Equation (72), we obtain the following with $F_r(1) = 1$ and $G_r(0.33) \approx 1$

$$k_r^2 = 3 \cdot 10^{-8}. \tag{73}$$

Therefore, we obtain the following for the power density

$$s = 3 \cdot 10^{-8} \frac{P_o^2}{c/D} \cdot Ma^{5,2} \cdot F_r^2(St) \cdot G_r^2(He) \tag{74}$$

and for the level of the power density

$$10 \log s/s_o = 20 \log (P_o/\tilde{p}_o) + 20 \log Ma^{2,6} + 20 \log F_r(St) + \\ + 20 \log G_r(He) - 10 \log \frac{c/D}{Hz} - 75 \text{ dB}. \tag{75}$$

A control calculation carried out for the point He = 1, Ma = 0.174 showed that the calculated level of power density is only 1 dB larger than the measured value.

## 10.6. Similarity of the Power Spectrum Functions and System Frequency Characteristics

The scatter of the curves in Figure 30 and 31 is a measure for the similarity of the power spectral functions or the system frequencies, respectively, determined for the rotors D = 100, 140, 280 and 560 mm. If one considers the course of the power spectral functions, then significant deviations from the other curves occur at high frequencies and only in the case of the small rotor. For this rotor, the diameter step is 1:1.4 in contrast to the other rotors, the diameters of which have the ratio 1:2. The influence of the wheel size on these deviations must therefore be excluded. Therefore, they are due to dissimilar flow processes at the blade trailing edge. A comparison of the rotors showed that the blade trailing edge of the smallest rotor is not as sharp as compared with the blade thickness as in the case of the larger wheels, so that there is not a strict geometrical similarity at this point. This similarity of the other power spectral

/53

functions is satisfactory, because the deviation from an average imaginary course is about $\pm$ 2 dB.

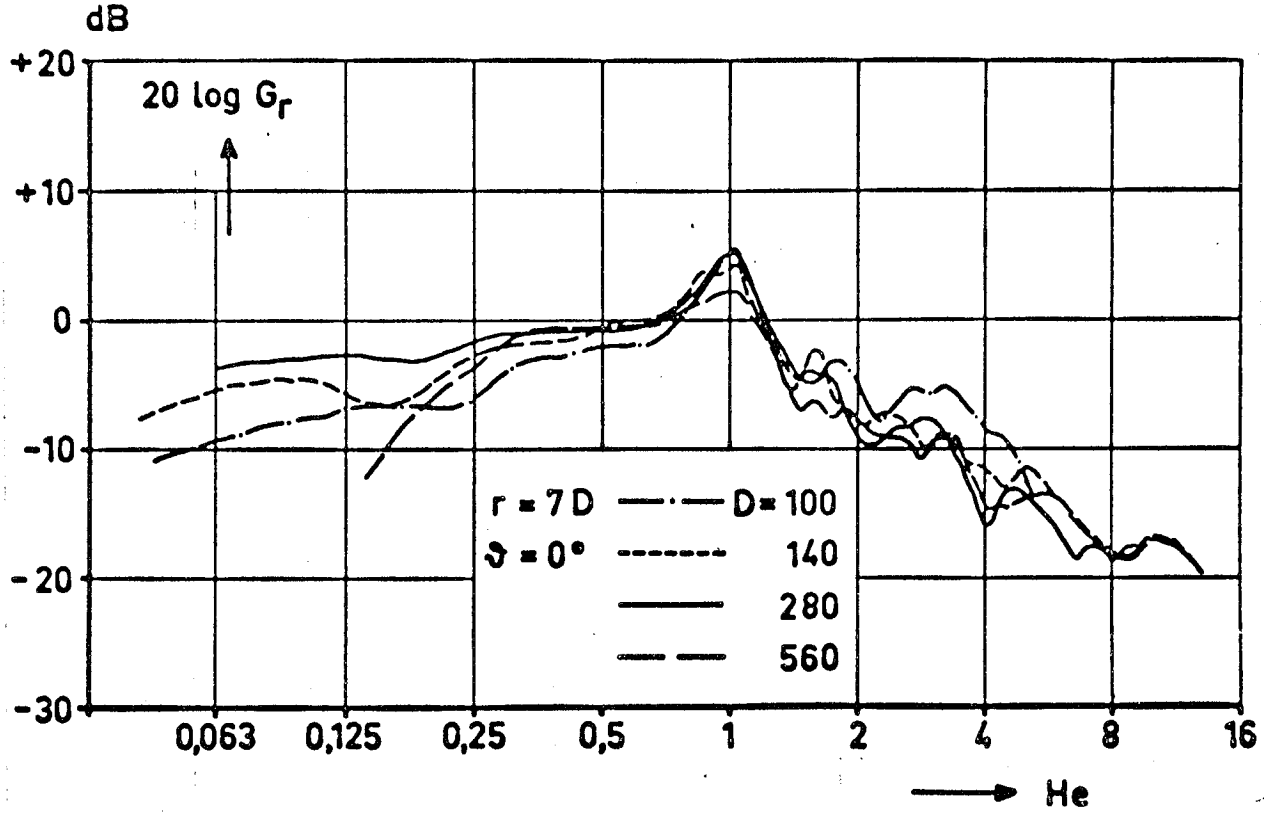


Figure 31. Similarity of the system's characteristics.

Deviations for the system frequency characteristics are about the same order of magnitude. At the low frequencies in the case of the largest rotor, they can be traced to the influence of the chamber with a low reflectivity, because at He = 0.2 the frequency is already lower than its limiting frequency. The same is true for the measurements of the rotational sound, as can be seen from Figure 22. Above the limiting frequency the deviations of the four system frequency characteristics from an average curve amount to $\pm$ 3 dB.

## 11. COMPARISON OF THE NOISE COMPONENTS

Equations (50) and (74), as well as the functions $F_d$, $F_r = F(St)$ and $G_d$, $G_r = F(He)$, make it possible to determine the total level averaged over

all frequencies at the measurement position. This can be done for the rotational sound and the flow noise separately. Comparison of the components shows which of the two have the decisive influence on the unweighted noise levels. Here the two system frequency characteristics $G_d$ and $G_r$, which are compared in Figure 28, are replaced by an average frequency characteristic G(He), which essentially does not consider the level cancellations in the case of the rotational sound. Figure 28 also shows that it is sufficient to consider a frequency range only up to about He = 2, because higher frequency components only yield a total noise which is within the measurement accuracy.

## 11.1. Total Sound Level of the Rotational Sound

Let:

$U = 60$ m/s
$D = 0{,}28$ m
$i = 1 \ldots 7$
$z = 6$
$c = 345$ m/s
$\nu = 0{,}15 \cdot 10^{-4}$ m$^2$/s
$P_o = 1$ bar

$Ma = 0{,}174$
$Re = 1{,}12 \cdot 10^6$
$He = \frac{z}{\pi} 0{,}174 \cdot St = \frac{St}{3{,}0}$

In order to determine the level of the rotational sound, the squares of the amplitudes of the harmonics must be formed and added. From Equation (50) it follows that

$$\tilde{p}^2_{d,tot} = (0{,}14 \cdot 10^{-4} \cdot P_o)^2 \cdot Ma^{5,2} \cdot Re^{0,4} \sum_{St=1}^{7} F_d^2(St) \cdot G_d^2(He) \cdot \qquad (76)$$

With these values we obtain

TABLE 1

| St | He | $F_d$ [dB] | G [dB] | $F_d^2 \cdot G^2$ |
|---|---|---|---|---|
| 1 | 0,33 | 0 | -1 | 0,794 |
| 2 | 0,66 | -2 | -2 | 0,4 |
| 3 | 1,0 | -1,5 | +5 | 2,5 |
| 4 | 1,33 | -3 | -1 | 0,4 |
| 5 | 1,66 | -4 | -2,5 | 0,224 |
| 6 | 2,0 | -6 | -8 | 0,04 |
| 7 | 2,33 | -7,5 | -9 | 0,025 |

$$\sum F_d^2 \cdot G^2 = 4{,}383$$

After a numerical recalculation for the effective value of the total sound pressure of the rotational sound and using the numerical values of the other parameters, we obtain

$$\tilde{p}_{d,tot} \approx 5 \text{ µbar}$$

and for the level we obtain

$$20 \log (\tilde{p}_{d,tot}/\tilde{p}_o) \approx 88 \text{ dB}. \quad (77)$$

11.2. Total Sound Level of the Flow Noise

If the power spectral density in Equation (74) is integrated over all frequencies, then the effective value of the total sound pressure of the flow noise is obtained:

$$\tilde{p}^2_{r,tot} = \int_0^\infty s \cdot df = (k_r \cdot P_o)^2 \cdot Ma^{5,2} \cdot \int_0^\infty F_r^2(St) \cdot G_r^2(He) d(He). \quad (78)$$ /55

For an estimation of the flow noise it is sufficient to select frequencies as the integration limits for which the power spectral function or the system characteristics have dropped by 10 dB, as was done for the rotational sound. Using the same values of the parameters as for the rotational sound and also considering that

$$St = 3,0 \, He,$$

we obtain the following after a graphic integration for the integral

$$\int_{0,1}^{2} F_r^2(St) \cdot G^2(He) d(He) = 1,4 .$$

After substituting Equation (73) $P_0$ = 1 bar and $Ma^{5.2} = 1.12 \cdot 10^{-4}$ in Equation (78), the following is obtained for the effective value of the total sound

pressure of the flow noise

$$\tilde{p}_{r,tot} \approx 2{,}2 \text{ µbar}$$

and for the level

$$20 \log (\tilde{p}_{r,tot}/\tilde{p}_o) \approx 81 \text{ dB}. \tag{79}$$

11.3. Noise Synthesis

Comparison of the level of both noise components shows that the rotational sound of the flow noise is higher by 7 dB. The total noise, which consists of both components, is obtained as

$$\tilde{p}^2_{tot} = \tilde{p}^2_{d,tot} + \tilde{p}^2_{r,tot}$$
$$\tilde{p}_{tot} = \sqrt{5^2 + 2{,}2^2} \text{ µbar} = 5{,}45 \text{ µbar}. \tag{80}$$

The total sound pressure level therefore is

$$20 \log (\tilde{p}_{tot}/\tilde{p}_o) = 89 \text{ dB}. \tag{81}$$

The total level read off at the microphone amplifier directly is, on the other hand,

$$20 \log (\tilde{p}_{tot}/\tilde{p}_o) = 90 \text{ dB}. \quad /56$$

This comparison shows that the error is only -1 dB and is within the measurement accuracy. The simplifications used in the calculation of the spectrum, that is to ignore frequencies above He = 2 and to merge the two system frequency characteristics, are therefore permissible.

The Table for the evaluation of the rotational sound shows how the system frequency characteristic influences the level of the total noise. For the

selected maximum circumferential velocity, the third harmonic is greatly increased at the measurement position, because the system frequency characteristic takes on its maximum value at just He = 1. If it would be possible to attenuate the third partial tone, then the rotational sound level would decrease by 3.6 dB and the total noise level would decrease by 2.8 dB. This means that almost half of the total sound energy radiated in the direction $\vartheta = 0°$ is due to the third harmonic of the rotational sound.

## 12. ADDITIONAL MEASUREMENTS

### 12.1. Influence of the Perturbing Body

In the investigations of sound production mechanisms the question arises of how the spectra will differ when the measurements are carried out with the perturbing body and without it. Measurements show directly that when the perturbing body is absent the rotational sound disappears, but it essentially remains in the flow noise. We must now test whether the flow noise properties are maintained.

In order to answer this question, measurements were carried out on the rotor with D = 140 mm. In order to demonstrate the differences, both spectra taken with and without the perturbing body were written above each other, and the spectrum determined without the perturbing body was increased by 23 dB using a frequency linear method. As Figure 32 shows there are relatively small differences between the curves which are emphasized by shaded surfaces. The deviations which occur in the same direction in the spectrum can be traced to changes of the system frequency characteristic, because the deviations occur at the same Helmholtz numbers. The total measured level is about 60 dB /57 without the perturbing body. With the perturbing body it is 81 dB, see Equation (79). However, the second value was determined for the larger wheel for D = 280 mm at a geometrically similar measurement position. Within the framework of the possible acoustic similarity of both wheels, this level difference agrees relatively well with the level by which the spectrum of the smaller

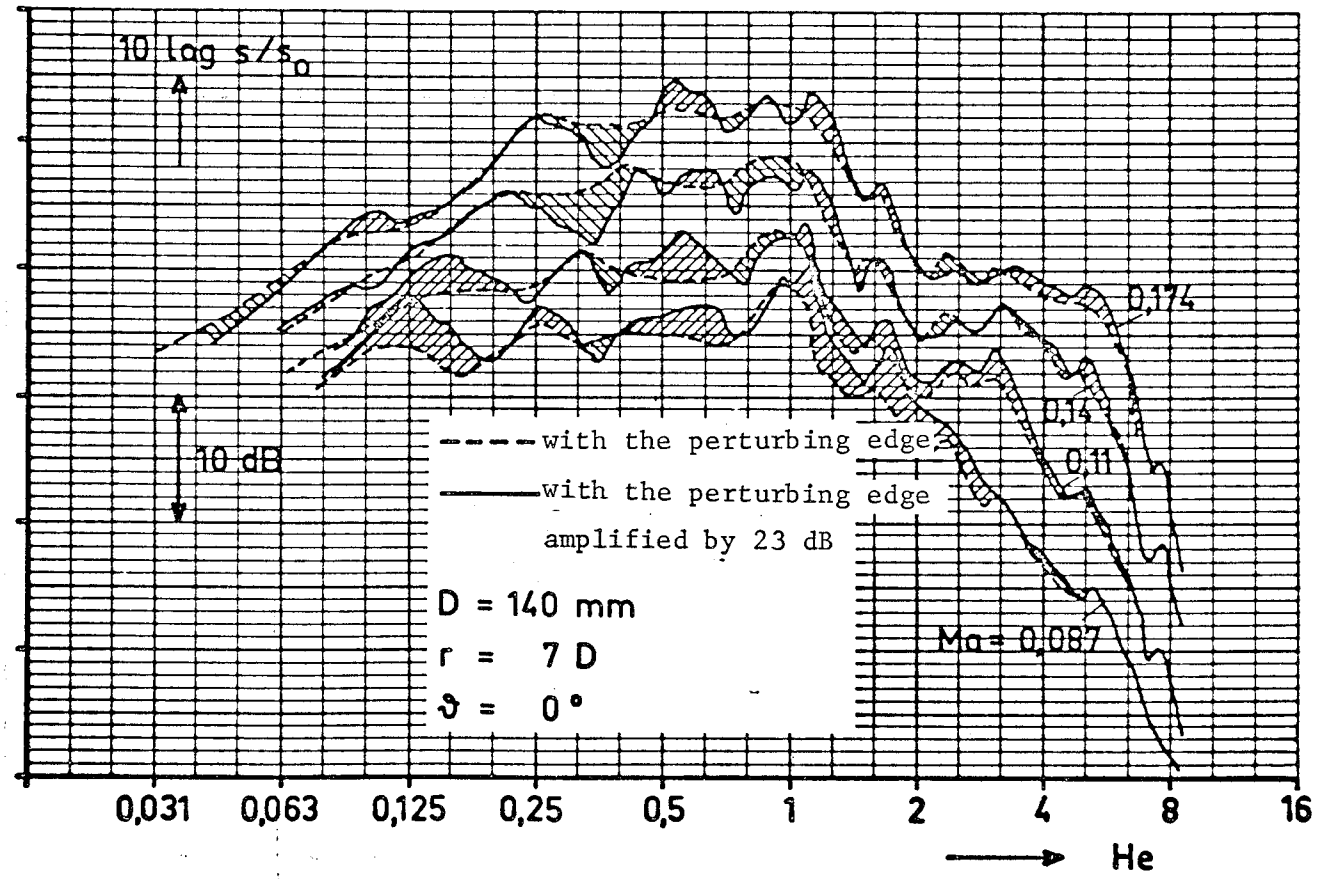


Figure 32. Influence of the perturbing body on the flow noise.

rotor without the perturbing body must be raised for best agreement.

From these results it follows that:

1. The perturbing body has no decisive influence on the system frequency characteristic. The fundamental course of the power density is maintained.

2. The flow noise is amplified by more than 20 dB by the presence of the perturbing body. This means that only the flow processes at the edge of the perturbing body are important for the sound production of this noise component. The production of the flow noise at the other parts of the rotor circumference can therefore be neglected.

3. The level of the noise measured without the perturbing body is a lower limit value for a given circumferential velocity which is reached for arbitrary enlargement of the edge distance. As the distance is increased, the rotational sound component increases more than the flow noise component. Thus, for example, the radiated sound energies of both noise components are equal at a certain distance.

## 12.2. Influence of the Edge Distance

The measurements described up to the present refer to an edge distance of $s = 0.01\ D$, as can be seen from Figure 4. In order to estimate the deviations during verification of the acoustic similarity, which may be caused by violating the similarity of the edge distance, measurements were also carried out at $s = 0.014\ D$. Figures 33 and 34, respectively, show the excitation spectrum and the system frequency characteristic determined from them.

The evaluation shows that the amplitude of the excitation spectrum decreases considerably when the edge distance is increased. This means that /58
the temporal course of the absolute velocity at the edge no longer increases as steeply and that it decreases just as in the immediate vicinity of the

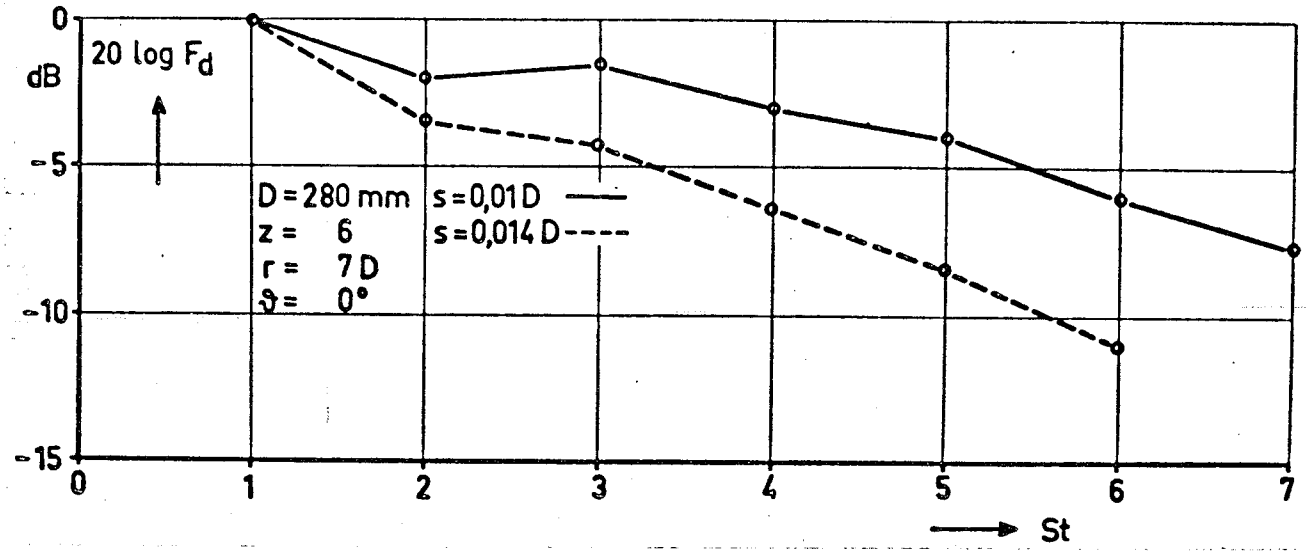


Figure 33. Influence of the edge distance on the excitation spectrum.

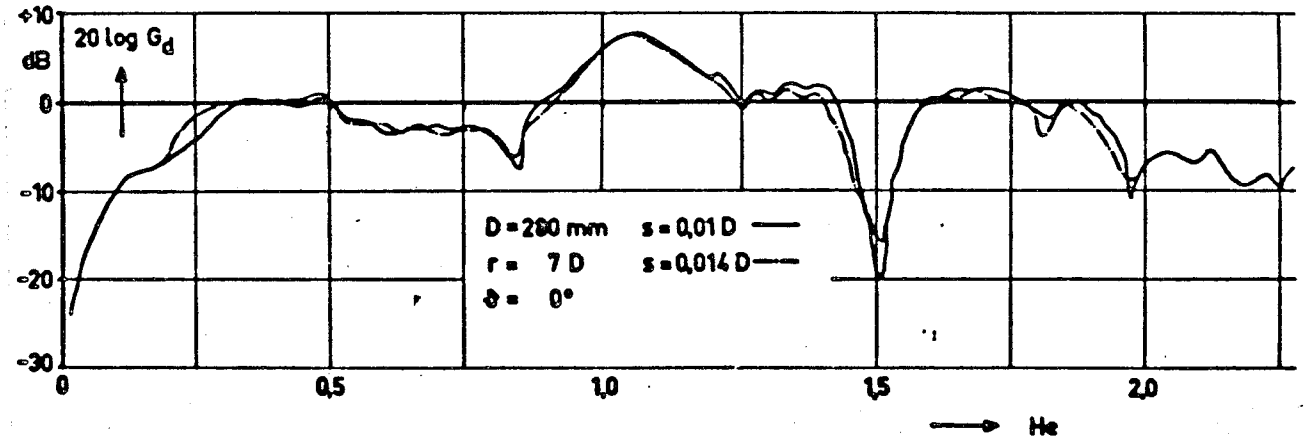


Figure 34. Influence of the edge distance on the system characteristics.

rotor. This means that the needle-shaped impulse shown in Figure 20 is broadened. This is also in agreement with experience. As the flow distance is increased, the inhomogeneities of the flow field, which are produced by the wake behind the blade, are equalized.

A comparison of the system frequency characteristics determined for various edge distances shows that there is good agreement among the curves. This result could be expected because, even when the perturbing body is removed, the course of the power density as a function of the Helmholtz number changes only slightly, as was shown in the preceding section.

## 12.3. Directional Effect of the Sound Radiation

In order to determine the influence of the microphone position on the measurement results, we first determine the system frequency characteristics and the corresponding excitation spectra for three fixed space points at r/D = const and $\vartheta$ = 0°, 45° and 90°. These are shown in Figures 35 and 36, respectively.

Figure 35 shows that the course of the system frequency characteristic depends strongly on the selection of the measurement position. The scatter of the curves usually amounts to 10 dB and is reduced in the high frequency part. The strong extinction at He $\approx$ 1.5 and $\vartheta$ = 0° is especially noticeable. Deviations in the similarity of the directional characteristics of the individual rotors, which may appear insignificant, must cause significant level differences for these values of the parameters. Apparently, the strong deviations in Figure 22 at He $\approx$ 1.5 can be attributed to such differences in the direction of maximum extinction, especially since there is no strict geometrical similarity of all elements of the test spans. The deviations indicated by shading at He = 0.8 could be interrupted in a similar way.

The excitation spectrum is quite reproducible, on the other hand, as Figure 36 shows and is therefore essentially independent of the measurement position at which it is determined. There are large deviations only at $\vartheta$ = 90°.

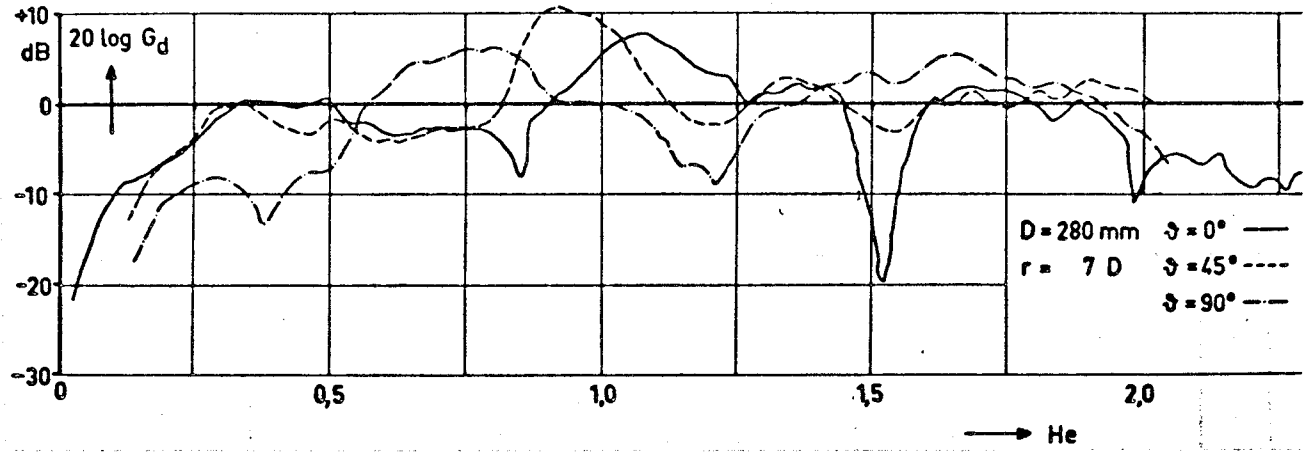


Figure 35. Dependence of the system characteristic on the measurement position.

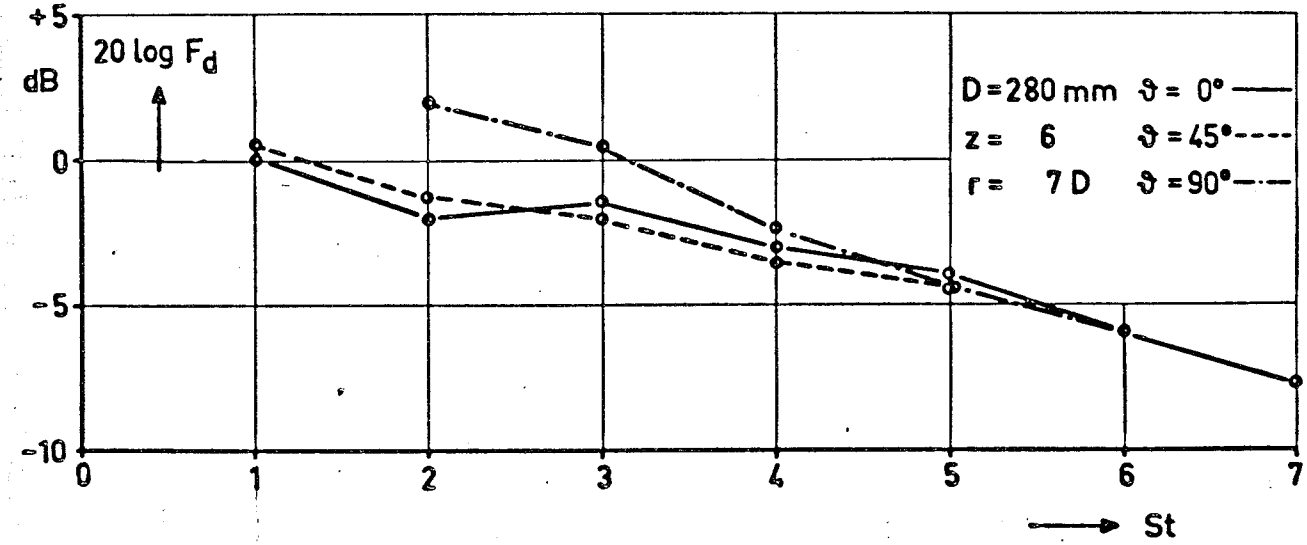


Figure 36. Dependence of the excitation spectrum on the measurement position.

In particular, it is not possible to give the amplitude of the first harmonic with certainty because the curve ST = 1 has a relatively low level, in contrast to Figure 9, and is curved in many places. In order to investigate the origin of this property, the angle $\vartheta$ was continuously varied in the region from -50° to +190° during recording of the measurement data for the first harmonic. Figure 37 shows the curves obtained in this way for various Mach numbers. From this representation it can be seen that by displacing the minimum as a function of Ma $\sim$ He, the level at $\vartheta$ = 90° decreases by 30 dB with respect to about 20 dB at $\vartheta$ = 0°, 45°. This means that the reason for the deviations in the first harmonic of the excitation spectrum is the fact that the extinction degree depends on Mach number, and the direction of maximum extinction depends on the Helmholtz number. Figure 37 shows typical properties of the radiation diagram of a line radiator which coincides with the edge of the perturbing body: the minimum sound propagation is in the direction of the expansion and is a maximum perpendicular to this direction. In order to test whether this law also holds for the other harmonic, the measurements were extended up to the sixth harmonic and are shown in Figure 38, but only for the maximum circumferential velocity corresponding to Ma = 0.174. As the frequency increases, the sound radiation as a function of the angle $\vartheta$ becomes ever more complicated. The curves clearly show that the total level of the rotational sound is determined by a third harmonic at angles of $\vartheta = \pm 60°$, as was already expressed in Section 11.1. In addition it can be seen that for larger angles the second and first harmonics dominate. Even though the harmonic levels are considerably different at $\vartheta$ = 0° and $\vartheta$ = 45°, this has very little influence on the excitation spectrum due to the good decoupling of the system frequency course from the other flow-acoustical properties.

/59

The total level of the rotational sound results from the action of all harmonics. It agrees with the level of the total noise within the framework of the measurement accuracy, as was shown in Section 11.3. The latter was measured directly and is shown in Figure 39. The angle of the microphone coordinates was also varied continuously here. It was found that the total noise level is only weakly dependent on the angle. The sound color changes

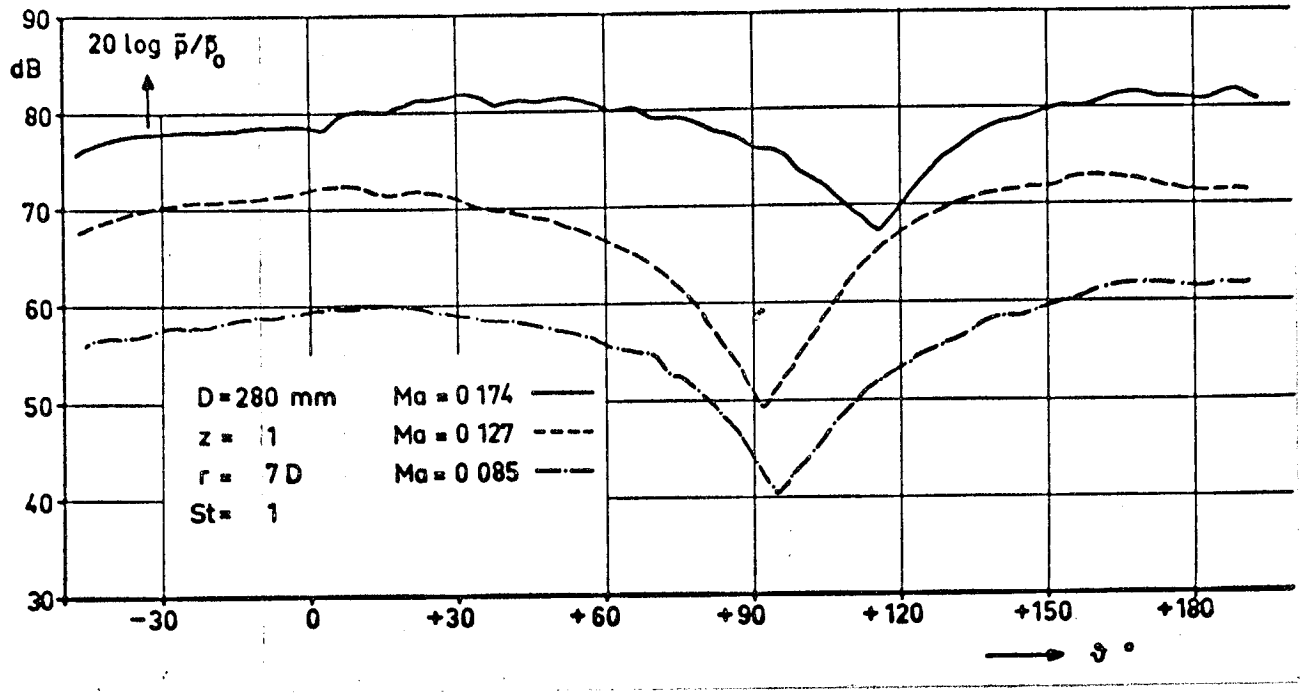


Figure 37. Directional characteristic of the first harmonic of the rotational sound.

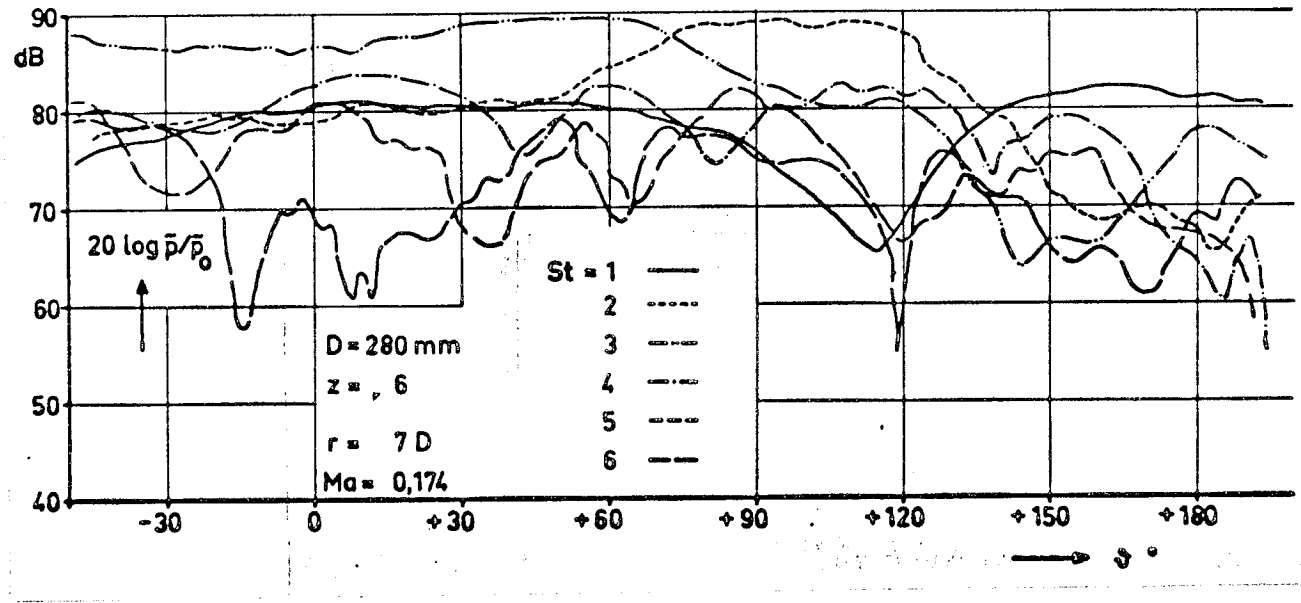


Figure 38. Directional characteristic of the rotational sound.

clearly when the microphone is moved and when one listens to the microphone signal. This is because the total level is decisively influenced by various harmonics in sequence, as is shown in Figure 38.

Therefore the investigations on the directional effect of the sound radiation show that the acoustic pressure recorded at the receiving point depends essentially on the ratio of the characteristic length divided by the acoustic wavelength /60

$$D/\lambda = He$$

On the other hand, if one considers only a small frequency band with the central frequency He = const, then the measurements in Figure 40 show that when the Strouhal number or the Mach number are varied there will only be slight deviations. The variation of the Mach number only brings about a uniform displacement of all levels, as the product trial solution specifies.

## 12.4. Reproducibility

Three measurements of the rotational sound were carried out in order to determine the reproducibility. These were taken one and one half years apart and one day apart. The test stand of the rotor D = 280 mm was rebuilt between the first two measurements, and the follower control device was improved. No changes were carried out between the two last measurements, and the important measurement instruments remained plugged in. In order to include the graphical evaluation in the reproducibility tests, the corresponding excitation spectra were determined and are compared in Figure 41.

The scatter of the two last functions lies within the measurement accuracy. This means that the determination of the average level distances between the curves in Figure 9 is therefore reliable. Slightly larger deviations can be found between the older and more recent measurements. The reproducibility is satisfactory for the maximum level difference of only +1 dB.

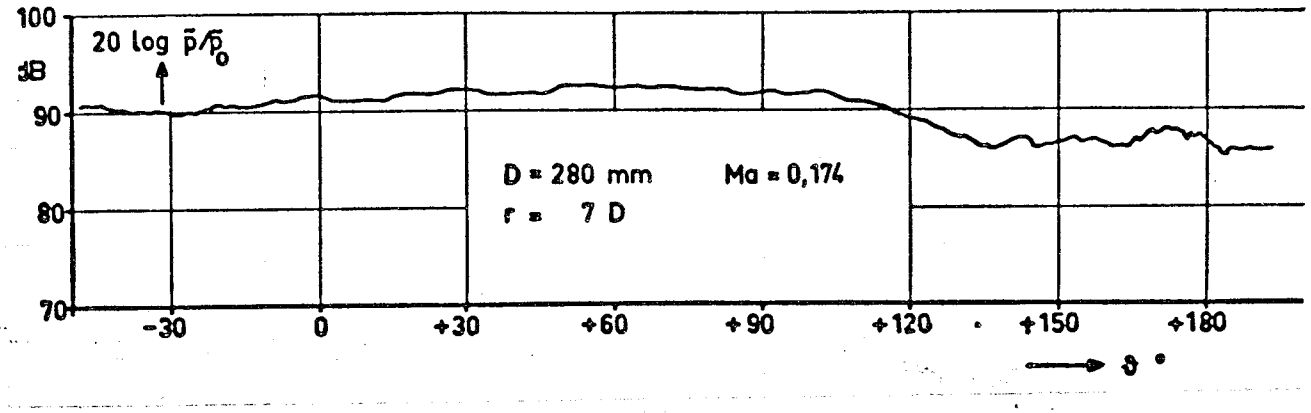


Figure 39. Directional characteristic of the total noise.

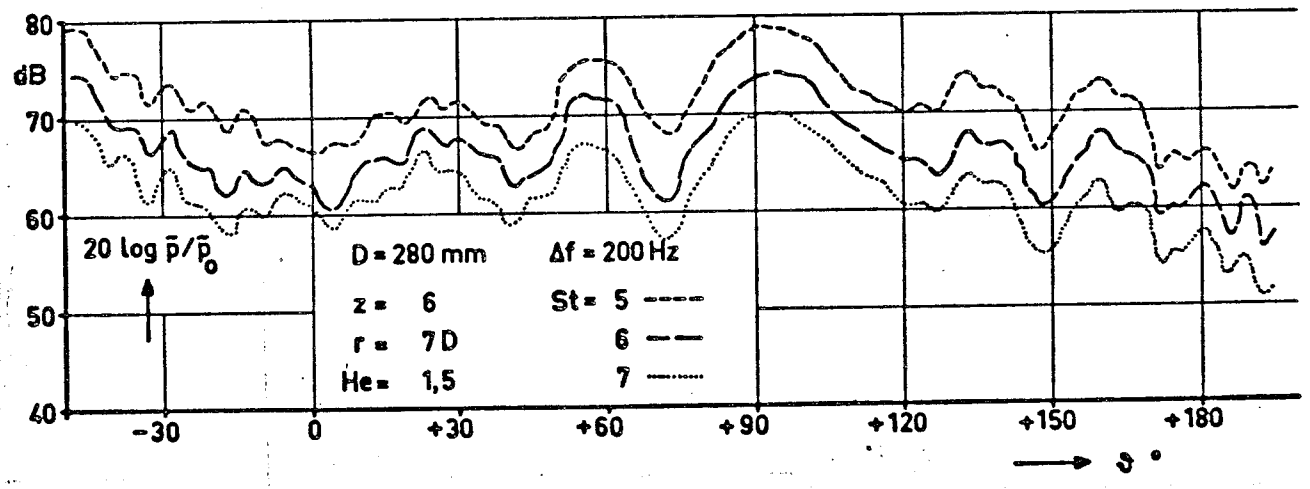


Figure 40. Directional effect of various harmonics for constant Reynolds number.

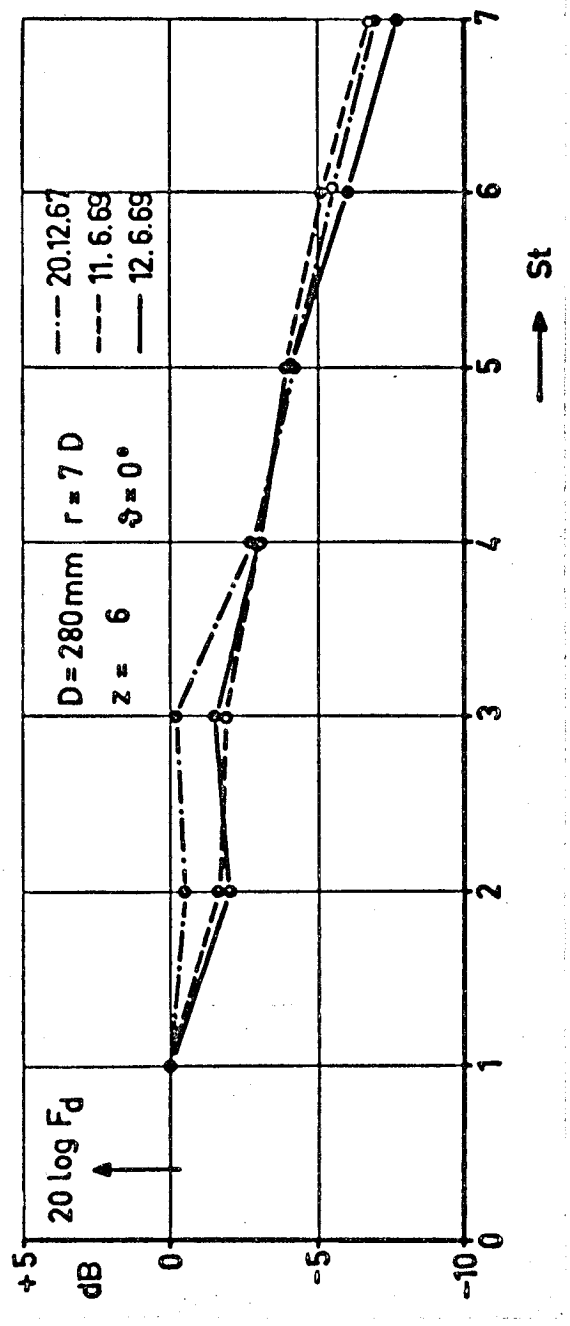


Figure 41. Reproducibility of the excitation spectrum.

Figure 34 makes it possible to estimate the reproducibility of the system frequency characteristic. Even for changes of 40% of the edge distance from the rotor, the deviations between the system frequency characteristic are of the order of magnitude of the measurement accuracy on the average. Larger deviations of about 3 dB only occur for the steep curves.

## 13. DISCUSSION OF THE RESULTS

In order to make a comparison with the known laws given in the literature, the results found in this paper have been transformed in a suitable way. According to Equation (41), the following holds for the rotational sound:

$$\tilde{p}^2 \sim U^{5,6} \cdot D^{0,4} . \tag{41}$$

Thus, the $U^{5.6}$ law for axial ventilators given by WIKSTRÖM [5] has been verified. He did not find a dependence on D, because D was only varied in the range from 1:1.3. In this case the power level would only be raised by 0.7 dB according to Equation (41). WIKSTRÖM explains the fractional exponent by the fact that the sound production increases as the boundary layer thickness increases. However, the laws determined in this paper do not agree with this explanation. Apparently the width of the wake behind the blade is of prime importance for the rotational sound, shown in Figure 20, because here is where the temporal course of the velocity fluctuations is determined, especially the amplitude of the impulse function. In Equation (42) it is stated that the acoustic pressure depends on the Reynolds number in the following way:

$$\tilde{p} \sim Re^{1/5} .$$

From boundary layer theory it is known [27] that in the case of turbulence the normalized boundary layer thickness $\frac{\delta}{D}$ depends on the Reynolds number in the following way:

$$\delta/D \sim Re^{-1/5} . \tag{82}$$

We find now that the exponent for the Reynolds number which we have found has the same magnitude as that given in Equation (82), so that in conjunction with Equation (42) we can establish the relationship:

$$\tilde{p} \sim U^{2,6} \cdot D/\delta \quad . \tag{83}$$

Equation (82) shows that $\delta/D \sim (UD/V)^{-1/5}$ and therefore, for the same circumferential velocities and the same working medium, the normalized boundary layer thickness decreases with increasing wheel size D according to $\delta/D \sim 1/D^{1/5}$. This results in an increase of the velocity change per unit time at the edge of the perturbing body, and therefore brings about an increase in the acoustic pressure in Equation (83). This result is based on measurements carried out /62 on five rotors having a diameter ratio of $D_{max}:D_{min} = 10$. In the investigations of MALING [13] and CHANAUD [16], this ratio was 1.4 and 2, respectively. The influence of the rotor size on the plotted power and pressure levels would have the effect of level changes of about 1 dB for constant and uniform circumferential velocities. This means that it can hardly be detected.

The exponent 2.6 in Equation (83) could be confirmed in two ways in the further evaluation of the acoustic pressure measurement in the present paper:

1. The universal functions $F_1(St)$ and $F_2(He)$ in Figure 15 and 13, respectively, were approximated by power functions with the exponent $x = 2.6$. The level differences which result due to the incompleteness of the approximation are shown in Figure 18 as excitation spectra. The decrease of the spectra obtained in this way only depends on the value of the exponent. It was found that the excitation spectrum determined directly with the hot wire method also shows the same strong drop as was obtained from the evaluation of the acoustic measurements taking the $U^{2.6}$ law into consideration.

2. From the measurements of the flow noise it could be determined that when the diameter was varied in the ratio range $D_{max}:D_{min} = 5.6$, it was not possible to observe a dependence of the normalized power density on the rotor

size. This means that there can be no separation of the velocity exponent as was done in Equation (37) and (38). Comparison of the laws found for the rotational sound

$$\tilde{p}^2 \sim U^{5,2} \cdot Re^{2/5}$$

and for the flow noise

$$s \sim U^{5,2} ,$$

taken from Figure 26 shows that after splitting off the influence of friction, both noise components increase with the same exponent for the circumferential velocity.

If we consider the sound power W which results from an integration of the sound intensity $\tilde{p}^2/\rho c$ over geometrically similar spherical surfaces having the area $S \sim D^2$ in the far field, then with

$$W \sim \frac{\tilde{p}^2}{\rho c} \cdot D^2 \qquad /63$$

and Equation (76) we obtain the following for the rotational sound

$$W_d \sim C_d \cdot Ma^{5,2} D^2 Re^{0,4} \qquad (84)$$

The following is obtained for the flow noise using Equation (78)

$$W_r \sim C_r \cdot Ma^{5,2} D^2 . \qquad (85)$$

The constants of both noise components $C_d$ and $C_r$ essentially consist of the quantities $k_d$ and $k_r$, respectively, and the sum in Equation (76) or the integral in Equation (78), respectively.

In this paper the acoustic pressure was normalized with the ambient pressure at the measurement location. But the flow field only depends insignificantly on this pressure. The circumferential velocity has a stronger influence on the flow phenomenon. Therefore, it is customary to use the dynamic pressure formed with the circumferential velocity as the reference quantity. The normalized acoustic pressure is then

$$K^* = \frac{\tilde{p}}{\frac{\rho}{2} \cdot U^2} .$$

If Equations (84) and (85) are added, then for this normalization we obtain the following for the sound power:

$$W \sim \frac{\rho U^3}{2} \cdot D^2 \cdot Ma^{2,2} \ (C_d \cdot Re^{0,4} + C_r). \tag{86}$$

Comparison with the power laws (1) to (3) shows that it is not possible to explain the sound production of the experimental installation using a single monopole, dipole or quadrupole model for the turbulent flow.

On the other hand, there is good agreement with numerous measurements of radial ventilators which are known in the literature and are given in Equation (4) in the form

$$W \sim U^5 \cdot D^2 \tag{4}$$

After transforming Equation (86) /64

$$W \sim U^{5,2} \cdot D^2 \ (C_d \cdot Re^{0,4} + C_r) \tag{87}$$

it can be seen that the difference is only given by the factor $U^{0.2}$ except for the expression in parentheses. The corresponding difference of the power levels is about 3.5 dB up to circumferential velocities of 60 m/s. However this is only true if the influence of viscosity can be neglected. As these investigations have shown, this is possible if the flow noise dominates, for

example for a large switchblade distance (see Section 12.2) or for drum rotors having a large number of short blades. However, since in the experimental installation selected here the rotational noise dominates, as can be seen from a comparison with Section 11, we found the law

$$W \sim U^{5,6} \cdot D^2$$

The circumferential velocity power law for the acoustic power depends on the values of the constants $C_d$ and $C_r$. This means that all intermediate values of the exponents $x = 5.2, \ldots, 5.5$ can be expected, depending on the switch-blade distance.

In addition it is notable that agreement was found with known results for different flow coefficients. This is because most reported results refer to flow rates in the vicinity of the optimum point. In the present work, the rotors remain unthrottled. This means that the power laws are independent of the flow coefficient to a large degree, at least in the over-load region, and the selected experimental installation is therefore suitable for a determination of the fundamental structure of ventilator noise.

The specific acoustic properties of the experimental installations are expressed in the excitation spectrum, the system frequency characteristic and the power spectral function. These curves are only valid for geometrically similar models. The advantage of the representation of these functions is their clarity. They make it possible to interpret many physical mechanisms and they can be tested by parallel experiments using other methods. The course of the system frequency characteristic depends strongly on the selection of the measurement point. As Figure 35 shows, the extreme values of the curves are /65 situated at various frequencies. This means that the resonance properties do not determine the frequency characteristics. The resonance properties always influence the levels at the same frequency and in the same direction. This should not be expected, because the ratio of the uncovered surface to the

enclosed volume is relatively large. At least it is larger than when the rotor is operated inside a ventilator housing. This shows that the system frequency characteristics essentially determine the frequency dependence of the directional characteristic, at least for the present experimental installation.

## 14. MEASUREMENT INSTALLATIONS

### 14.1. Measurement Apparatus and Control Apparatus Used

The following apparatus were used in carrying out the measurements. They could be connected in any way using a cross bar distributor:

| | | |
|---|---|---|
| 1. | Condensor microphone, 1/2 inch, Type 4133, Brüel and Kjaer | ±0.2 dB |
| 2. | Tertiary analyzer, type 2112, Brüel and Kjaer | ±0.5 dB |
| 3. | Logarithmic converter, Type 7560AM, Hewlett Packard | ±0.5 dB |
| 4. | X, Y plotter, Model 7000AM, Hewlett Packard | ±0.2 % |
| 5. | Frequency counter, Model 5211B, Hewlett Packard | ±0.1 % |
| 6. | Digital-Multimeter, Type DM 68, System Elektronik GmbH | ±0.2 % |
| 7. | Heterodyne analyzer, Type FTA·BN 48302, Rohde and Schwarz | ±0.5 dB |
| 8. | Simultaneous movement generator for 7., BN 483011, Rohde and Schwarz | |
| 9. | Hot wire anemometer, Type HDA II, DVL | |
| 10. | Hot wire linear unit, developed here, | dynamic 0.3 dB |
| 11. | Frequency/voltage converter, developed here | ±0.5 % |
| 12. | Frequency divider 1:5, developed here | |
| 13. | Direct current power amplifier, developed here, output 200 V, 1A | |
| 14. | Low frequency mixing amplifier, developed here, output 8 W | |
| 15. | Potentiometer angle transducer, developed here | ±0.2 dB |
| 16. | Oscillograph, Type 503, tectronics | |

## 14.2. Follower Control Device for the Measurement of the Rotational Sound /66

The measurement program for determining the rotational sound in Section 9.1 specifies that the ratio of the central frequency of the analyzer to the rotational frequency is made constant, as expressed by Equation (36). As shown in Figure 42, the rotational rate measurement is reduced to a measurement of the frequency $f_n'$ and results by using the induction principle derived from the number of teeth of an impulse wheel. Sixty teeth were selected so that the counter would give the number of revolutions per minute. In the case of six blades, the following is obtained for the Strouhal number

$$St = \frac{f_d}{z} \cdot \frac{60}{f_n'} = \frac{10 \cdot f_i}{f_n'} = 1,2,3 \ldots 7 \; .$$

In order to reduce the frequency ratio from the maximum of $70 \cdot f_i/f_n'$, the rotational frequency is divided by the number 5 in a divider, so that $f_n'/5 = f_n$. In order to tune the analyzer to the desired harmonic of the rotational sound, the following frequency conditions must be adjusted and maintained constant:

$$f_i/f_n = 1/2; \quad 1; \quad 1,5; \quad 2; \quad \ldots \; 3,5.$$

Both signals were added in a mixing amplifier and the frequency mixture can be heard on a loud speaker. Stated in musical terms, primarily consonant intervals are produced which lie within two octaves. For zero beats the harmonics coincide with the central frequency of the filter, which are output to the mixing amplifier through a following generator. A characteristic figure is seen on the screen of an oscillograph which is determined from the frequency ratio. The sign of the frequency deviations can be determined from the direction of rotation when beats occur. The central frequency output by the following generator is transformed into a proportional direct current in a f/U converter. It is then directed to a direct current power amplifier over a continuously variable attenuater. Its output signal then excites a

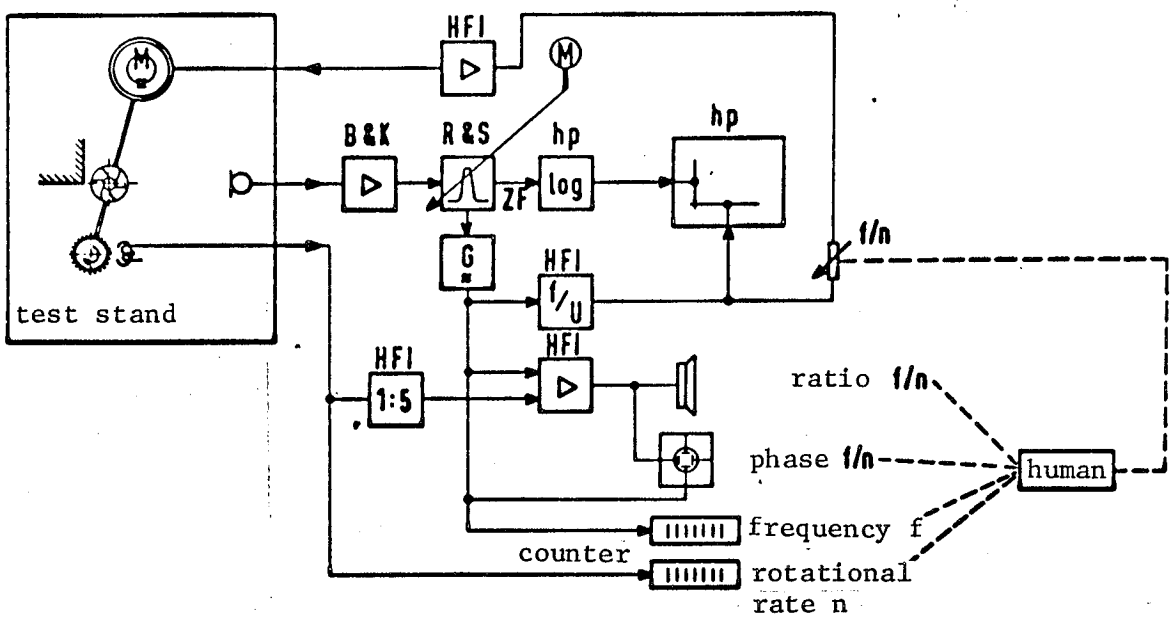


Figure 42. Block diagram for the measurement of the rotational sound.

Leonard generator which feeds the drive motor for the ventilators. This means that the rotational rate and, depending on the setting of the attenuator, also the individual harmonics of the rotational sound follow the central frequency of the analyzer, which is monotonically increased by about 6 Hz/s by means of a servomotor. The operator closes this control loop to form an automatic /67
control system. When phase rotations occur on the screen, erroneous frequency deviations are regulated by hand using the attenuator. During each running up experiment, the logarithm of the output signal of the heterodyne analyzer is plotted versus the central frequency using a X, Y plotter. The rotational sound component is determined after seven passes, as is shown in Figure 9. The amplification in the X channel is adjusted proportional to the rotor diameter, so that plots versus He are obtained directly.

This type of data recording for the rotational sound has several advantages:

1. Such a completeness of the measurement data can only be obtained by an arbitrary number of recordings, as is shown in Figure 8, and this is what is customarily obtained. Then the rotational rate would have to be divided into arbitrarily small steps, so that the required time would be increased by several orders of magnitude.

2. The buildup behavior of the filter is not critical to a large degree. Since the recorded levels are primarily monotonic, the state of buildup depends primarily on the control processes. The rate of starting can be adjusted to the course of the curves in order to save measurement time.

3. If uncertainties are suspected in the recorded curves, then they can be immediately clarified by retracing the same process on the graph.

4. The automatic data recording shown in Figure 9 is represented in such a way that it can be immediately evaluated. The observer of the curves will immediately be aware of the results.

During recording of the flow noise in Figure 7, the control chain is interrupted, and the logarithm of the X signal of the recorder is taken.

## 15. SUMMARY /68

Investigations on the structure of ventilator noise were carried out with five experimental installations having geometrically similar radial wheels and the diameters of which varied in the ratio 1:10. We also wanted to experimentally verify the similarity of the spectral noise properties. The rotors have six blades curved toward the back and are operated in the free mode as well as in the unthrottled mode. A rectangular and geometrically similar perturbing body is used to simulate the switchblade. Its sharp edge is located at a distance of 1% of the rotor diameter.

The measurements were carried out in a chamber having low reflectivity. The microphone can be rotated around the wheel center at a distance of seven rotor diameters. The microphone signal is sheltered by means of a heterodyne analyzer at a bandwidth of 7 Hz. The rotational sound can be continuously recorded using a special measurement technique and for continuous variation of the rotational rate. The noise component of the spectrum is determined by other conventional measurements. However, it is evaluated in the same way as the rotational sound.

Dimensionless characteristic numbers, which describe the problem, have been determined by means of a dimensional analysis. It is possible to immediately test the similarity of the spectra by comparing the normalized results.

A product trial solution is introduced in which it is assumed that the acoustic pressure and the power density depend on the circumferential Mach number and the Reynolds number in the form of exponential laws. It is also assumed that they depend on other normalized functions, namely the excitation spectrum of the rotational sound, the power spectral function of the flow noise and a "system frequency characteristic". Whereas the first two only depend on the Strouhal number, the latter is only a function of the ratio of the wheel size to the acoustic wavelength. The system frequency characteristic is suitable for a description of the frequency dependence of the directional characteristic and the near field interferences, as well as the resonances of the system under consideration.

The power law has been verified by evaluating the measurements. The sound intensity integrated over all frequencies depends on the $5.2^{th}$ power of the circumferential velocity and the $0.4^{th}$ power of the Reynolds number. A dependence on the Reynolds number was only determined in the case of the rotational sound.

Only three normalized curves give an indication of the details of the line spectrum and the power spectrum. They are valid for a large range of rotational rates, and the system characteristic depends only on one measurement direction. The spectral properties of the acoustic sources themselves describe the excitation spectrum and the power spectral function, which are no longer colored by the frequency dependence of the acoustic radiation. This means that several physical mechanisms can be interpreted and verified.

We were able to experimentally verify the general validity of these results for geometrically similar experimental installations, taking the scatter given in Table 2 into account. It is possible to calculate the sound intensity integrated over all frequencies using these curves and to calculate the corresponding equations for arbitrary rotational rates with an error of less than 2 dB.

TABLE 2. REPRESENTATION OF THE ERRORS AND THE VERIFICATION OF SIMILARITY.

| $\frac{D_{max}}{D_{min}}$ | Measurement quantity | Range | Scatter | Figure |
|---|---|---|---|---|
| | **Drehklang** | | | |
| 1:10 | $\tilde{p}_{d,tot}$ | U = 30..60 m/s | ±1 dB max. | 11 |
| 1:5,6 | excitation spectrum | Oct. 3 | ±2 dB max. | 21 |
| 1:5,6 | system frequency characteristic | Oct. 4 | ±3,5 dB on the avge. | 22 |
| | Flow noise | | | |
| 1:5,6 | $\tilde{p}^2_{r,tot}$ | U = 30..60 m/s | ±2 dB max. | 25 |
| 1:4 | power spectral function | Oct. 6 | ±2,5 dB max. | 30 |
| 1:5,6 | system frequency characteristic | Oct. 6 | ±2,5 dB max. | 31 |
| | Comparison of the System frequency characteristic | | | |
| 1 | $G_d/G_r$ | Oct. 4 | ±2 dB on the avge. | 28 |

## APPENDIX

/71

The present paper represents a contribution to the investigation of ventilator loss. An attempt was made to represent them in a clear way and to point to ways in which these laws could be generalized for a number of geometrically similar radial ventilators.

This work was done in Berlin during my seven-year stay as Scientific Researcher at the Hermann-Föttinger-Institut for Flow Technology of the Technical University and the Turbulence Research Institute of the German Research and Experimental Organization for Aerodynamics and Space Flight.

I am especially indebted to the director of both institutes, Professor Dr.-Ing. R. WILLE. I thank him for being able to have received additional experience in flow technology and for his generous support connected with this work.

I am indebted to Dr.-Ing. C. SCHRECK for the supervision of this work and for consultations especially in the area of flow machine problems.

I am indebted to Professor Dr.-Ing. L. CREMER for valuable comments and suggestions in connection with the acoustic developments.

In addition, I would like to thank Professor Dr.-Ing. H. SCHADE, Dr.-Ing. D. BECHERT and Dipl.-Ing. K. GIESE for critical discussions.

Finally, in addition to the unmentioned collaborators, I would like to thank the German Research Association for their financial support of this project.

Dipl.-Ing. Johannes WEIDEMANN
1 Berlin 12, Müller-Breslau-Str.8

## 16. REFERENCES /72


1. Ernsthausen, W. Investigations of Propeller Noise. Akustische Zeitschrift, Vol. 3, 1938, pp. 141-146.

   —. Radiation Groups with a Rotating Phase. A.Z., Vol. 3, 1938, pp. 380-389.

   —. The Influence of Aerodynamic Properties on the Acoustic Field and Jet Performance of a Propeller. A.Z., Vol. 6, 1941, pp. 245-261.

2. Lighthill, M. J. On Sound Generated Aerodynamically. Part 1: General Theory. Proceedings of the Royal Society of London, Vol. 221, 1952, pp. 564-587.

   —. Part 2: Turbulence as a Source of Sound. Proc. Roy. Soc., Vol. 222, 1954, pp. 1-32.

3. Curle, N. The Influence of Solid Boundaries upon Aerodynamic Sound. Proc. Roy. Soc., Vol. 231, 1955, pp. 505-514.

4. Doak, P. E. Acoustic Radiation from a Turbulent Fluid Containing Foreign Bodies. Proc. Roy. Soc., Vol. 254, 1960, p. 129.

5. Wikström, B. Contribution to a Convenient Determination and Representation of Ventilator Noise as the Foundation for the Acoustic Calculation of Ventilation Installation. Dissertation at the Technical University, Berlin, 1964.

6. Yeow, K. W. Centrifugal Fan Noise Research: A Brief Survey of Previous Literature. Institute of Sound and Vibration Research Memorandum No. 143, 1966, pp. 1-112.

7. Beranek, L. L., J. L. Reynolds and K. E. Wilson. Apparatus and Procedures for Predicting Ventilation System Noise. The Journal of the Acoustical Society of America, Vol. 25, No. 2, 1953, pp. 313-321.

8. Peistrup, C. F. and J. E. Wesler. Noise of Ventilating Fans. Journ. Acoust. Soc. Am., Vol. 25, No. 2, 1953, pp. 322-326.

9. Allen, C. H. Noise from Air Conditioning Fans. Noise Control, Vol. 3 /73
   No. 1, 1957, pp. 28-34.

10. Madison, R. D. and J. B. Graham. Fan Noise Variation with Changing Fan Operation. Transactions of ASHRAE (American Society of Heating, Refrigerating and Airconditioning), Vol. 64, 1958, pp. 319-341.

11. Goldmann, R. B. and G. C. Maling. Noise from Small Centrifugal Fans. Noise Control, Vol. 1, No. 6, 1955, pp. 26-29.

12. Madison, R. D. Fan Engineering (Handbook), 5th Edition. Buffalo, New York: Buffalo Forge Company, 1949.

13. Maling, G. C. Dimensional Analysis of Blower Noise. Journ. Acoust. Soc. Am., Vol. 35, No. 10, 1963, pp. 1556-1564.

14. Sharland, I. J. Sources of Noise in Axial Flow Fans. Journal of Sound and Vibration, Vol. 1, No. 3, 1964, pp. 302-322.

15. Stüber, B. Investigation of Aerodynamically Produced Acoustic Fields Using the Model Method. Dissertation at the Technical University, Munich, 1967.

16. Chanaud, R. C. Aerodynamic Sound from Centrifugal-Fan Rotors. Journ. Acoust. Soc. Am., Vol. 37, No. 6, 1965, pp. 969-974.

17. Embleton, T. F. W. Experimental Study of Noise Reduction in Centrifugal Blowers. Journ. Acoust. Soc. Am., Vol. 35, No. 5, 1963, pp. 700-705.

18. Lyons, L. A. and S. Platter. Effects of Cut-Off Configuration on Pure Tones Generated by Small Centrifugal Blowers. Journ. Acoust. Soc. Am., Vol. 35, 1963, pp. 1455-1456.

19. Leidel, W. Influence of the Housing Shape on the Characteristic and Noise of a Radial Ventilator. Dissertation at the Technical University, Berlin, 1967.

20. Daly, B. B. Investigations of Ventilator Noises (II). klima-technik, No. 2, 1964, pp. 8-14.

21. Van Niekerk, C. G. Measurement of the Noise of Ducted Fans. Journ. Acoust. Soc. Am., Vol. 28, No. 4, 1956, pp. 681-687. /74

22. Langhaar, H. L. Dimensional Analysis and Theory of Models. New York: John Wiley and Sons, Inc., 1951.

23. Berger, E., P. Freymuth and E. Froebel. Application of Control Technology to the Development of a Constant Temperature Hot Wire Anemometer. Parts I and II. Report No. 282 and 283, 1963 of the Deutschen Versuchsanstalt for Luft- and Raumfahrt.

24. Giese, K., and C. Schreck. Hot Wire Measurements on Rotating Rotors of Flow Machines. Technica, No. 5, Abs. 5, 1969, p. 106.

25. Giese, K. and C. Schreck. Hot Wire Measurements on Rotating Rotors of Flow Machines. Technica, No. 6, Abs. 8, 1969, p. 498, Figure 27.

26. Roshko, A. On the Drag and Shedding Frequency of Two-dimensional Bluff Bodies. National Advisory Committee for Aeronautics, Washington, July 1954.

27. Schlichting, H. Boundary Layer Theory, 5th Edition, Chapter II, p. 40. Karlsruhe: Verlag G. Barun, 1964.

Translated for National Aeronautics and Space Administration under Contract No. NASw 2035, by SCITRAN, P. O. Box 5456, Santa Barbara, California, 93108.